University of Huddersfield Repository

Alashter, Aisha M Alashter

A Graphical Causality based Modelling Approach for Condition Monitoring

Original Citation

Alashter, Aisha M Alashter (2020) A Graphical Causality based Modelling Approach for Condition Monitoring. Doctoral thesis, University of Huddersfield.

This version is available at http://eprints.hud.ac.uk/id/eprint/35419/

A Graphical Causality based Modelling Approach for Condition Monitoring

By

Aisha M Alashter Alashter

A thesis submitted to the University of Huddersfield in partial fulfilment of the requirements for the degree of Doctor of Philosophy

January 2020

School of Computing and Engineering

University of Huddersfield

Abstract

The wide use of electromechanical systems in critical applications motivates the need for condition monitoring (CM) of such systems. Signal-based methods require simulating all possible malfunction conditions of a system which in reality not possible. Model-based CM is a promising solution and provides a cost-effective and appropriate approach for simulation of all possible operating conditions and can be used for early fault detection and diagnosis. Many models have been utilized to simulate the behaviour of electric machines; however, most of these simulations are based on abstract numerical models rather than a structured illustration of the system. To overcome these problems, a Bond Graph (BG) model with qualitative simulation has been used in this thesis. BGs are efficient at modelling the dynamics of system behaviour based on physical structure, causality and mathematics.

Qualitative simulation (QS) represents semantic knowledge concerning the performance of a particular system for qualitative reasoning. QS could be applied with minimum knowledge of system variables and even with incomplete system model . Therefore, this study focuses on the investigation of QS procedures to develop a more effective and realistic approach to monitor an industrial machine. Significantly, the study has also developed a qualitative BG fault detection approach based on temporal causal graphs (TCGs), qualitative reasoning and, forward propagation. It mainly describes the dynamics of an AC induction motor (ACIM), which is commonly used in numerous industries. It also used to detect ACIM electrical faults (broken rotor bar and stator winding imbalance that commonly occur in ACIM). Further promotes the diagnostics performance of by introducing an algorithm for ACIM diagnosis, which is based the qualitative influence of the faults on the motor current.

In order to evaluate the proposed QS approach, to enhance the knowledge of the dynamic behaviour of ACIM, a BG model of the AC induction motor has been introduced. The developed BG model can simulate the motor behaviour under different conditions, including a healthy motor, a motor with two broken rotor bar levels (one and two broken bars), and a motor with two different levels of stator winding imbalance. The investigation was based on the motor current spectrum analysis using the FFT signal processing technique.

An experimental study investigates the effects of broken rotor bars and stator imbalance on the motor current. The BG model results and corresponding results from the experimental study

have been in good agreement. Moreover, it has also been shown that these outcomes are agreed upon with outcomes reported in the literature.

The TCG and forward propagation results indicated that this approach could be used for the CM of ACIMs. It can detect the effects of broken rotor bars and stator imbalance on the whole system behaviour, showing that this developed QS approach is an efficient technique for extracting diagnostic information, ending up with accurate fault detection using TCG and qualitative reasoning.

The QS technique was validated based on a 20-SIM simulation of the ACIM BG model. The observed results show that a QS approach can accurately detect a broken rotor bar and stator imbalance faults.

The investigation continued by examining the qualitative influence of the seeded electrical faults on the motor current signatures. The results from the experimental study confirm that the BG model and qualitative influence give accurate diagnoses.

Comparison evaluation has been done to compare the graphical causality-based approach with work in the literature. The graphical causality-based approach represents an efficient and meaningful technique for simulating the dynamic system behavior. The diagnostic approach based on TCG is very effective for the detection of ACIM electrical faults. Moreover, it overcomes the limitations of some qualitative studies in the literature.

Copyright Statement

i. The author of this thesis (including any appendices and/or schedules to this thesis) owns any copyright in it (the "Copyright") and s/he has given The University of Huddersfield the right to use such Copyright for any administrative, promotional, educational and/or teaching purposes.

ii. Copies of this thesis, either in full or in extracts, may be made only in accordance with the regulations of the University Library. Details of these regulations may be obtained from the Librarian. This page must form part of any such copies made.

iii. The ownership of any patents, designs, trademarks and any and all other intellectual property rights except for the Copyright (the "Intellectual Property Rights") and any reproductions of copyright works, for example graphs and tables ("Reproductions"), which may be described in this thesis, may not be owned by the author and may be owned by third parties. Such Intellectual Property Rights and Reproductions cannot and must not be made available for use without the prior written permission of the owner(s) of the relevant Intellectual Property Rights and/or Reproductions.

Declaration

I hereby state that I am the lone contributor of this thesis, this original work is my own, and that neither the all nor part of this thesis has been submitted to this university or any other institution for any other qualification.

Aisha M Alashter

Dedication

This work is dedicated to:

The *soul of my father, my mother, my siblings, my husband and my lovely children (Alaa, Abd Almuizz, Mohamed, Ikhlas and Roaa)*

For their kindness, affection, support and prayers of day and night make me able to accomplish much achievements.

Acknowledgement

I would like to express my deep and sincere gratitude to my supervisor **Professor Andrew Ball** for his guidance and support throughout my PhD study.

I sincerely express my thanks and appreciative gratitude to my co-supervisor **Professor Fengshou Gu,** for his help, encouragement, and guidance which play a crucial role in the completion of my research study. Those words are not able to perfectly express my gratitude and greatest thanks to him.

I also would like to convey my special warmest, deep gratitude and thanks to my **mother** and my **brothers and sisters** for their encouragement, support and prayer.

I convey my special thanks to my **husband**, for his support and encouragement to do my best. Without his help, I would not be able to complete this research study. A special thanks to my lovely children **Alaa- Abd Al Muizz- Mohamad- Ikhlas** and **Roaa** for their patience.

I express my thanks to the Libyan government for their support and sponsor of my study.

Last but not least, I would like to take this opportunity to thank all my friends and colleagues who have given their support and help.

Publications

1. **Alashter, Aisha**., Gu, F., Ball, A. D., & Cao, Y. (2019, September). Fault Diagnosis of Broken Rotor Bar in AC Induction Motor based on A Qualitative Simulation Approach. In 2019 25th International Conference on Automation and Computing (ICAC) (pp. 1-6). IEEE.

2. **Alashter, Aisha,** Cao, Y., Rabeyee, K., Alabied, S., Gu, F., & Ball, A. D. (2020). Bond Graph Modelling for Condition Monitoring of Induction Motors. In Advances in Asset Management and Condition Monitoring (pp. 511-523). Springer, Cham.

3. Rabeyee, K., Xu, Y., **Alashter, A.**, Gu, F., & Ball, A. D. (2020). A Componential Coding Neural Network Based Signal Modelling for Condition Monitoring. In Advances in Asset Management and Condition Monitoring (pp. 559-572). Springer, Cham.

Table of Contents

List of Figures

List of Tables

Abbreviations

AC	Alternative Current
ACIM	Alternative Current Induction Motor
ARR	Analytical Redundancy Relations
ASAF	Analytical Signal Angular Fluctuation
BG	Bond Graph
BRB	Broken Rotor Bar
BL	Baseline
CM	Condition Monitoring
DAQS	Data Acquisition System
DC	Direct Current
EMF	Electromagnetic Force
EPRI	Electric Power Research Institute
FDI	Fault Detection and Isolation
FFT	Fast Fourier Transform
GY	Gyrator
IM	Imbalance
K	Kurtosis
MCSA	Motor Current Signature Analysis
MSe	Modulated Effort Sources
MSf	Modulated Flow Sources
PCA	Principle Component Analysis
P2P	Peak to Peak
QDE	Qualitative Differential Equation
QR	Qualitative Reasoning
QS	Qualitative Simulation
QSI	Qualitative Scheme Identification
QSIM	Qualitative Simulation
QTA	Qualitative Trend Analysis
RMS	Root Mean Square
SDG	Signed Directed Graph
SK	Skewness
Se	Effort Source
Sf	flow Source
TCG	Temporal Causal Graph
Te	Electromagnetic Torque
TF	Transformer
VFD	Variable Frequency Drive
WT	Wavelet Transforms

List of Notations

C-elements	Capacitor
E1	Voltage source for stator phase (a) in ACIM BG model
E2	Voltage drop across R_{sa} in ACIM BG model
E3	Voltage source for stator phase (b) in ACIM BG model
E4	Voltage drop across R_{sb} in ACIM BG model
E5	Voltage source for stator phase (c) in ACIM BG model
E6	Voltage drop across R_{sc} in ACIM BG model
E7	Voltage drop across Inductance Stator A in ACIM BG Model
E8	Voltage drop across Inductance stator B in ACIM BG model
E9	Voltage drop across Inductance stator C in ACIM BG model
E10	Voltage drop across Inductance rotor A in ACIM BG model
E11	Voltage drop across Inductance rotor B in ACIM BG model
E12	Voltage drop across Inductance rotor C in ACIM BG model
E13	Motor induced torque in ACIM BG model
E14	Inertia torque in ACIM BG model
E15	Load torque in ACIM BG model
E16	Voltage drop across R_{rc} in ACIM BG model
E17	Voltage drop across R_{rb} in ACIM BG model
E18	Voltage drop across R_{ra} in ACIM BG model
E19	Rotor phase A voltage in ACIM BG model
E20	Rotor phase B voltage in ACIM BG model
E21	Rotor phase C voltage in ACIM BG model
$e(t)$	The effort at a Bond in BG Model in ACIM BG Model
$e = c. \int f.dt$	The effort at C-elements
$e1 = r.f2$ $e2 = r.f1$	The relation between effort and flow at the GY(Gyrator)
$e = R.f$	The Relation Between effort and flow at R-elements
$e1 = m\,e2$ $f2 = m\,f1$	The relation between effort and flow at the TF(Transformer) , m is constant
F1	Phase A current flow in ACIM BG model
F2	Current go through Rsa in ACIM BG model
F3	Phase B current flow in ACIM BG model
F4	Current go through Rsb in ACIM BG model
F5	Phase C current flow in ACIM BG model
F6	Current through Rsc in ACIM BG model
F7	Current flow through Inductance stator C in ACIM BG model
F8	Current flow through Inductance stator B in ACIM BG model
F9	Current flow through Inductance stator A in ACIM BG model
F10	Current flow through Inductance rotor A in ACIM BG model
F11	Current flow through Inductance rotor B in ACIM BG model
F12	Current flow through Inductance rotor C in ACIM BG model
F13	Rotor speed in ACIM BG model
F14	Rotor speed in ACIM BG model
F15	Rotor speed in ACIM BG model

F16	Current go through R_{rc} in ACIM BG model
F17	Current go through R_{rb} in ACIM BG model
F18	Current go through R_{ra} in ACIM BG model
F19	Rotor current phase A in ACIM BG model
F20	Rotor current phase B in ACIM BG model
F21	Rotor current phase C in ACIM BG model
$f = \frac{1}{I}.\int e\,dt$	The flow at I-elements (integral of the effort)
$f = \frac{d}{dt}(c^{-1}.e)$	The flow at I-elements
f_{brb}	broken rotor bar frequency
f_{IMs}	Stator winding imbalance frequency component
f_s	Supply Frequency
$F(t)$	The flow at a bond in BG model
I-elements	Indicator
I_r	Rotor Current
$i_{ra,rb,rc}$	Current for rotor phases a,b,c
I_s	Stator current
$i_{sa,sb,sc}$	Current for stator phases a,b,c
Jm	Machine Inertia
L	Inductance matrix
L_{lr}	Rotor winding leakage inductance
L_{ls}	Stator winding leakage inductance
L_m	The mutual inductance
L_{rr}	Rotor winding self-inductance
$L_{rs=}[L_{rs}]^T$	Stator to rotor inductance/Rotor to stator inductance
L_{ss}	Stator winding self-inductance
N	The number of turns
N_b	Number of rotor bars
n_{brb}	Number of broken bars
P	momentum
Pl	The number of poles
$p(t)$	The energy (power) of a bond in BG model
q	displacement
R2	The resistance of stator phase A in TCG
R4	The resistance of stator phase Bin TCG
R6	The resistance of stator phase C in TCG
R18	The resistance of rotor phase A in TCG
R17	The resistance of rotor phase B in TCG
R16	The resistance of rotor phase C in TCG
r_b	The bar resistance
R_{fs}	Stator resistance fault
R-elements	Resistive
R_r	Rotor Resistance
R_{ra},R_{rb},R_{rc}	The resistance of the rotor phases A,B,C
R_s	Stator Resistance
R_{sa},R_{sb},R_{sc}	The resistance of the stator phases A,B,C
S	Slip
S_r	Rotor speed
S_s	Synchronous speed

$(1 - 2s)fs$	Left-hand BRB sideband component
$(1 + 2s)fs$	The right-hand BRB sideband component
T_e	Electromagnetic torque
T_l	Load torque
u_r	Rotor voltage
u_{ra}, u_{rb}, u_{rc}	The rotor three phases Voltage
u_s	Supply voltage
u_{sa}, u_{sb}, u_{sc}	The stator three phases Voltage
ω_r	Rotor mechanical speed
Ψr	The rotor flux
$\Psi_{ra}, \Psi_{rb}, \Psi_{rc}$	The flux at rotor phases A,B,C
Ψs	The stator flux
$\Psi_{sa}, \Psi_{sb}, \Psi_{sc}$	The flux at stator phases A,B,C
$\emptyset$	Magnetic flux
θ_r	Rotor angle
Δr	The resistance fault
$\Delta r_{ra}, \Delta r_{rb}, \Delta r_{rc}$	The resistance changes (fault) of the three rotor phases

Chapter 1 Introduction

The wide use of the electromechanical systems and the increasing demands from end-users for improved reliability, efficiency, and overall performance are the major motivations for research into and developing fault detection and diagnosis systems. The target of this research study is to develop a qualitative simulation condition monitoring approach accomplishing a viable AC induction motor fault detection.

This chapter introduces to the background and motivation for the research undertaken for this thesis into the condition monitoring of alternating current induction motors using Bond Graphs to more efficiently model the dynamics of system behaviour. The aim and research objectives are presented and the organisation of the thesis is described.

1.1. Background

Induction motors are crucial in providing mechanical energy from electrical energy. They are widely utilized in numerous industrial sectors, including manufacturing, construction and transportation. The induction motor has gained its position as a vital part of power conversion systems due to its many advantages, in particular its relatively low unit cost and low maintenance costs (its construction is not complicated). In particular, the squirrel cage AC induction motor (ACIM) used widely because of its added benefits; long life span and premium energy efficiency [1, 2].

To ensure reliability, consistency, and longevity not only squirrel cage ACIMs but also all-electric machines need to be monitored to detect any faults that exist, minimize maintenance costs and avoid unplanned breakdowns [3].

Machine condition monitoring (CM) is an essential task carried out in most industries to identify machine faults early and prevent sudden and disruptive machine shutdowns. CM has a fundamental role in ensuring that machines continually operate in a reliable and healthy state. Importantly, CM offers the opportunity to detect a fault or monitoring the progress of the detected fault before they cause costly damage. Many different approaches to CM have been reported and used to improve the reliability, applicability, and precision of CM schemes, using various machine quantities (e.g., current, voltage, speed, and productivity) and different sensors (e.g., vibration, speed, and temperature) [4]. Many studies have been carried out into detecting failures in ACIMs, including signal-based, knowledge-based, and model-based techniques. However, all these approaches require sensors to accurately measure the relevant parameters to monitor the condition of the ACIM. Qualitative Simulation (QS) models such as qualitative Bond Graph (BG) involve the semantic representation of the system behaviour dynamics. It could diagnosis the fault based on qualitative behaviour without needing specific values of the parameters [5, 6].

1.2. Motivations of Research

To obtain accurate diagnostic information, modelling a machine system is often required to provide system characteristics under different fault conditions [7]. It has been found that CM based model/simulation of the system is a cost-effective approach and can be particularly useful for the detection of faults in their early stages [8]. Several models have been used to describe the behaviour of electric motors. However, most of them are based on mathematical

abstractions from physical models rather than a structured representation of the motor. They often have problems with uncertainties in the parameters and data distribution. Thus, this study attempts to select a modelling procedure that can be used to analyse an electric motor system's behaviour to accurately describe relations between system components for the detection of motor faults. To overcome these problems, BG modelling and qualitative simulation approaches can be a potential solution as qualitative models can be derived from quantitative models but simulation studies are less parameter-dependent and hence more computationally efficient. This is the reason why this research opts for using BGs.

A BG can be more efficient because it can simulate dynamic system behaviour based on physical structure, causality, and mathematics [9]. Although BGs have been used successfully for simulation of numerous engineering systems, there has been limited research carried out using BGs as a tool for monitoring the condition of ACIMs (alternating current induction motors) [3]. This study develops and evaluates the use of a BG model for CM of a squirrel cage ACIM. The BG model has been constructed using the causal relationship between the system's components in a manner that allows the presence of faults to be detected based on the motor current. Using the "natural reference frame" whereby the currents in the three phases are represented by sinusoids A-B-C with phase differences of 120°, the behaviour of the ACIM has been simulated. This model simulates motor behaviour under different conditions: baseline (BL - assumed healthy), with two levels of rotor bar breakage (BRB) and two levels of stator winding imbalance (IM).

Then this model is used as a benchmark for the BG QS approach for monitoring the ACIM system, based on a temporal causal graph (TCG) and qualitative equations. The qualitative BG model aims to detect ACIM electrical faults based on TCG and qualitative reasoning by investigating the qualitative changes caused/induced by a broken rotor bar(s) and stator winding imbalance faults. Later the study evaluates the proposed quantitative and qualitative models using a test rig and experimental data sets.

1.3. Research Aim and Objectives

The aim of this study is to develop a method for the diagnosis of induction machine faults, based on a qualitative simulation study. It will be fulfilled through the accomplishment of the following objectives:

Objective 1 To review and understand CM techniques used in condition monitoring systems including quantitative and qualitative methods, and complete a comprehensive review of the electrical induction machines' diagnostics.

Objective 2 To investigate the effects of electrical faults on an AC induction motor's performance, which includes the effects of stator windings imbalance, and broken rotor bars. This is accomplished by analysing the cause and effects of these faults.

Objective 3 To understand the models of ACIMs and develop a BG model of a healthy motor, the motor with a broken rotor bar, and motor with stator winding imbalance.

Objective 4 To develop a qualitative simulation approach for the detection of ACIM faults, including broken rotor bar and stator winding imbalance.

Objective 5 To build a three-phase AC induction motor bench rig suitable for testing different ACIM faults with different severity levels and collecting experimental data sets.

Objective 6 To examine the performance of the techniques developed in Objectives 3 and 4 above, based on the acquired experimental datasets.

Objective 7 To suggest recommendations that may be considered for future research in this area of study.

1.4. Thesis Structure

This thesis includes ten chapters to represent the tasks that were performed to achieve the aim and objectives of this study.

Chapter One- The first chapter comprises the background, motivation, aims, and objectives of the research, and it concludes with the thesis organization.

Chapter Two- Provides a brief review of previous work on machine CM, and gives an overview of CM techniques. These are followed by a review of ACIM fault detection methods.

Chapter Three- Gives an overview of qualitative simulation methods. It begins with the principle of qualitative simulations and existing qualitative simulation methods. Next, it gives some qualitative BG fault diagnostic approaches and concludes with a general view of the proposed approach adopted for this research.

Chapter Four- Provides a description of ACIM construction and principles of operation, including speed, torque and load. This is followed by a description of relevant types of motor faults. The chapter ends with the relations between motor specification and modes of failure.

Chapter Five- This chapter provides BG modelling theory. It starts with a brief introduction to BG modelling techniques, including BG principles, variables, and standard elements. Next, it presents a general explanation of the causality concept. Then, it gives an example to show how to build a BG model and generate equations from the BG model. Afterward, it provides a brief review of some BG fault detection procedures. It also introduces the proposed quantitative BG model. Finally, it provides a description of the proposed qualitative simulation approach that will be used in this study.

Chapter Six- This chapter covers the details of experimental test facilities and describes the rig instruments. Additionally, it presents an explanation of the addressed faults and the procedure for collecting the data. Then it provides the results obtained from the measured signal in the form of graphs. The tests were conducted with an adjustable load and different motor conditions: baseline/broken rotor bar/stator winding imbalance. The acquired data were processed and the baseline data was compared with data from the tests with seeded faults.

Chapter Seven- This chapter covers the development of the BG model of a three-phase ACIM in the stationary frame. First, it provides the mathematical description of a healthy motor, followed by the motor's description with a broken rotor bar then motor with stator imbalance. Finally it provides the BG model of the three phase induction motor.

Chapter Eight-This chapter provides the implementations of the BG model introduced in Chapter Seven. Then, it presents the evaluation of the BG model by comparing the results acquired from the BG model to the corresponding experimental results obtained from the test facilities described in Chapter Six. Finally, the current signal spectrum results for both seeded faults (broken rotor bar and stator winding imbalance) are presented.

Chapter Nine- This chapter provides BG qualitative approach modelling. It presents the temporal causal graph of the ACIM, qualitative equations and fault detection procedure. Next, it gives the qualitative fault detection results for the seeded faults, providing validation of the qualitative fault detection result by comparison with the corresponding simulation results. Finally, it presents a qualitative fault diagnosis based on the changes in the current signal spectrum's amplitudes at frequencies $(f_s + 2sf_s)$ and at $3f_s$, caused by a broken rotor bar and

stator imbalance. Validation of the method is provided by comparing corresponding results from simulated (data from the bond graph model) and measured data (experimental data).

Chapter Ten - This chapter outlines objectives and achievements, draws conclusions, describes the contribution to knowledge made in this thesis, and makes suggestions and recommendations for future work.
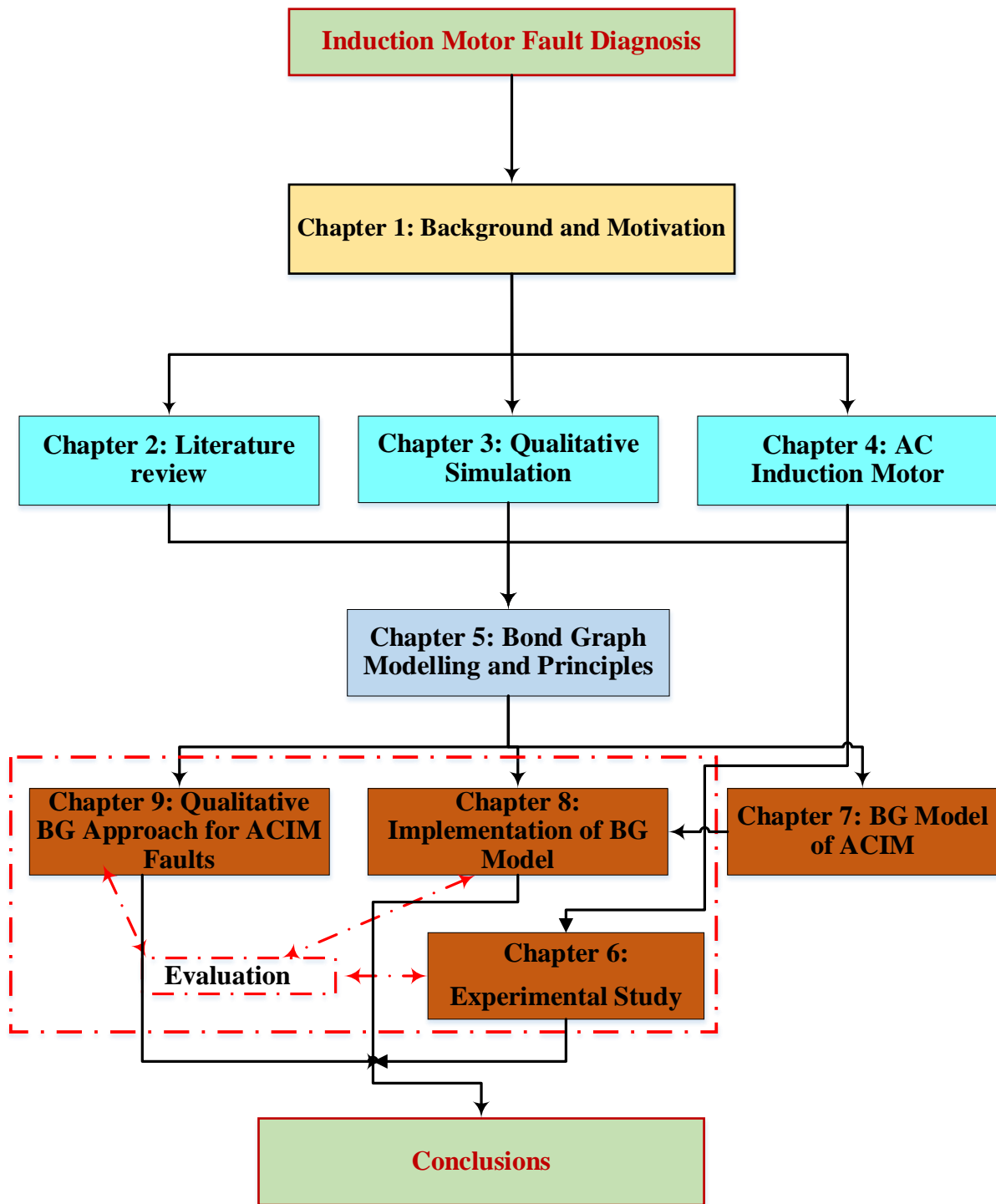
Figure 1-1 Thesis Structure

Chapter 2 Literature Review

This chapter gives a general overview of the condition monitoring of electrical motors. Then it gives a brief description of condition monitoring procedures and fault detection and diagnostic approaches. Next, it provides a review of methods used for the detection of common induction motor faults.

2.1. Overview of Condition Monitoring of Electrical Machines

The primary purpose of condition monitoring (CM) is to monitor the essential system specifications and search for unanticipated changes or unusual behaviour that would demonstrate a possible, or likely, deficiency in the system. Due to the widespread use of electrical machines in most, if not all, industries, it is essential to monitor the machine's behaviour to enhance reliability and ensure low-cost maintenance and human safety. Having a dependable CM framework for induction motors utilized as a part of numerous, different industrial applications, would minimize downtime and reduce the occurrence of costly repairs [10].

If an existing fault is not detected and diagnosed promptly, there is a strong possibility that the machine will start to malfunction or even stop working. The fundamental concept of a fault diagnosis scheme is to monitor the performance of every vital component. Essentially this is accomplished by matching the output of the system to reference values [11]. Many fault observation strategies have been proposed and utilized to identify machine problems at an early stage using diverse machine quantities, for example, motor current, voltage, and speed, or machine vibration, temperature, pressure, and lubricant condition. CM's function is to select one or more of these measurable parameters that best reflect the machine's condition.

The maintenance technician and engineer should regularly monitor the chosen parameters and then take appropriate action when any significant change(s) is detected. When a difference in parameter behaviour is identified, it is a sign to the maintenance engineer to make a detailed analysis to detect and determine system irregularities quickly. The use of CM to identify abnormal operation allows the maintenance personnel to circumvent the consequences of the fault before a failure takes place [12]. Potential advantages of CM are [13]: increased machine reliability and availability; improved efficiency of operation; reduction of unexpected shut-downs; better system performance and decreased machine preparation costs; improvement of health and safety; enhanced awareness of the machine's condition; extended operational life; and improvement of relations with customers. However, CM related cost should be taken into accounts, such as the cost of the necessary sensors and the computerized instrumentation utilized for data analysis [14].

2.2. Condition Monitoring Techniques of Electrical Machines

CM techniques are typically used in industrial applications to control the performance and monitor the conditions of machines. It detects and identifies faults, thus enabling the prevention of machine damage, reducing maintenance costs, increasing machine reliability, extending the machine's operational life, and improving overall system efficiency.

The well-known CM measurement procedures include; vibration level, temperature, oil quality, voltage, and current measurement. However, the common disadvantage of these techniques is that they often require the presence of additional sensors.

Researchers have investigated a variety of approaches to observing the operations of induction machines. With reviews of fault diagnosis methods, their findings have been summarized in relevant surveys, in particular [5, 15-18]. Some of these methods used sensors that measured the speed or vibration, torque, temperature, and magnetic flux. For fault detection and condition monitoring, the most popular methods reported in the literature can be categorized as follows [10, 19-22]:

Signal-based techniques: committed sensors can be implanted into the machine to distinguish the level of damage. This technique is usually based on time and frequency domain analysis of some quantity, such as vibration, machine motor current, and/or temperature.

Model-based techniques: This includes building up a mathematical model of the system of interest to examine the system under different conditions rather than actualizing tests.

Knowledge-based techniques: These methods depend on qualitative approaches instead of quantitative numerical models and include artificial intelligent systems and case based reasoning. This approach can be used when the system is too complex to model mathematically or for which there is incomplete knowledge.

Merging of techniques: The strategies mentioned above can be combined to accomplish a more precise, reliable, and cost-effective CM system.

The standard steps of the condition monitoring techniques can be summarized as:

1- Data collection: acquiring system parameters
2- Data processing and,
3- Decision-making.
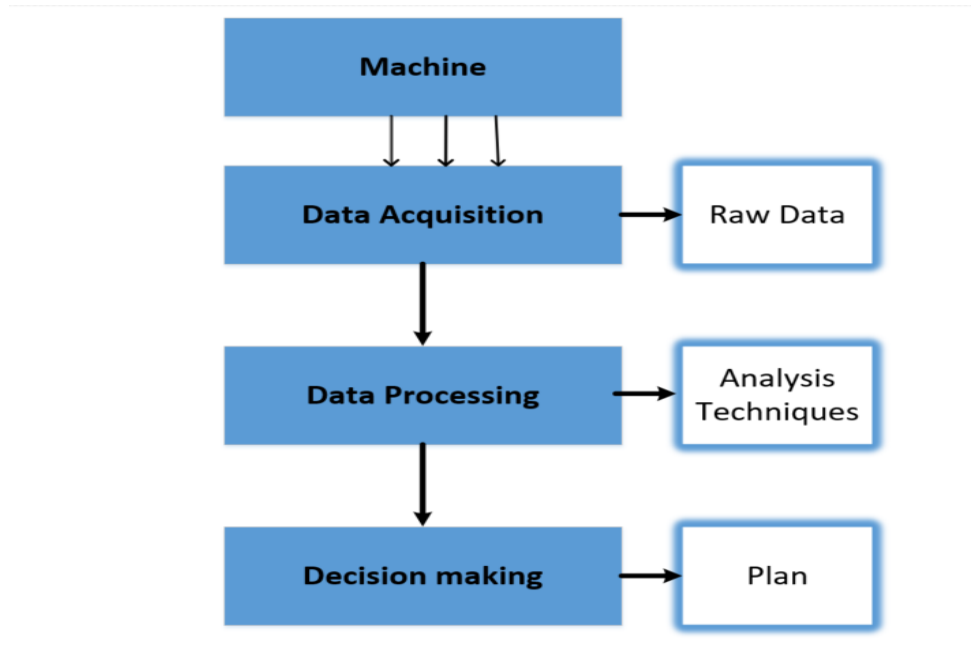
Figure 2-1 Steps of condition monitoring procedure

This section gives a brief overview of some fault detection and diagnosis approaches.

2.2.1. Vibration Monitoring

Even a perfectly healthy induction machine will have a slight vibration. However, massive vibration signals can be induced when the machine has an internal fault [23]. Monitoring of vibration levels is a typical technique for detecting bearing fault [24], rotor faults and gear mesh problem in induction machines [23]. Vibration signals can be measured by placing suitable transducers (usually accelerometers) on bearings. Vibration supervising is considered among the oldest fault detection methods. Although it is both effective and widely used to detect induction machine faults, particularly mechanical faults, it has two significant disadvantages. First, it needs transducers to be attached to the system that may disturb the machine's operations. Second, the vibration transducers can be expensive compared with the costs of other types of other sensors.

2.2.2. Temperature Monitoring

Temperature monitoring is a common approach for fault detection related to the change in temperature of all or part of a device. It is particularly useful for detecting a fault with, e.g., bearings and motor windings. The temperature can be measured with sensors such as resistance thermometers, but today the most common is the optical pyrometer [25] . This is a useful method because each component has a limited operating temperature; however, the change in

component (or device) temperature may take time, so it is not appropriate to detect faults in their early stages [26].

2.2.3. Human Senses Monitoring

A traditional and very widely-used fault detection method depends on the human senses; hearing, touch, sight, and smell. It offers a direct method of finding machine faults without the use of additional tools [27]. The human senses can be utilized to detect abnormal operating, e.g., excessive vibration, overheated machinery, leaking equipment, poor electrical/pipe connections, steam leaks, and surface roughness changes [25]. This method is cost-effective and can be used as a complement to other fault identification techniques. However, owing to the different individual experiences of different observers, fault diagnosis may vary between individuals [28].

2.2.4. Motor Current Signature Analysis

Motor Current Signature Analysis (MCSA) is a technique used to investigate electrical machines' health, such as induction motors. It has been used to successfully detect several induction machine faults such as broken rotor bars, abnormal air gap eccentricity, and stator winding faults [29]. The procedure consists of calculating the spectrum of the measured stator current of the induction motor from which the fault can be detected. Amongst fault detection approaches, MCSA has many advantages. Firstly, it deals with simple electrical quantities and does not require additional instruments as other methods do, which makes it cost-effective [4]. Secondly, it is capable of detecting a fault in the early stage and prevent damage from occurring. Thirdly, the fault influences in the current signals are unique for some faults such as BRB and imbalanced stator winding. Most crucially, it has the advantage of being able to improve the efficiency and reliability of a system [30, 31].

Diverse signal processing procedures have been introduced to process the current signal to extract diagnostic features from raw data. These can be categorized into three general groups: Time domain, Frequency domain and Time-frequency domain.

2.2.4.1. Time domain analysis

The current signals are functions of time [32], and time-domain analysis can be applied for fault detection either by visual observation of the signal or using statistical parameters [33]. There are different statistical measures utilized to generate diagnostic characteristics from the

raw data; these include Root Mean Square (RMS), Peak to Peak Value (P2P), Kurtosis (K), and Skewness (SK). Compared to a fault-free condition each of these statistical measurements changed in magnitude as a machine fault develops.

RMS gives a proportion of the energy evolution of the input signal. Its value shows the change in the signal that indicates a fault has occurred but does not indicate which fault is occurring. It is defined as [34]:

$$RMS = \sqrt{\frac{1}{N}\sum_{i=1}^{N} x_i^2} \qquad\qquad (2\text{-}1)$$

P2P utilized to measures the maximum difference with the input signal based on the following formula [34]

$$P2P = \frac{max(x_i) - min(x_i)}{2} \qquad\qquad (2\text{-}2)$$

SK is widely used for measuring the asymmetry of the input signal about its mean value as [35]

$$SK = \frac{\frac{1}{N}\sum_{i=1}^{N}(x_i - \overline{x})^3}{S^3} \qquad\qquad (2\text{-}3)$$

Where $\bar{x}$ is the mean, N is the number of data point and S is the standard deviation.

K is utilized to measure the peakedness of the signal and the weight of tail for the entered signal based on this calculation [36]:

$$K = \frac{\sum_{i=1}^{N}(x_i - \overline{x})^4}{N*(\sigma^2)^2} \qquad\qquad (2\text{-}4)$$

Where N the total number of data points is, xi is the raw time series, $\bar{x}$ is the mean of the data, and σ is the variance of the data.

2.2.4.2. Frequency domain analysis

All time-domain signals whose amplitude varies will contain frequency components. Induction machines faults, including rotor breakage and stator winding imbalance faults, can be detected based on current analysis. Commonly, to detect abnormal conditions, the current spectrum is much more useful than the current amplitude for monitoring the motor's condition. As a fault occurs in the motor, peaks occur in the current spectrum. The most spectral analysis used for motor fault detection has been achieved utilizing the Fast Fourier Transform (FFT) [37]. The FFT is used to transform the input signal into an infinite series of sinusoids and could be utilized to extract the characteristic of the current signal for defect identification [38]. For instance, [39-

41] have utilized the FFT for stator current analysis to detect rotor faults. The FFT can be defined by the flowing equation [42]

$$X_k = \sum_{n=0}^{N-1} x_n \cdot e^{-i2\pi kn/N} \qquad (2\text{-}5)$$

$$x_n = \frac{1}{N} \sum_{k=0}^{N-1} X_k \cdot e^{-i2\pi kn/N} \qquad (2\text{-}5)$$

2.2.4.3. Time-frequency domain analysis

When the signal is transformed from the time into the frequency domain, time information is lost [43, 44] making it challenging to identify when a specific event occurs. The time-frequency analysis is a great tool that describes the signal's component with respect to its frequency and time. Lately, approaches for addressing time-frequency have been introduced, such as Short-Time Fourier Transform (STFT) and Wavelet Transform (WT).

2.3. Fault Detection Procedures for ACIM

It has long been known that to avoid unscheduled stoppages and consequential financial loss and to lower maintenance costs, ACIMs need to be continuously monitored, and system faults need to be identified at the earliest possible stage. ACIM faults can be mechanical or/and electrical. This study focuses on two types of electrical faults: broken rotor bar (BRB) and stator winding imbalance (IM). These are common faults that substantially impact motor efficiency and system safety, and early detection is strongly recommended. Previous studies have reported different methods that have been used to identify ACIM faults, including signal processing, model-based, and knowledge-based techniques. Liu and Bazzi [45] carried out a wide-ranging review of methods for the CM of ACIMs; the methods were grouped into four domains based on their usage.

Another review of stator faults was presented in [46], in which it was concluded that the quickest method for fault detection was to use an analytical model. These authors found that motor current signature analysis (MCSA) was the most common fault detection method and that MCSA has been used successfully to detect various sorts of electric machine faults. In this study, the literature review focuses on detection BRB and stator winding faults using MCSA and model-based fault detection procedures.

2.3.1. Fault Detection Procedures based on MCSA

MCSA is a steady-state technique. It involves measuring the current from an induction machine's stator and identifying the fault from the spectrum. The MCSA approach relies on

finding particular harmonic elements in the stator current, which is induced by the rotating flux due to the presence of faults. MCSA is a viable approach for detecting electric motors faults. Because it uses just stator current, it is also relatively simple [47]. A brief review of MCSA, including a description of its principles, practical detection techniques, and different faults' signatures, is given in [48]. It has also been addressed by several other authors [49, 50]. In particular, [50] have investigated a new method for broken rotor bar fault identification utilizing motor current signals. The method is based on modulation signal bi-spectrum analysis of the stator current. This method overcomes the deficiency of the conventional bi-spectrum.

A description of BRB's fault detection is given in [47], based on MCSA and FFT. In [51] MCSA was applied, first using the FFT and then using a WT to extract the features for the BRB detection and classification. In another example, [52], MCSA and an extended Park vector method were used to detect a stator turn fault. In [53], a stator inter-turn fault diagnosis was achieved based on motor current signals and discrete WT. A description of fault detection of a BRB and load oscillation based on Analytical Signal Angular Fluctuation (ASAF) of the current signal is given in [54].

2.3.2. Model Based Fault Detection Approaches

Fault detection model-based approaches generate an analytical description of the dynamic system to identify faults of the system under investigation. Mathematical models have been utilized to reveal machine operations under various conditions. For instance, a model has been developed by [55] to examine the machine conditions under a BRB fault using a set membership identification. A BRB diagnostic has been achieved utilizing a model-based method and a Prony analysis of the motor current by [56]. Their results were verified by comparison with experimental data. A new mathematical model to detect a BRB was developed [41], based on a winding function approach with fault severity addressed using motor current and rotor speed.

The authors in [57] have studied the effects of the broken rotor bar fault on the magnetic flux density using an analytical model. Their results indicated that the broken rotor bar characteristic could be investigated around 300 Hz at the electromagnetic spectrum. They plan to apply this method to the double cage induction motor.

In [58], the authors developed a complete mathematical model to represent inter-turn winding faults in a three-phase induction motor in the ABC reference frame. The short circuit was

considered as a new phase to obtain the short circuit current. It simulated the inter-turn short circuit fault by matching a resistance with phase A of the stator. Results of an experimental investigation corresponded with the predictions of the simulated model. A methodical model was used by [59] to examine the machine conditions under a stator fault by observing the instantaneous power of the stator as well as line current spectra.

A transient model for an induction motor developed to detect a stator winding fault has been given by [60]. This model was based on reference frame conversion theory and used a state-space model to estimate the fault. This model can present the fault level, but it cannot identify the location of the fault.

A dynamic model of a squirrel cage induction motor has been reported in [61] to simulate both normal and faulty rotor conditions. It is based on the rotating field theory and coupled circuits. The simulated results agreed with the experimental in the healthy condition, but the model was limited when a rotor fault was present. In [62] a comprehensive three-phase induction motor dynamic analytical model was developed to investigate the influence of temperature on machine parameters. Another mathematical model proposed by [63], simulates a squirrel cage induction motor's healthy and abnormal conditions and can detect a broken rotor bar fault. A simplified model of three-phase induction motor has been used by Khater et al. [64] to examine the effect of a broken rotor bar on the torque-speed characteristic. Their result indicated that the machine damping was reduced as the rotor resistance was increased. There was no experimental study to evaluate the model results.

Another model-based approach has been developed by Bednarz and Dybkowski [65] for the detection of broken rotor bar and stator winding faults. The fault detection was based on the changes of the motor parameters. The broken rotor bar fault caused increasing the rotor resistance while the stator winding fault increased the stator resistance. Two estimators have been used in the reported method to estimate the rotor and stator resistance based on the model reference adaptive system. Also, a fault identification algorithm was proposed. They indicated that their method was useful for fault detection based on experiment evaluation.

Nemec et al. [66] reported a model-based broken rotor bar fault detection. It depends on observing the contrast between the angles of rotor-flux vectors calculated through voltage and current models. It used a simplified model of an AC induction motor. The detection was based on the angle change to differentiate between healthy motor and motor with a broken rotor bar fault. Also, they showed the current spectrum result. The reported method demonstrates a high

performance of the broken rotor bar fault detection; however, its shortage is the need to measure the amounts of the current, voltage, and rotor angle.

Though many models have been used for fault detection of induction machine, most of these reported models are based on the abstract mathematical model instead of system structure. This propels the need for structured models such as bond graph modelling.

Moreover, although extensive research has been carried out on detecting rotor and stator faults, to the best of this author's knowledge, not much research exists which uses the qualitative reasoning simulation models for ACIM fault detection. Thus the next section introduces the qualitative simulations. Then Chapter Three would review the qualitative simulation approaches.

2.4. Summary

Model-based approaches provide low-cost and appropriate methods for the detection of faults in their early stages. Many models have been utilized to simulate the behaviour of induction motors. But, most of them are based on abstract mathematical models rather than a structured presentation of the motor. From our perspective, selecting a modelling procedure that is apt for analysis of electric motor behaviour and describes the relations between system components would be more accurate for fault detection. This is the reason for using bond graph modelling in this research. Bond graphs are more efficient in that they can model the dynamics of system behaviour based on a combination of three different aspects; physical structure, causality, and mathematics. This approach has been used widely for the modelling of engineering systems [67, 68]. However, it has been found that there has been limited research work utilizing bond graphs for induction motor process simulations.

This study aims to address this gap and proposed a qualitative simulation bond graph approach for the CM of a three-phase squirrel cage AC induction motor. A bond graph model will be constructed based on system structure and the causality relations between its components. It will simulate the AC machine under different conditions namely, baseline, broken rotor bar and stator winding imbalance. It aims to identify the existence of such faults based on MCSA.

Chapter 3 Qualitative Simulation

In this chapter, a brief introduction is given to the significance of Qualitative Simulation (QS) approaches. It reviews typical implementations of QS methods used for CM, in which the major tools used with QS are highlighted. Next, it gives some qualitative BG fault diagnostic approaches and concludes with a general view of the proposed approach adopted for this research.

.

3.1. Qualitative Simulation

The rapidly increasing complexity of engineering systems such as wind energy conversion, aircraft, and medical systems, and the parallel development of security needs, has accelerated the need for automatic system observation. This has encouraged the development of fault detection tools for monitoring the system by simulating system behaviour. QS was first established to characterize complex physical events in the lack of quantitative data [69].

3.2. Principle of Qualitative Simulations

Qualitative simulations would be a prevalent common sense or reasoning technique that includes simulation technologies to figure out the qualitative values and the variation direction of system variables [70]. Qualitative fault diagnosis models can be established based on two different approaches; causal models or abstraction hierarchies. Causal approaches are based on cause and effect relations between the system components. The digraphs/bond graphs approach to the system is a set of nodes connected by edges on the basis of relationships of known causes and effects. A fault tree is a description of the failure mode and interprets the relations between component faults and observed symptoms [71]. Qualitative physics approaches are based on the derivation of qualitative behaviour from the differential equations [5]. The abstraction hierarchy approach is dependent on the deductions of system behaviour based on the behaviour of its subsystems [72]. This approach can be built based on system structure or the system functionality.

Figure 3-1 depicts a classification of qualitative model strategies.
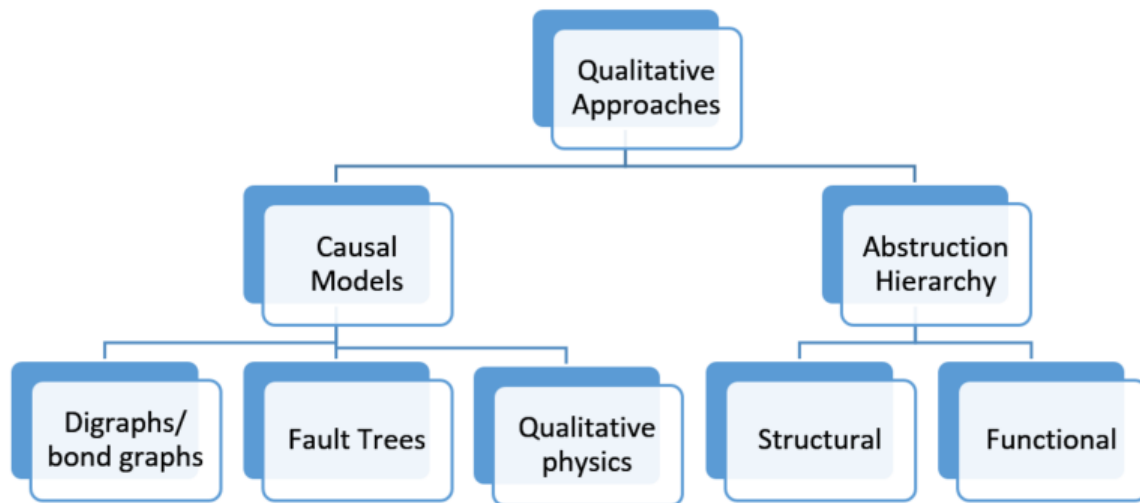
Figure 3-1 Types of qualitative knowledge amended from [5]

According to [70], "Qualitative simulation is defined as a reasoning technique, which is utilized to model human reasoning approach". Qualitative Reasoning (QR) has several positive attributes compared to forms of reasoning, as done in conventional numerical approaches [73]. Firstly, QR can be utilized to develop a system model to illustrate the connections between cause and effect in the system's components and behaviour. Secondly, QR denotes variable values using [+, 0, -], (+) means the variable value increases, (-) means the variable value decreases, and (0) means there is no change. Such associations between variables are generally stated easily without referring to specific values or even units. Finally, QR used reasoning in both its illustration and inferences, it represents a status regards to overall features, providing useful concepts and distinct states without the need for precise numerical information [74]. As a result, a system can be presented and investigated with incomplete knowledge. On the other hand, precise data could be introduced into QS models to enhance their accuracy. Subsequently, QR offers the possibility of monitoring techniques that include both inference ability and accuracy [74].

The goal of QS is to provide a description of the possible future behaviour of the addressed system. QS is described as a reasoning procedure that utilizes simulation; it produces possible

values and changes in their directions using qualitative information concerning the system being simulated [70].

In order to describe physical systems, QS utilizes qualitative state variables, including interval-valued, ordinal valued, and signed variables, to help describe the modelled system [75]. It reliably estimates the conceivable behaviour of the system under investigation with a qualitative differential equation model. Its value is a result of its ability to identify the expected information from limited knowledge of the system [76] and the aptitude to develop whole conceivable behaviour patterns. However, even so, the model is incomplete. It begins with a description of the system structure and its initial state, and it concludes with possible future states of the system. Qualitative simulations calculate the possible behaviour with a qualitative differential equation (QDE) model and an initial state. According to [77], "a qualitative differential equation model (QDE) is an abstraction of an ordinary differential equation, consisting of a set of real-valued variables and functional, algebraic and differential constraints among them."

Quantitative models have been used extensively in machine monitoring systems for machine faults detection. However, there are major concerns about machine parameters, which may often be insufficient, and model accuracy may be hard to meet [73]. On the other hand, QS models do not depend on the parameters significantly, hence affecting the computational aspect. In QS models, semantic knowledge is extracted from the description of both the construction and the system's behaviour. After the description of the system behaviour, qualitative reasoning is used with algebraic rules to derive the system's state, based on semantic relations.

In general, QS based fault detection and diagnosis may be less accurate compared with the quantitative approaches. However, it is more resistant to noise and could be more convenient for computing [5, 6, 78]. These merits make it more appropriate for CM in conventional industrial systems, which often have incomplete system design details and limited resources (finance and computation) for implementing a fully quantitative method.

3.3. Existing Qualitative Simulation Models

Much research on fault detection methods have been reported in the literature, so only qualitative approaches are considered in this section.

3.3.1. Qualitative Simulator (QSIM)

The well-known qualitative simulation algorithm (QSIM) presented in [79] is a good example of QS. QSIM requires a description of the system, its construction and its base state. It describes the behaviour of the system's mechanism using (+, 0, -), which represents an increase, stability, and decrease, respectively, in the given variables. Its output is the most likely imminent state of the system. QSIM is a means of addressing how quantities described qualitatively can be used to build an algorithm that can be used to solve quantitative equations. More detail on QSIM can be found in [79, 80]. QS is an interesting area for research into CM and could play an essential part in ACIM fault diagnosis.

3.3.2. Qualitative Scheme Identification

Another formulation of QS is "Qualitative Scheme Identification" (QSI), which is reported in [81]. The input of the QSI is information regarding the qualitative behaviour of a physical system and then provides a constraint model. QSI is a machine-learning procedure that adapts the QSIM method, as a good example see the U-tube and spring-block system in [81]. Both QSIM and QSI described the system using QDE, a group of qualitative constraints that characterize the investigated system. Table 3-1 shows a list of qualitative constraints utilized in the QSIM and QSI models.

Table 3-1 Examples of qualitative constraints

Constraints	Meaning
ADD(X, Y, Z)	$Z(t)=X(t)+Y(t)$
DERIV(X, Y)	$dx/dt = Y$
M+(X, Y)	$X(t)=f(Y(t))$, where f>0
M- (X, Y)	$X(t)=f(Y(t))$, where f <0
MINUS(X, Y)	$X(t)= -Y(t)$

3.3.3. Signed Directed Graph

Signed Directed Graph (SDG) is one of the most used qualitative models and, in the last three decades, has increasingly been used for fault detection [82]. It represents the causes and effects that explain the relationship between the actions that determine a system's behaviour, as a graph. It is used to illustrate the relevant characteristics between processes in the system being investigated [83] using the set of nodes connected by arcs as the graph G= (X, R) where X represents the variables of the system and R the edges that connect the graph. Multiple fault

detection using a signed digraph has been proposed in [84]. To reduce the complexity that arises with a number of faults and increase the resolution of SDG, a knowledge base was used to swap out the node that has less probability. Fault detection using SDG combined with a neural network to identify abnormal operation in a nuclear power system was reported in [85]. The results indicate that the simulation result of the hybridized method was able to detect abnormal conditions.

An inclusive technique for QS has been developed in [86, 87] using sign digraph models and qualitative equations. The system was the automation of a chemical process and used a graph model to generate a mathematical description of the procedure. A generic model of the system was used to reduce the number of spurious solutions that could have resulted from the predictive behaviour. The shortage of SDG-based fault detection is the lack of diagnosis resolution [88]. A SDG developed by [88] coupled with qualitative trend analysis (QTA) did improve detection resolution. First, the signed digraph of the system behaviour was constructed and then the QTA algorithm was used to examine the connection between nodes. The results obtained indicated an improvement in efficiency.

3.3.4. Automatic Qualitative Trend Simulation

A fully automated QS method for fault detection in industrial processes has been reported in [83]. It involves the prediction of the patterns of behaviour that result from a variety of faults. Qualitative models can derive specious solutions, and this research limited the number of such solutions via the systematic derivation of qualitative equations from the quantitative model of the system. These authors began by constructing the equations that describe the system's basis, then introduced a fault into the system, reconstructed the quantitative equations, and then derived the qualitative equations automatically using a MATLAB code. Later, a solver algorithm, based on the algebraic manipulation proposed in [22], was applied. One example given of using the automated QS model was the lubrication system of a centrifugal compressor. These plants are difficult to monitor using numerical methods, so QS was used. The QS model considered different lubrication systems faults, such as pipe leakage at the pump discharge, and increased lubricant temperature. Although the obtained results indicated that the number of specious solutions was reduced, this method was limited to the stationary situation of the system.

3.3.5. Qualitative Fault Isolation

Qualitative fault isolation has been introduced by Bregon et al. [89]. It is based on the structure model, and the fault is detected by investigating the qualitative information of the residual deviations. The technique was utilized for a simple circuit system.

3.3.6. Qualitative Event Based

Daigle et al. [90] reported a qualitative event-based method to predict the fault effects. They stated that their qualitative approach could be utilized for fault detection based on qualitative event-based information. They applied this method to a tank system, and claimed that it was shown a good performance.

3.3.7. Bond Graph Qualitative Simulation

Another QS technique is a bond graph (BG) in which the interactions between system components are presented as bonds that convey power, energy, and causations between power variables [91]. There are two variables linked to each bond, known as effort and flow, indicated by the use of e_i and f_i respectively, where i denotes the number of the bond [92]. BG affords a unified modelling tool appropriate to all domains of physics (e.g., electrical, mechanical, hydraulic). BG modelling is a pictorial method utilized to construct the system behaviour using the causality procedure. On this basis, BG language has been shown to be a useful technique for the modelling of systems [93].

3.4. Bond Graphs for Fault Diagnosis

BGs represent a logical structure for constructing consistent models of dynamic physical systems through multi-domains. Because they are built on the basis of cause and effect constraints, they are a good diagnostic tool. Moreover, these features give the BGs the power to be used as qualitative approaches. Once qualitative information is applied within the principal protocols of the BG structure's basic elements, the resulting model can be described as qualitative BG [94]. BG models have been applied widely in the published literature to present different systems. Relatively few researchers have reported using BGs for qualitative analysis. This section presents qualitative BG models of interest for this research.

A qualitative BG has been reported in [95] for the diagnosis of continuous-valued systems. It was constructed based on four steps. Firstly, it decomposed the system into subsystems. Next, it built BG models of the systems. Then, it constructed the relevant equations based on the

behaviour of the components of the system being addressed. Finally, it produced conflict sets utilizing causality and qualitative analysis.

A QS BG approach was introduced by [96] for analysing and simulating the behaviour of a dynamic physical system. It was based on two forms of qualitative investigation; the first was to use known states to acquire unknown states. The second was the prediction of the impacts of parameter deviations on the entire system. Another qualitative BG approach for fault diagnosis has been introduced in [73]. It was based on qualitative reasoning analysis between system elements and system structure. The inference mechanism was introduced to address fault localization utilizing qualitative equations and qualitative reasoning.

A qualitative bond graph fault detection approach has been proposed by Mosterman and Biswas [6]. It was based on applying a new causal graph named a temporal causal graph (TCG) produced by considering the causal relations between the BG power variables. Effort and flow were the vertices of the TCG, and the relations between them have been the edges. When an edge is linked to system elements, it illustrates the relation between them, so that for the simplest electrical circuit, i.e., a resistor with effort causality, the edge linking the effort and flow has the value of the resistance (R). The system's behaviour is modelled by the relationships allocated to control junctions and to those between the components of the system. An edge allocated a "1" shows the variables are directly proportional; similarly, a "-1" shows the two variables are inversely proportional. A graph edge assigned an "=" indicates that the two variables linked by this edge are equal in value [6]. They have applied the TCG fault detection procedure into different experiments for the monitoring of two-tank, three-tank, and the secondary sodium cooling loop. Their results were feasible.

Another BG study for fault detection in a cooling system has been produced by [78]. It was based on TCG. Their emphasis was on unknown faults. Their results were evaluated with an experimental study.

The TRANSCEND [97] system is a combination of quantitative and qualitative fault diagnosis approaches. It used BG for the quantitative state-equation based on an observer model and the TCG. It first derived the qualitative fault residual then used a quantitative fault isolation observer. An experiment was performed based on a three-tank system and stated that the proposed methodology was effective for monitoring the three-tank system. However, they did not apply this methodology to more complex systems. A bond graph-based fault detection has

been developed by Lo et al. [98]. It is based on hypothesis variables and the construction of the causal links between these variable from the qualitative equations. Their simulation result on the single and double tanks was feasible. Mekki et al. [99] have also proposed using BG fault diagnosis, combining qualitative and quantitative diagnosis approaches. The qualitative method was based on the temporal causal graph, and the quantitative method was a global analytical redundancy interaction acquired using a BG. Their findings indicated that the qualitative diagnostic approach was quicker and could overcome the problems associated with the quantitative approach, such as convergence and accuracy when dealing with complex and non-linear systems.

3.5. Qualitative Simulation for the Diagnostic of AC Induction Motor

ACIMs used in power conversion systems need to be monitored due to their importance in production processes, where a sudden shut-down can lead to severe economic losses. Many quantitative techniques have been used to diagnose ACIM faults, but this can be a complex process in terms of assessing the many parameters of the machine. In this type of system, [100] claim that QS methods can achieve better detection and diagnosis than quantitative methods. Quantitative methods require continuous accurate monitoring, and some of the parameters not necessarily associated with the presence of a fault may change over time, e.g., load and speed in electrical machines.

SDG is a QS method that has been used widely, especially for fault detection in industrial processes, but limits on diagnosis resolution make the SDG insufficient for fault diagnosis. Using qualitative reasoning equations and qualitative semantic reasoning that link the dynamics of machines as causes and effects can play a crucial role in system diagnostics. Qualitative BG modelling has been reported in the literature as used for fault detection. BG modelling can present a crucial cause and effect analysis for system conditions. Therefore, this research proposes to use BG and qualitative reasoning equations to represent the behaviour of a dynamic system to derive a QS approach for induction motor CM. This research plans to use a quantitative BG model and qualitative BG based on a temporal causal graph (TCG) and qualitative equations to detect the electrical faults (broken rotor bar and stator winding imbalance) in an AC induction motor.

3.6. Summary

This chapter presented general information on qualitative simulation approaches. Then it gave a brief review of qualitative simulation methods. Next, it introduced the qualitative bond graph fault detection approaches. Further, it described the proposed qualitative bond graph approach that will be based on the temporal causal graph and qualitative equations.

Chapter 4 AC Induction Motor Construction and Working Principles

The squirrel-cage induction motor is a common type of induction machine that employed widely in various industrial applications and will be the basis of this study. This chapter provides a description of the squirrel-cage AC induction motor with details of its construction, working principle, and failure modes. Finally, it gives an overview of the relation between motor specification and failure mechanism.

4.1. Introduction

An induction machine transfers mechanical energy from electrical energy. They are vital machines in a huge number of power conversion systems because they have a number of important advantages, such as low capital cost, reliable with low maintenance costs (its construction is not complicated), relatively efficient, long life span and a premium energy efficiency [1, 2].

4.2. AC Induction Motor Construction

The construction of induction motors involves of two main parts namely the stator, and a rotor fixed on bearings. A narrow air gap separates the stator and rotor. There are two different types of rotors namely, the squirrel cage and wound. This study considers only the squirrel type since that is the rotor in the test motor being used. *Figure 4-1* shows the typical structure of the three-phase AC Induction Motor. A photograph of an exposed ACIM is shown in Figure 4-2. The alternating current is supplied to the stator and passes to the rotor via induction. The magnetic circuits of the stator and rotor are illustrated in Figure 4-3. The winding of the phases are shifted from each other by 120 electric degrees around the air gap [101].
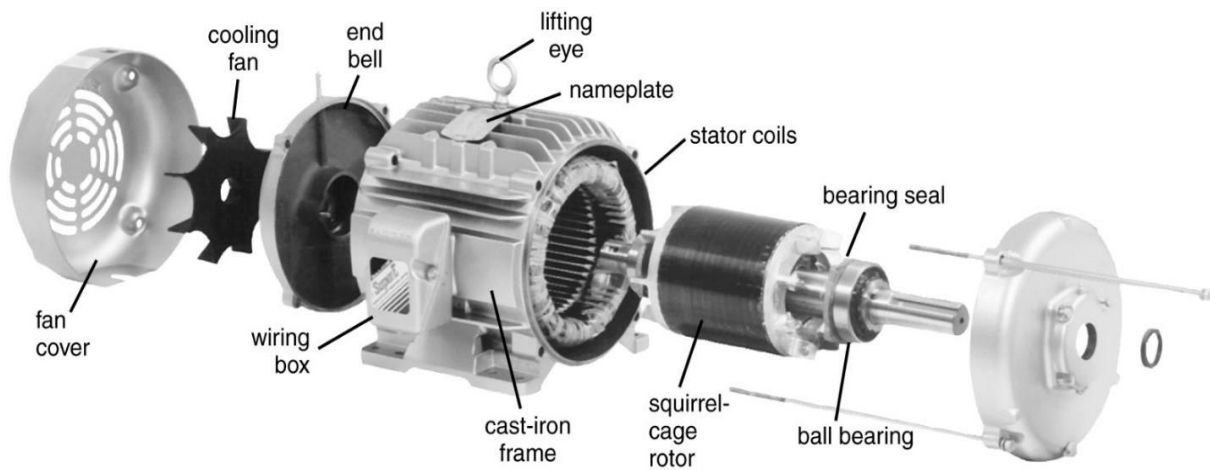
Figure 4-1 Representation of the typical structure of AC induction motor [102]
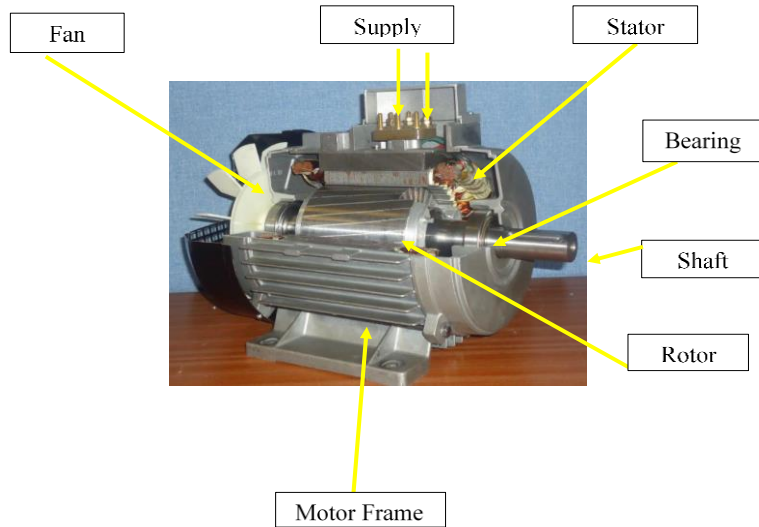
Figure 4-2 photograph of ACIM construction
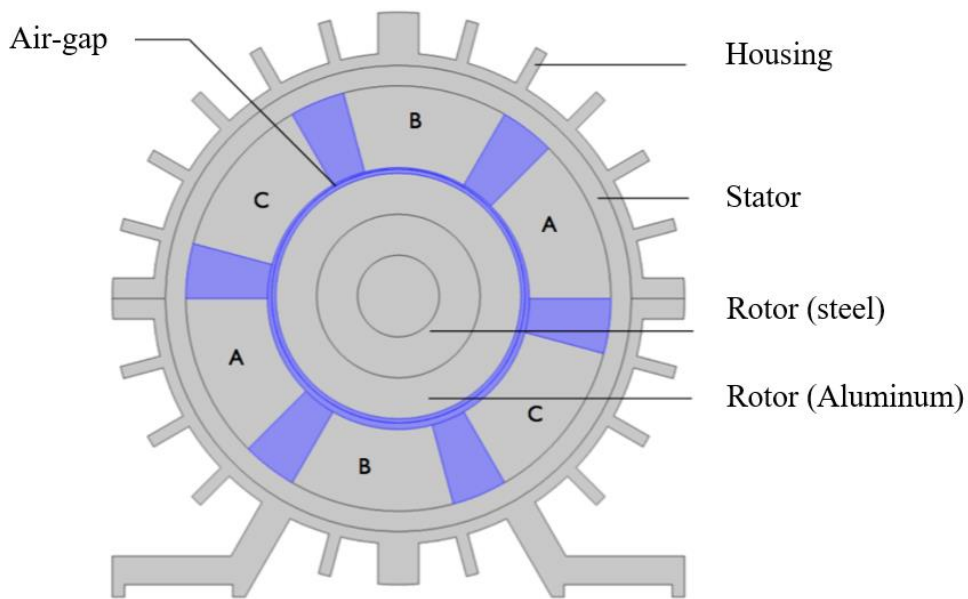
Figure 4-3 Magnetic circuit of stator and rotor of ACIM amended from [103]

4.2.1. Stator

As indicated by its name, the stator is the stationary part of the induction motor. A three-phase electrical supply is given to the stator of the induction motor. The stator is made up of three parts namely, frame, laminated core, and three-phase windings coupled in star or delta arrangement [104]. The laminated core is punched and clamped together to form a hollow cylinder (stator core) with slots, as shown in Figure 4-4.
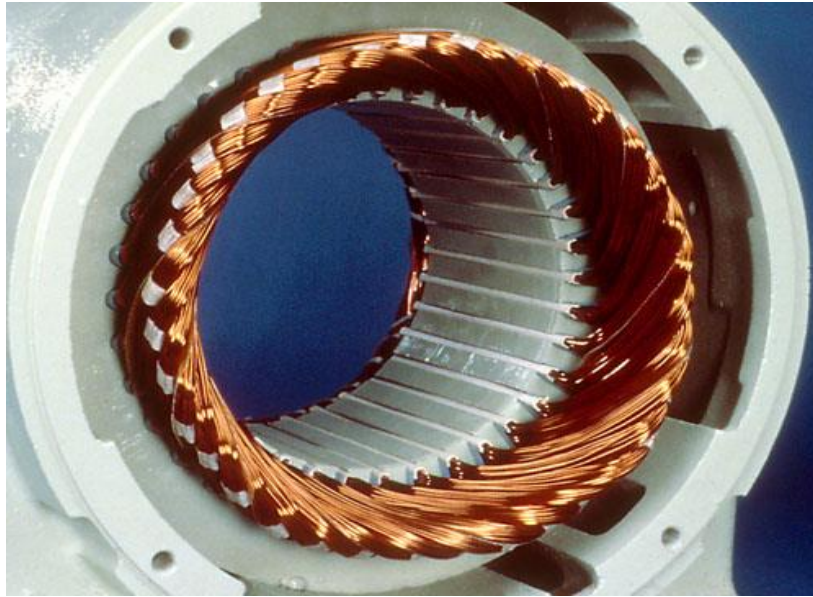
Figure 4-4 Stator of three phase induction motor

4.2.2. Rotor

The rotor is the moving (rotating) part of the induction motor. As shown in Figure 4-5, the motor comprises a squirrel cage rotor made up of copper or aluminium bars with end rings, which act as short circuits. For small-sized motors, the bars are usually made from aluminium, and copper is used for greater power motors. The mechanical load is connected to the rotor via a central shaft.
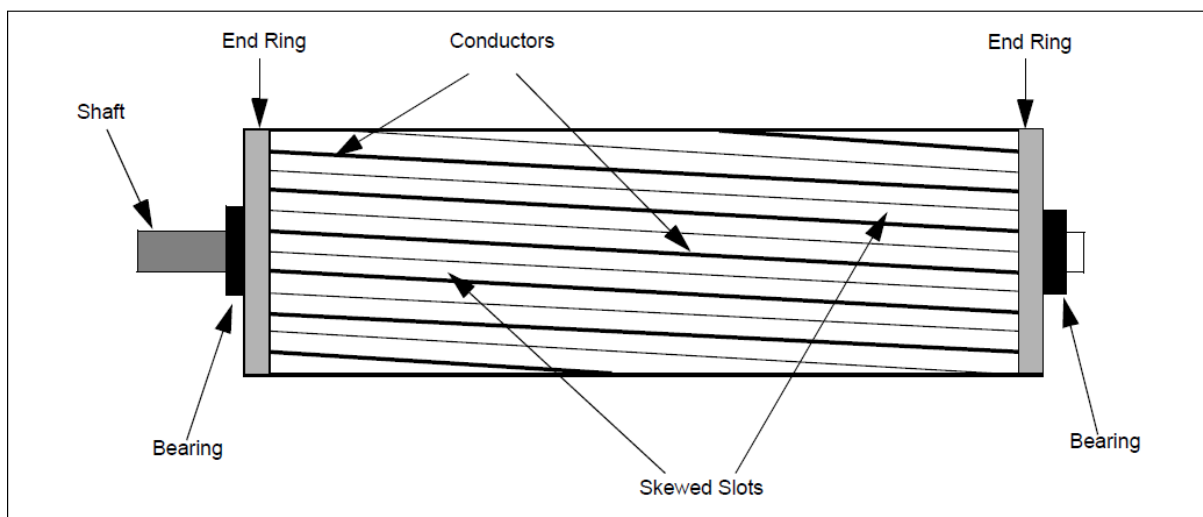
Figure 4-5 The rotor of induction motor [105]

4.2.3. Other AC Motors Parts

As presented in Figure 4-1, the ACIM construction includes more than just rotor and stator. There are other parts, including a fan, bearings, cover, and various spring washers and screws.

4.3. Operating of AC Induction Motor

Faraday's laws determine the action of 3-phase ACIMs; see Equation (4-1). A three-phase alternating stator current, with each phase in the windings displaced from the others by a phase difference of 120º, see Figure 4-6, and induce an Electromagnetic Force (EMF) in the rotor. The result is an interaction between the generated electromagnets which results in a rotating torque with the motor rotating in the direction of the torque.

$$EMf = N\frac{\Delta\Psi}{\Delta t}$$ (4-1)

Where N is the number of turns and Ψ is the Magnetic flux
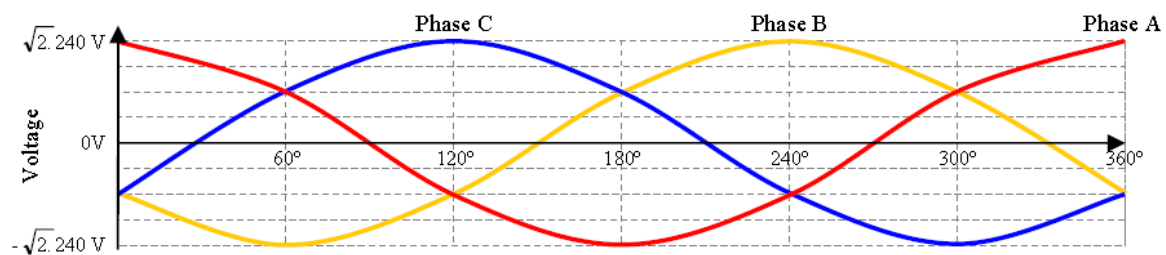
Figure 4-6 Depiction of three phase power supply [106]

4.3.1. Motor Speed

The synchronous speed of the ACIM is the speed that the magnetic field rotates. The motor's synchronous speed is dependent on the number of poles in the motor and the electrical supply frequency as in Equation (4-2) [107] .

$$S_s = \frac{120f_s}{p1}$$ (4-2)

S_s = synchronous speed, Hz

f_s = frequency of the power supply, Hz

p1 = number of poles

The slip S, commonly presented as a percentage, is stated for being among the most advantages of ACIM, which is the speed difference between the rotor S_r and magnetic field speed (synchronous speed) S_s see Equation (4-3). It is one of the significant features of ACIMs, and

it based on the size of the machine. In motor operations, the slip is usually in the range 10 to 3% [108]

$$S = \frac{S_s - S_r}{S_s} * 100 \tag{4-3}$$

Where S is slip, S_s is motor synchronous speed, and S_r is actual rotor speed.

4.3.2. Motor Torque and Load Principle

The torque produced by the ACIMs changes considerably with motor speed, from a relatively low value at start-up to a maximum at about 80% of S_s, see Figure 4-7.

At the start-up of the ACIM, the current through the rotor is at its maximum, and is commonly termed "the Locked Rotor Current", which induces the similarly named "Locked Rotor Torque". As it accelerates, the rotor's speed increases, both the current and torque will change, with constant supply voltage the torque rapidly decreases to a most low referred to as "Pull-up torque" which is about 20% of Ss. With further increase in rotor speed, at about 80% of the mechanical speed the torque gets to its highest value, denoted as the "Pull-out torque". Under no-load conditions, as the rotor speed nears its rated speed, current and torque drop dramatically [1, 63].
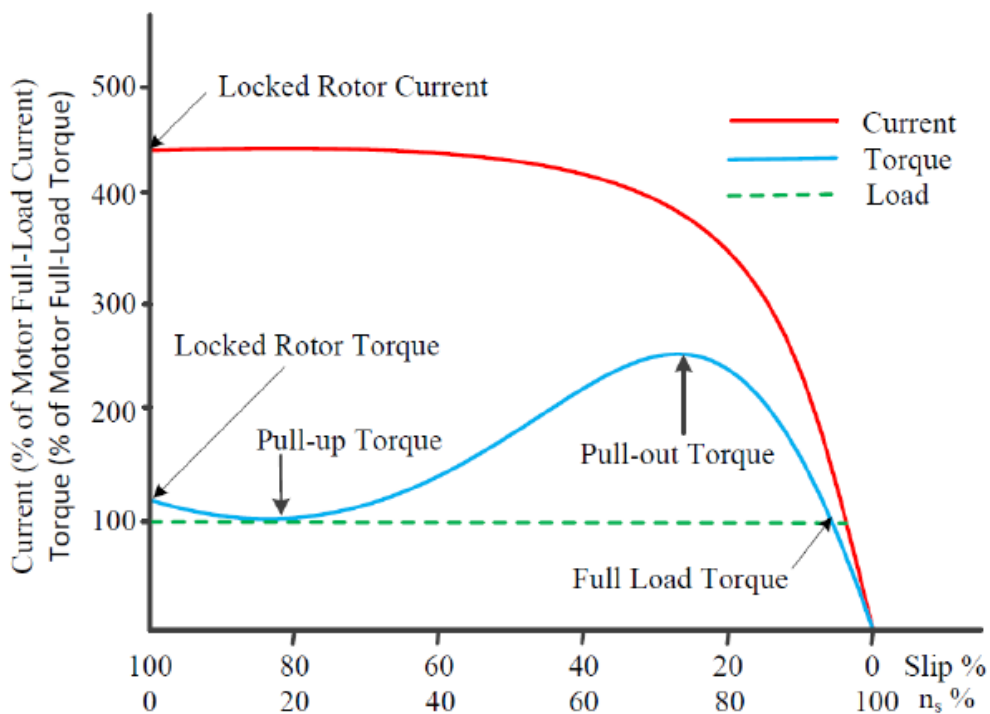
Figure 4-7 Torque-speed curve of ACIMs [63]

4.4. Induction Motor Failure Modes

Induction motors are symmetrical machines, and any fault will change their symmetrical properties. They are subjected to several modes of failures, which can be categorized as follows [11, 77, 109]:

1- Electrical faults such as open or short circuits of the stator winding, wrong connections of the windings, high resistance contact to the conductor, broken rotor bars, and cracked end-rings.

2- Mechanical faults such as a bent shaft, bearing failure, misalignment, and air gap irregularity.
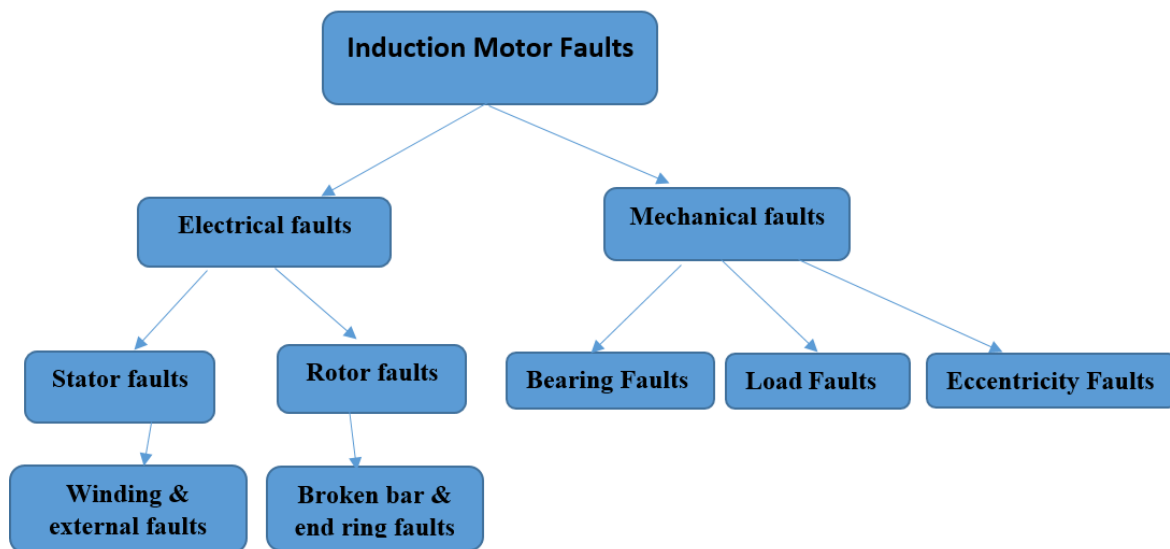
Figure 4-8 The categorisation of induction machine faults [109]

A classification of induction motor faults is shown in Figure 4-8. The relative percentages of ACIMs faults are illustrated in Figure 4-9. Based on the Electric Power Research Institute (EPRI) survey and [110], almost 40% of ACIM failures are related to bearings fault, and 38% are due to a stator fault, 10% are due to rotor faults, and 12% are related to other types of faults.
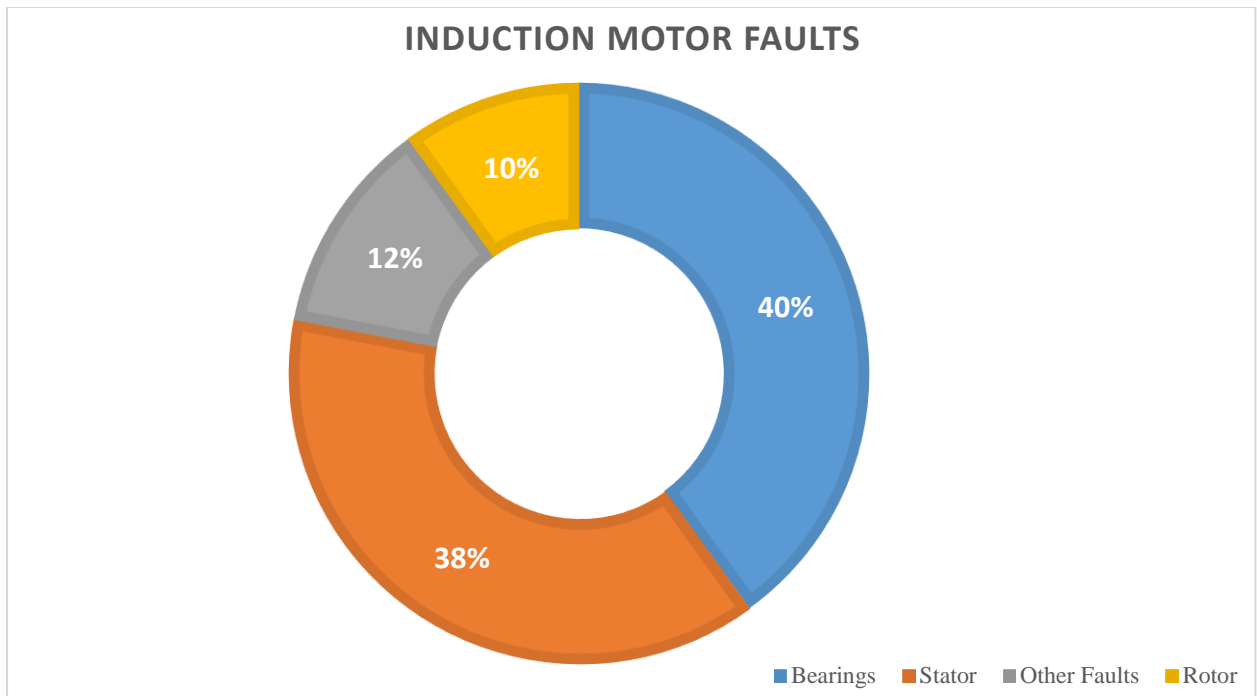
Figure 4-9 Represents the percentages of induction motor faults

These faults could cause one or more of the following symptoms: [63, 111, 112]:

- Unbalanced voltages and line currents,
- Increased losses and efficiency reduction,
- Reduced average torque,
- Incremented torque pulses,
- High degrees of heating, and
- Unbalanced air-gap eccentricity.

4.4.1. Rotor Faults

A broken rotor bar is one of the most prevalent induction motor faults that leads to a sudden drop in efficiency, or even an unexpected failure. Studies [45, 113] have indicated that the most common reason for a BRB faults is high starting current, heating the bars and causing thermal stress as well as mechanical and environmental stresses.

A BRB leads to asymmetric behaviour resulting in an unstable air gap and unstable current. A BRB causes a critical lowering of the efficiency of the induction motor and can significantly shorten its working life. Figure 4-10 shows a depiction of the current flows through the rotor of a healthy motor and with a rotor with two broken bars. With a BRB, the current that would

have travelled through the broken bar will now be diverted through the adjacent bars and cause unbalance in the rotor's magnetic flux [114].

(a)

(b)
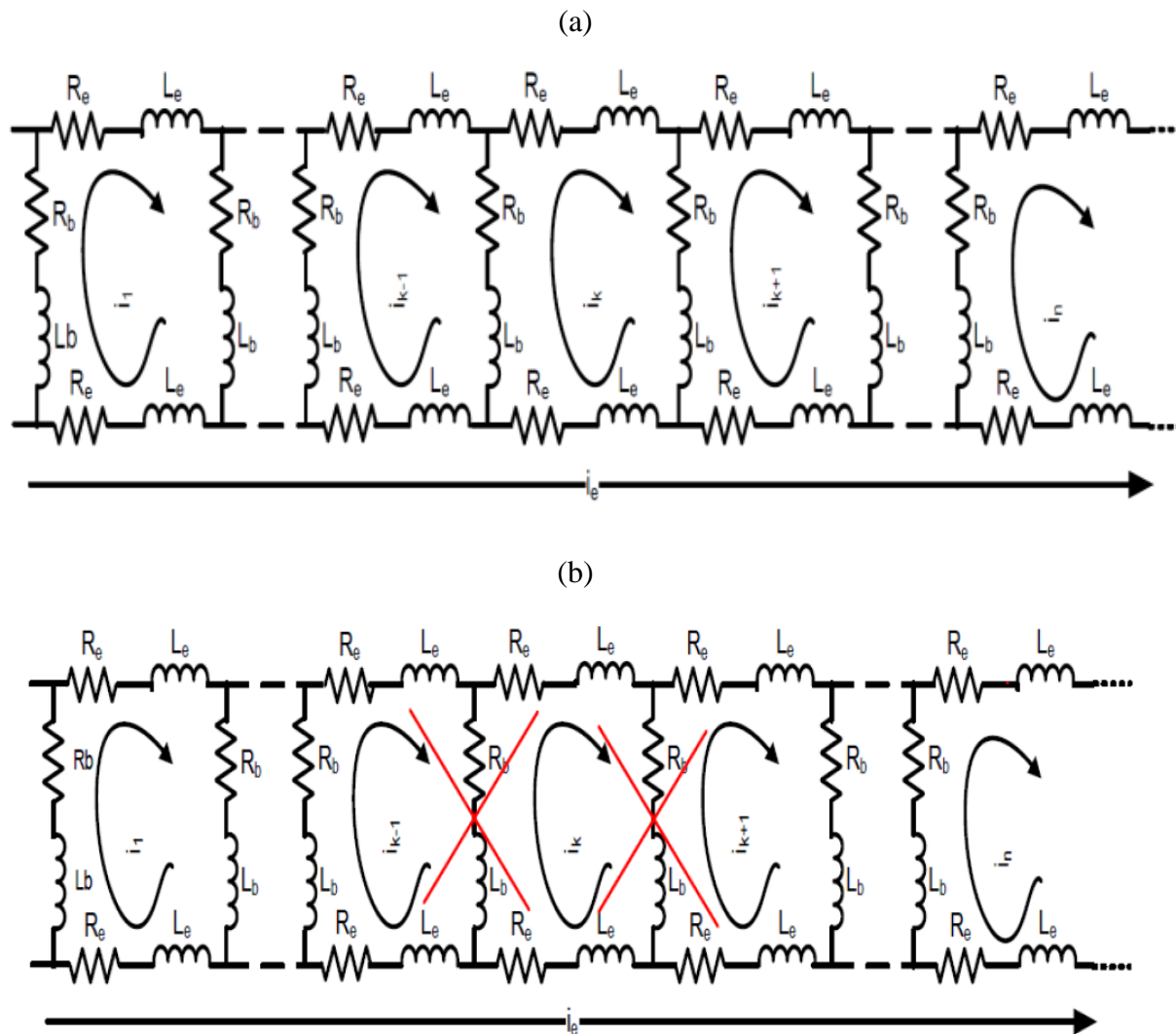
Figure 4-10 Depiction of current flow through the rotor of (a) healthy motor, (b) motor with two broken bars[63]

The diverted current hastens consequent breakdowns in adjoining rotor bars [45]. The motor is considered to be in failure mode when the fault severity is higher than about a third of the rotor bars [56]. A BRB increases the electrical resistance of the rotor [115], and introduces into the stator current frequency components at $2sf_s$ around the supply frequency. BRBs are identified by these characteristic frequencies, which are given by [113]:

$$f_{brb} = (1 \pm 2ks)f_s \tag{4-4}$$

Where, s is the slip, f_s, f_{brb} are the supply frequency and broken rotor bar frequency, Hz, and k is a harmonic integer, $k = 1,2,3, \ldots n$

Actually, the left-hand sideband $(1 - 2s)f_s$ component is affected by rotor asymmetry at $2sf_s$ directly. The right-hand sideband $(1 + 2s)f_s$ component is caused by the speed ripple due to the machine load inertia rate [116].

As the BRB fault develops it has a significant effect on motor dynamics and a corresponding effect on the mathematical model that describes the system behaviour.

4.4.2. Stator Winding Asymmetry

The ACIM is built so that the three phases of the stator are balanced. Any asymmetry or lack of equivalence of stator winding and supply impedances will result in the stator winding producing a so-called "backward rotating field" [110]. A slight change of stator winding resistance will cause an imbalance in the machine. That leads to an increase in the stator winding temperature and it may lead to damage of the machine. Therefore early detection of stator windings asymmetry could avoid subsequent damage, decreasing maintenance costs and motor downtime [117]. Many reasons exist for the occurrence of imbalance stator faults, including unequal line voltage of the AC motor, power factors, and windings faults [112, 118].

It has been stated that a good indicator of stator imbalance is the harmonic frequency component at $3f_s$ in the stator current spectrum [119-122]. An imbalance in the stator winding induces a component in the spectrum of the ACIM current at these frequencies [123] as in equation (4-5).

$$f_{IMs} = (1 + 2n)f_s \tag{4-5}$$

Where n is the order of the harmonic: n=1, 2, 3…

f_{IMs} : stator imbalnce frequency, Hz.

f_s : Fundamental frequency of supply, Hz.

4.4.3. Stator Faults

Stator faults are usually caused by insulation failure between two adjacent turns in a coil. An additional current will be produced when an asymmetric stator winding fault has occurred, which will generate an additional MMF across the air-gap. Stator asymmetry could happen due to a short circuit that causes a significant decrease of winding resistance or an open circuit fault that caused an increase of winding resistance. As shown in Figure 4-11, stator faults are commonly categorized as: open circuit, turn-to-turn, phase to phase and phase to ground shorts.
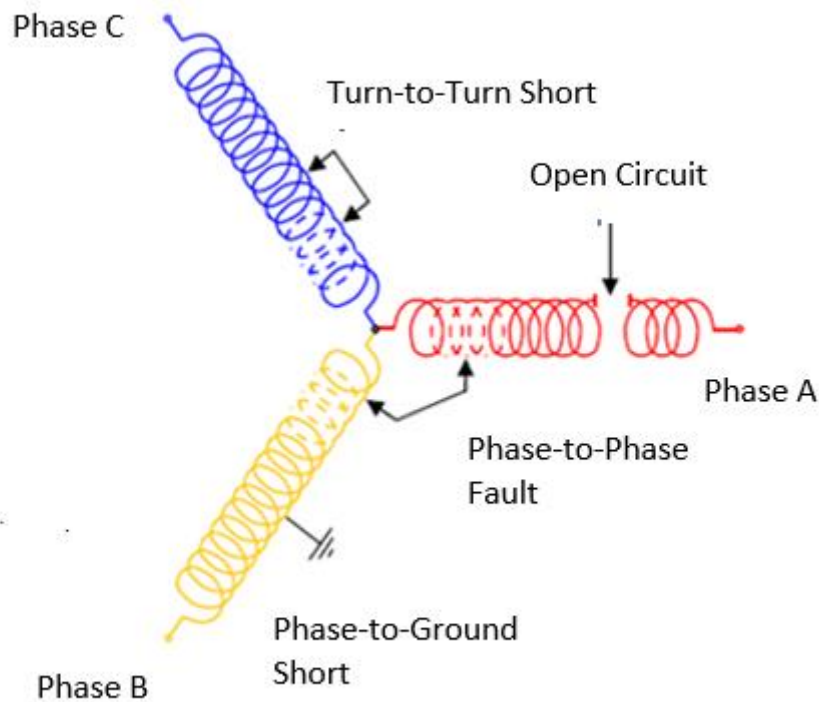
Figure 4-11 Common stator winding faults amended from [63]

According to [124] Stator faults occur because of the reducing of insulation due to:

- High temperatures in the stator core or in the windings.

- Magnetic effects caused by electromagnetic forces, magnetic asymmetries, electromagnetic noise and vibration.

- Core laminations and loose joints.

- Contamination due to oil, moisture, and dirt.

- Leakage in cooling systems.

- Electrical discharges.

Studies [124, 125] indicated that stator short circuit faults create asymmetry motor impedance and flux waveforms that lead to unbalanced phase currents with an unbalanced air gap flux. Subsequently, the defects caused by these faults are related to the changes in stator winding's resistance and inductance. The number of stator windings will decrease on the effected stator phase. Stator short circuit causes overheating in the stator winding, and this could cause the motor to fail in a very short time [119, 126].

In the literature, various kinds of signals have been utilized as a sign of stator fault detection. These signals include magnetic flux, vibration, and stator current.

4.4.4. Bearings Faults

Bearings are system components used to reduce friction between moving parts. In an ACIM, the bearings will also maintain the air gap and support the shaft to transfer the electro-motive force as a rotational force. A depiction of bearing components is shown in Figure 4-12. In general, bearing failures occur due to wear, a situation that can lead to an increase in vibration and noise levels. Bearings can be damaged by other causes such as:

• Pollution and corrosion are caused by pitting and interaction with hard particles such as grit and abrasive liquids such as acids or water.

• Inadequate lubrication.

• Improper installation of the bearings (when incorrectly forcing the bearings into position) or cracks in the bearing surfaces in contact with the shaft or housing.

Bearing faults could be categorized into four different kinds [45]: ball element, inner race, outer race, and cage. These faults are not addressed in this research.
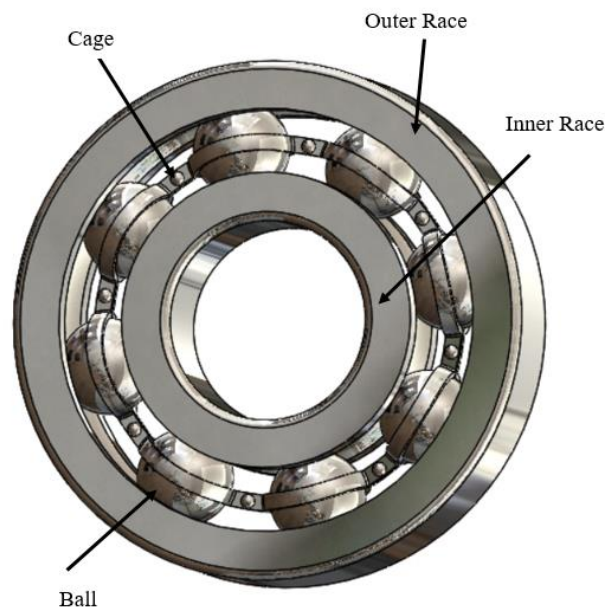
Figure 4-12 Components of Roller Bearing amended from [127]

4.4.5. Other Types of ACIM Faults

Another type of fault is air-gap eccentricity, an irregular air gap between a stator and a rotor. These irregularities may occur because of shaft deflection, stator movement, bearing wear, etc. As shown in Figure 4-13, the presence of air gap eccentricity produces an unbalanced magnetic pull (an unbalanced radial force), which leads to damage to the stator windings and stator core. There are two types of eccentricities:

 a) Static eccentricities,

 b) Dynamic eccentricities

• The static eccentricity originates by incorrect positioning of the rotor with respect to the stator. The static eccentricity of the air gap means that the position of the length of the minimum radial air gap is fixed in space. With dynamic eccentricity, or misalignment, the centre of rotation and centre of symmetry of the rotor do not coincide, the result is that the location of the minimum air gap also rotates. Such eccentricity can be the result of numerous factors including a bent rotor shaft or asymmetrically worn bearings. Such mechanical faults would also be likely to induce resonances at certain critical speeds.
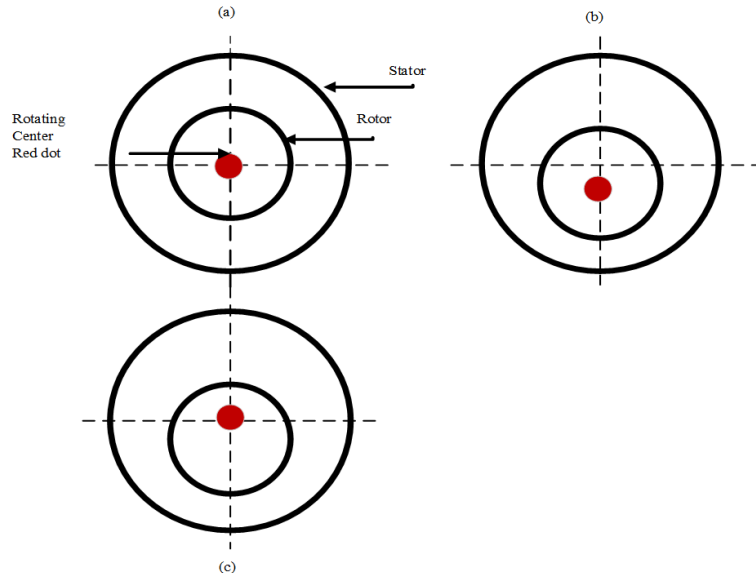
Figure 4-13 Displays air-gap eccentricity conditions (a) healthy air gab (b) static eccentricity, (c) dynamic eccentricity [45]

4.5. Relation between Motor Specification and Failure Mechanism

Inappropriate specifications lead to different ACIM malfunctions. Motors are electromechanical systems, so the motor specification should take into consideration both the electrical and mechanical conditions and the working environments of the motors. Table 4-1 presents how some of these working conditions can affect the monitored parameters.

Table 4-1 Effect of machine specification on failures

Mechanical conditions	Electric conditions	Environment conditions
Loading conditions can lead to different failures such as • Overloading can cause over-heating and bearing failure. • An oscillating load could lead to bearing damage; • Vibrations transmitted to the machine can lead to bearing failure.	Motor malfunction could be a consequence of the electrical power characteristic or the load feeding into the motor. These can be categorised as [128]: • Slow fluctuations of voltage can cause losses of power. • Rapid fluctuations of voltage can cause failure in the insulation.	Regarding environmental conditions, a malfunction could be a result of the operation itself, and the way in which the motor is being utilized. Among the main such problems are [128]: • High temperatures can lead to insulation damage. • Ingress of moisture and pollutants can lead to the generation of faults.

It is clear that the malfunctions in electro-mechanical systems depend not only on the type of the machine but also on the working environment. It is important to realise that motor faults invariably begin life as incipient faults and gradually grow from an initial defect to a real malfunction. The occurrence of a fault is associated with many different factors, but usually, there is an early indication of its existences, and it is exactly these initial indications that a good predictive maintenance scheme must detect and diagnose [128].

4.6. Summary

This chapter has given a general introduction to AC induction motors, including ACIM construction, operating principles, common faults, and the effects of these faults on the motor operations. It gives more details on a broken rotor bar and stator imbalance faults, which will be addressed in this research. It concludes with the relation between motor specifications and their failure.

Chapter 5 Bond Graphs: Modelling and Principles

This chapter presents a description of the proposed fault detection approaches, which are based on bond graph modelling. It starts with a brief introduction to BG modelling techniques, including BG principles, variables, and standard elements. Next, it presents a general explanation of the causality concept. Then, it gives an electrical circuit example that shows how to build a bond graph model and generate equations from it. Subsequently, it provides a brief review of some BG fault detection procedures. Next, it introduces the proposed BG model of the ACIM. Finally, it describes the proposed qualitative simulation approach.

5.1. Introduction

The BG is a pictorial representation of how power is exchanged between system elements and is a powerful and relatively simple modelling technique. A BG graphical representation of a dynamic physical system allows the complicated energy flows in a physical system to be determined and has been shown to be an effective means of fault diagnosis. The task of modelling complex systems becomes easier when using BG methodology because BGs offer a graphical interface, applying an energy analysis instead of examining the relations between forces and torques [129]. BG provides a unified modelling tool appropriate to all the physical domains, including electrical, mechanical, and hydraulic, found in machines. BG modelling was presented by Henry Paynter [130] and extended by Karnopp and Rosenberg [131]. The idea behind the BG approach begins with the interaction of energy flows between the components of the modelled system in a graphical form, and then simulated using specialist software such as 20-SIM [132], Camp-G [133], and SYMBOLS [134].

BG works as a mediator between the physical system and the analytical models describing it [135]. In BG modelling, the systems are modelled as a set of elements that exchange energy in a power-conserving way. BG or link graph builds a model based on cause and effect on energy and energy exchange. A BG model could be progressed by graphically including additional components such as inertial and resistive effects, without the need to restart the process. The causality relations enable the modeler to perform the algorithmic level of modelling a system. Moreover, the causality of the BG can be readily utilized for use in control systems. The BG approach comprises the building of a behavioural model and structural and causal analysis that is usually necessary to build control and monitoring systems [9].

Three-level of modelling are often presented when utilizing BG models:

1. The physical level. In this stage the physical phenomena are presented by the BG components (storage, resistive, etc.). At this stage, the BG is utilized as a common language for all the different fields of physics.
2. Mathematical level. In this stage, the system behaviour is represented using the constitutive equations of BG elements and constraints.
3. Algorithmic level. This stage shows how the dynamic model is calculated, which is based on the causality assignment procedure.

BG modelling has several advantages which can be summarized as [9]:

- BG is a specific language suitable for all physical domains.
- BG modelling represents the cause and effect relations (causality) in the model.
- A BG model can be amended for development by adding elements.
- It is suitable for analysing a system's structural properties.
- BG provides a visual representation of the system.

BG models present a graphical structure for analyzing dynamic system behaviour. This structure [136] can be utilized to generate:

1- Constraints among locally related variables from the causal links associated with the bond of the graph.
2- Temporal relations from the analytic models of system behaviour.
3- Steady state behaviour.

Although the most accurate process for constructing BG models of engineering systems varies between different domains, generally, to develop a system BG model the processes are as follows [95]:

- Determine the distinguished variables of the domain. For instance, these variables in electrical and mechanical domains would be the effort (voltage) and the flow (speed), respectively.
- Set up a junction connection for the variables, i.e. the common effort (a 0-junction) or the common flow (a 1-junction).
- Generate bonds from the junctions into the storage elements (I-elements and C-elements)
- Link the junctions to each other, adding R-elements in those cases where the system has dissipative elements.
- Define the source of the effort and flow and link it to the appropriate junctions.
- Specify the bond's direction (causality).
- Simplify the graph whenever it is possible; for example, replace 0-/1- junctions with simple bonds.

5.2. Bond Graph Modelling

Usually, a BG is founded on two parameters: flow (f) and energy (e), which are taken to be independent of each other. The product, $e*f$ of these parameters is a measure of the instantaneous energy flow [137, 138]:

$$p(t) = e(t)f(t) \tag{5-1}$$

The variables are different physical quantities in different domains. The effort and flow variables can be voltage and current in the electric domain, force, and velocity in the mechanical domain. Table 5-1 shows the variables representing effort and flow for the main physical domains.

Table 5-1 Effort and flow variables in the major physical domains (amended from [139, 140])

Domain	Effort, e(t)	Flow, f(t)
Electric	Voltage	Current
Mechanical Translation	Force	Velocity
Mechanical Rotation	Torque	Angular Velocity
Hydraulic	Pressure	Volume flow rate
Thermal	Temperature	Entropy flow

The effort is placed either above or on the left of the bond line, the flow is placed either under or on the right of bond line, see Figure 5-1.
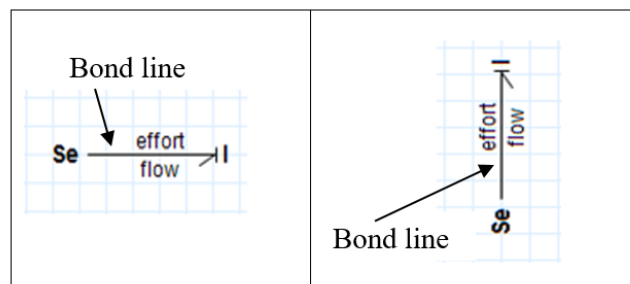
Figure 5-1 Representation of the effort and flow on the bond line

Interaction between effort and flow variables, and their mathematical relations are summarized in Figure 5-2.
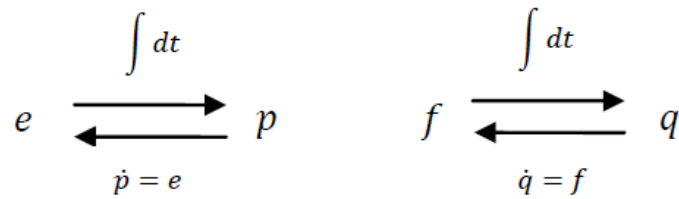
Figure 5-2 Association between effort and flow variables

5.3. Energy Variables

There are two types of physical quantum (energy variables) utilized in BG modelling, namely momentum $P(t)$ and displacement $q(t)$) used to represent a dynamic system. These are acquired by the integration of the power variables with respect to time as in the following equations [9]:

$$P(t) = \int_{-\infty}^{t} e(t)dt \tag{5-2}$$

$$q(t) = \int_{-\infty}^{t} f(t)dt \tag{5-3}$$

5.4. Standard Bond Graphs Elements

Elements in BGs represent the dynamic behaviour of the system, and they are the components of the modelled system. According to the number of bonds, there are three common categories of BG elements, namely, one port, two ports and multiport [91]. A depiction of BG elements, symbols, causality and equations, are shown in Table 5-2.

5.4.1. One Port Active Elements

One port elements interchange energy with the system via a single bond. Sources and passive elements are one port elements: energy sources are items that provide a unique type of power, and the energy flow starts when the device is connected to a system. A BG can only command energy and flow factors [141]. Given that energy sources can provide only one type of energy to the system, they are single ports. A BG has two active source elements: effort source and flow source.

5.4.1.1. Effort Source

An effort source (Se) is an energy resource that provides the system with a precise effort level (e). The effort source is denoted, utilizing a half arrow that is directed out from the source symbol[9]. Figure 5-3 represents the effort source. See Table 5-2 for more details.

$$Se \xrightarrow[f]{e}$$
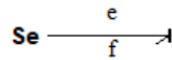
Figure 5-3 Representation of the effort source

5.4.1.2. Flow Source

A flow source (Sf) is an energy resource that offers a specific flow level, f, to the system. It also denoted utilizing a half arrow that is directed out from the flow source symbol [9]. Figure 5-4 represents the flow source. See Table 5-2 for more details.

$$Sf \vdash \xrightarrow[f]{e}$$
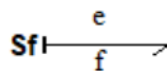
Figure 5-4 Representation of the flow source

5.4.1.3. Modulated Sources

Besides the typical effort and flow sources, BG modelling enables the usage of modulated sources. These modulated sources are controlled by a signal and represented by MSe or MSf, where M represents modulation. The modulated sources have a fixed causality, as shown in Figure 5-5.

$$\text{Effort} \quad \textbf{MSe} \xrightarrow[f]{e}$$
$$\text{Flow} \quad \textbf{MSf} \vdash \xrightarrow[f]{e}$$
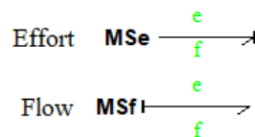
Figure 5-5 Representation of effort modulated source and flow modulated source

5.4.2. One Port Passive Elements

In BGs, there are three different types of passive elements, resistor R, capacitor C and inertia or inductor I. These are known as "passive elements because they transform the received power into dissipated power (R-elements), store power of potential energy (C- elements) or kinetic energy (I-elements)" [68].

5.4.2.1. Resistive R-elements

The resistive, R-elements, are derived from electrical resistances and have a functional relation between the effort and the flow as [142]:

$$e = Rf \qquad\qquad 5\text{-}4)$$

$$F = R^{-1}e \qquad\qquad (5\text{-}5)$$

5.4.2.2. Capacitor C-elements

The C-elements transform the received power into (potential stored) energy without loss. In BGs, C-elements could be a frictionless spring of an electrical capacitor with no resistance. C-elements have integral causality is as shown in Equation (5-6), and derivative causality is as shown in Equation (5-7)

$$e = c \int f dt \qquad\qquad (5\text{-}6)$$

$$f = \frac{d}{dt}(c^{-1}e) \qquad\qquad 5\text{-}7)$$

5.4.2.3. Indicator I-elements

I-elements store the received power as kinetic energy. It represents the electrical inductance or mechanical mass. It is the product of flow and integral of effort, as in Equation (5-8), see Table 5-2 for more details.

$$f = \frac{1}{I} \int e \, dt \qquad\qquad (5\text{-}8)$$

C-elements and I-elements are known as storage elements.

5.4.3. Two Port Elements

Two ports elements possess two-fold bonds for energy interchange with the system, which are the transformer (TF), and gyrator (GY). These receive energy in one port, convert it to another form, and transfer it to the output port, see Table 5-2 for BG elements, causality, equations, and rules.

5.4.3.1. Transformer

The TF-element links the inlet and outlet effort, and inlet and outlet flow as in Equation (5-8).

$$\begin{cases} e1 = m\,e2 \\ f2 = m\,f1 \end{cases} \qquad\qquad (5\text{-}9)$$

5.4.3.2. The Gyrator

The (GY) associates the effort of one port with the other port's flow and vice versa. The mathematical expression of GY is shown in Equation (5-10), where a constant is:

$$\begin{cases} e1 = rf2 \\ e2 = rf1 \end{cases} \qquad (5\text{-}10)$$

For instance, electric motors and centrifugal pumps can be modelled in BG using GY elements. On the other hand electrical transformers and mechanical gear boxes may be modelled by a TF element [143].

5.4.4. Multiport

There are two sorts of BG junctions that are used to connect BG elements, namely parallel (or 0-junction) and serial (or 1-junction).

The parallel junction connects elements with the same efforts. The efforts are, equal as shown in Equation (5-11), and the flows add up to zero as in Equation (5-12).

$$e1 = e2 = e3 = e4 \qquad (5\text{-}11)$$
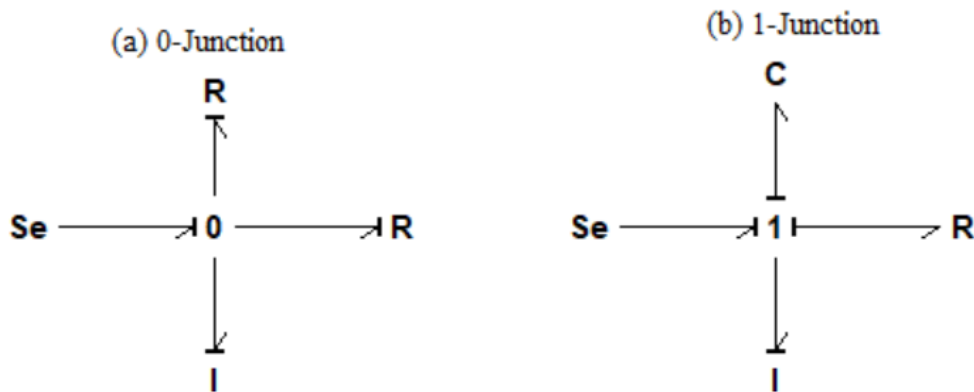
Figure 5-6 Representation of junctions connection and causality

(a) 0-junction, (b) 1-junction

$$F1 + F2 + F3 + F4 = 0 \qquad (5\text{-}12)$$
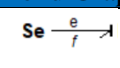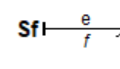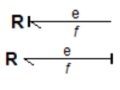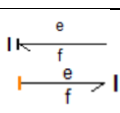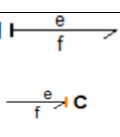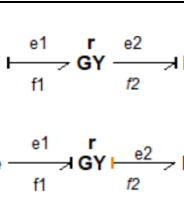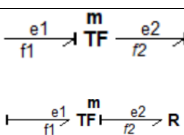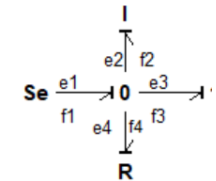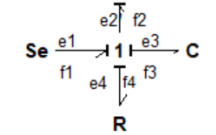
However, with the serial junction the efforts add up to zero, see Equation (5-13) and the flows are equal, see Equation (5-14).

$$e1 + e2 + e3 + e4 = 0 \qquad (5\text{-}13)$$

$$f1 = f2 = f3 = f4 \qquad (5\text{-}14)$$

In the serial-Junction (1- junction), one and only one bond has the flow information, which is should be the open end, known as the strong bond where other bonds must be stroked with the causality stroke. In the parallel-junction (0-junction), one bond only has the causality stroke nearer the parallel junction. It is the strong bond that decides the effort information to the junction. The BG representations of a 0-junction and 1-junction are shown in Figure 5-6.

Table 5-2 Common elements of BGs; causality, equations and rules (derived from [9, 144])

Element Name	Bond Graph	Causality Equation	Rules
Source of effort	$Se \xrightarrow[f]{e}$	e is known	Output of Se is an effort and it is input for the system. The causality is compulsory
Source of flow	$Sf \xrightarrow[f]{e}$	f is known	Output of Sf is a flow and it is an input for the system.
Resistor	$R \xleftarrow[f]{e}$ $R \xleftarrow[f]{e}$	$f = \dfrac{1}{R}\, e$ $e = Rf$	Conductance causality: Output is a flow. Resistance causality: the effort is an output.
Indicator	$I \xleftarrow[f]{e}$ $\xrightarrow[f]{e} I$	$f = \dfrac{1}{I}\int e\, dt$ $e = \dfrac{d}{dt}(I\,f)$	Integral causality: flow is an output. Derivative causality: effort is an output.
Capacitor	$\xrightarrow[f]{e} C$ $\xrightarrow[f]{e} C$	$e = c\int f dt$ $f = \dfrac{d}{dt}(c^{-1}e)$	Integral causality: effort is an output. Derivative causality: flow is an output.
Gyrator	$\xrightarrow[f1]{e1} GY \xrightarrow[f2]{e2} I$ $\xrightarrow[f1]{e1} GY \xleftarrow[f2]{e2} I$	$\begin{cases} e1 = rf2 \\ e2 = rf1 \end{cases}$ $\begin{cases} f2 = \dfrac{1}{r}\, e1 \\ f1 = \dfrac{1}{r}\, e2 \end{cases}$	Two efforts or flows are inputs. Two or no causality stroke near to the GY.
Transformer	$\xrightarrow[f1]{e1} TF \xrightarrow[f2]{e2}$ $\xrightarrow[f1]{e1} TF \xrightarrow[f2]{e2} R$	$\begin{cases} e2 = \dfrac{1}{m}\, e1 \\ f1 = \dfrac{1}{m}\, f2 \end{cases}$ $\begin{cases} e1 = m\, e2 \\ f2 = m\, f1 \end{cases}$	Only one effort and one flow are inputs. Only one stroke near to TF (the number of causality strokes near the TF must be only one)
0-junction	$Se \xrightarrow[f1]{e1} 0 \xrightarrow[f3]{e3}$ with e2/f2 in, e4/f4 out, R	$\begin{cases} e1 = e2 = e3 = e4 \\ f1 = f2 + f3 + f4 \end{cases}$	Only one bond has causal stroke near to the 0 junction. One effort is input – here it is e1.
1-junction	$Se \xrightarrow[f1]{e1} 1 \xrightarrow[f3]{e3} C$ with e2/f2 in, e4/f4 out, R	$\begin{cases} f1 = f2 = f3 = f4 \\ e1 = e2 + e3 + e4 \end{cases}$	Only one bond can have a causal stroke away from the 1-junction. The flow is equal for all bonds that linked with serial junction.

5.4.5. Fields

Besides the above basic elements, BGs have fields which are relevant for this research. This type of BG is known as a Vector Bond Graph [145] and has multidimensional bonds. Fields are used to model complex multidimensional systems [129]. Vector Bond Graphs have different fields including the I-field, C-field and IC-field which is relevant to this thesis. The effort vector can be considered as $e = [e_1, e_2, e_3 \ldots \ldots e_n]^T$, and an analogous flow can be identified as $f = [f_1, f_2, f_3 \ldots \ldots f_n]^T$ BG fields.

5.4.5.1. I-Field

The general form of the I-field is presented in Figure 5-7. The (I-field) stores the flow in the same manner as the basic I-element, but it has n-ports and n-state variables.

The state variables are $p_1 p_2 p_3 \ldots \ldots p_n$.
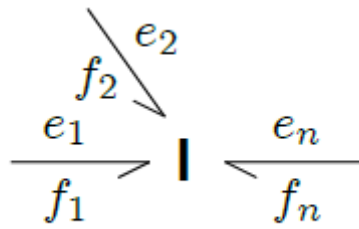
Figure 5-7 I-field port

An I-field relates a set of momentums to a set of flows as [146]:

$$
\begin{array}{llll}
\dot{p}_1 &=& e_1 & \qquad f_1 &=& \phi_1(p_1, \ldots, p_n) \\
\dot{p}_2 &=& e_2 & \qquad f_2 &=& \phi_2(p_1, \ldots, p_n) \\
&\vdots& & & \vdots & \\
\dot{p}_n &=& e_n & \qquad f_n &=& \phi_n(p_1, \ldots, p_n)
\end{array}
$$

(5-15)

Also it can be write as [68]:

$$
\begin{bmatrix} f_1 \\ f_2 \\ \vdots \\ \vdots \\ f_n \end{bmatrix} = \begin{bmatrix} m_{11} & m_{21} & \ldots & m_{1n} \\ m_{21} & m_{22} & \ldots & m_{2n} \\ \vdots & \vdots & \ldots & \vdots \\ \vdots & \vdots & \ldots & \vdots \\ m_{n1} & m_{n2} & \ldots & m_{nn} \end{bmatrix}^{-1} \cdot \begin{bmatrix} p_1 \\ p_2 \\ \vdots \\ \vdots \\ p_n \end{bmatrix}
$$

(5-16)

5.4.5.2. C- Field

A C-field, as in Figure 5-8, shows the stored energy E. There are n-ports in the C-field; if all ports are integral to the causality, this indicates that there are n state variables.
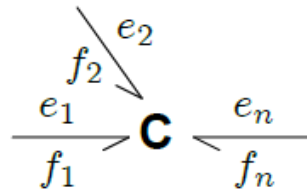
Figure 5-8 C-field port

The state variables are $q_1 q_2 q_3 \ldots \ldots q_n$. The associated set of displacements to a set of efforts is[146]:

$$
\begin{aligned}
\dot{q}_1 &= f_1 & e_1 &= \phi_1(q_1, \ldots, q_n) \\
\dot{q}_2 &= f_2 & e_2 &= \phi_2(q_1, \ldots, q_n) \\
&\vdots & &\vdots \\
\dot{q}_n &= f_n & e_n &= \phi_n(q_1, \ldots, q_n)
\end{aligned}
$$

$$(5\text{-}17)$$

5.4.5.3. IC- Field

The IC-field is a combination of I-and C- multiport, as illustrated in Figure 5-9. Usually, this arrangement is utilized to describe electromagnetic and mechanical systems [68].
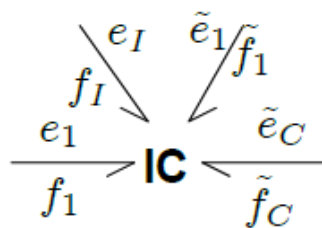
Figure 5-9 IC-field port

The constitutive relation for an IC-field associates a set of momentums to flows and associates a set of displacements to the efforts as[146]:

72

$$
\begin{array}{llll}
\dot{p}_1 & = & e_1 & f_1 & = & \phi_1(p_1,\ldots,p_I,q_1,\ldots,q_C) \\
& \vdots & & & \vdots & \\
\dot{p}_I & = & e_I & f_I & = & \phi_I(p_1,\ldots,p_I,q_1,\ldots,q_C) \\
\dot{q}_1 & = & \tilde{f}_1 & \tilde{e}_1 & = & \tilde{\phi}_1(p_1,\ldots,p_I,q_1,\ldots,q_C) \\
& \vdots & & & \vdots & \\
\dot{q}_C & = & \tilde{f}_C & \tilde{e}_C & = & \tilde{\phi}_I(p_1,\ldots,p_I,q_1,\ldots,q_C)
\end{array}
$$

$$(5\text{-}18)$$

5.5. BG Causality

In BGs, the bonds represent interactions between pairs of variables (flows and efforts) and their effects (or "causalities"). To represent the system components in a group of equations it is essential to create decisions reflecting cause-and-effect that algebraically express the associations between the relevant variables [141].

An important concept for BG theory is causality, where causality is the standard of which variables are independent and which are dependent. The causality is represented in a BG diagram by placing a stroke identified as a "causal stroke" as shown in Figure 5-10 . The half arrow on the end of a bond, see Table 5-2 and Figure 5-7, Figure 5-8, and Figure 5-9 show the positive direction of the bond's power. Figure 5-10 presents the causality strokes and the directions of effort and flow. The advantage of using causality is the ability to derive the equations and detect equation incoherence.
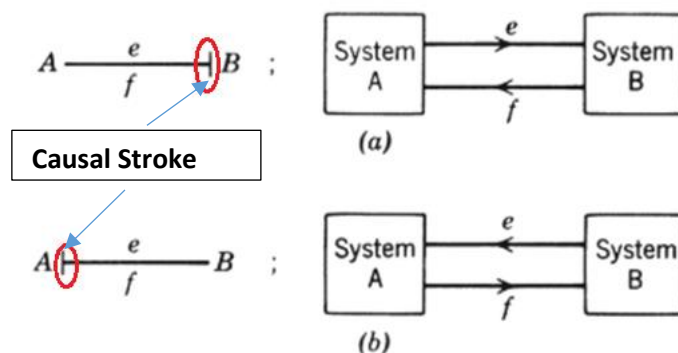
Figure 5-10 the causality stroke and the direction of effort/flow between the bond elements. (a) A represent the effort and B represent the flow. (b) B gives the effort and A gives the flow.

The effort source has only one causality. However, the resistance can take whatever value of causality that is assigned. In other words, given a voltage, the resistor will respond with a

current and vice versa. Also, I-elements and C-elements can have two causalities; integral causality where the input is integrated to produce the output, and derivative causality where the input is differentiated to produce the output.

5.5.1. Sequential Assignment Procedure

To be able to generate the equations from a BG model and to avoid inconsistencies, there are essential steps that should be followed in exact order:

First, the sources normally require one causality. Based on the given system, choose any source Se or Sf and allocate its causality. Then, straightway, extend the causal effects, using all of the 0- and 1-junctions, Transformers and Gyrators that may connect to the sources. These four elements are described as constraint components for the reason that only specific causal forms are possible [140]. Repeat this step until all effort (or, and) flow sources have been allocated their essential causality.

Second, select any storage elements (C or I) and allocate their preferred (integral) causality. Expand the causality effects using all 0-junctions, 1-junctions, TF, and GY constraints that apply, as illustrated in Table 5-2. Repeat this step till all storage elements (I/C elements) have been completely assigned their causality.

Third, select any resistance element R and assign it an arbitrary causality. Straightway extends the causal implications through the BG using constraint elements (0-junction, 1-junction, GY, and FT). Repeat this step until all R elements have been assigned a causality.

Fourth, choose any unassigned BG elements and assign causality based on causality constraints, utilizing the constraints elements, 0-junction, 1-junction, GY, and FT.

5.5.2. Temporal Causal Graphs

The temporal causal graph (TCG) was introduced by Mosterman and Biswas [6]. This is a distinctive form of causal graph, based on cause and effect relations, with efforts and flows as vertices and the relations between them as edges. When an edge is linked to system elements, it illustrates the relation between them so that for the simplest electrical circuit, i.e., a resistor with effort causality, the edge linking the effort and flow has the value of the resistance (R). The system's behaviour is modelled by the relationships allocated to control junctions and to those between the components of the system. An edge allocated a "1" shows the variables are

directly proportional; similarly, a "-1" shows the two variables are inversely proportional. A graph edge assigned an "=" indicates that the two variables linked by this edge are equal in value.

The TCG presentation has an identical structure for representing the magnitude and temporal constraints among system variables [147]. It can be used for the prediction of future behaviour in a state of system malfunction. TCGs are usually used either onwards or reverse directions from an observed or hypothesized fault (in a signal or a parameter). The reverse propagations are applied for generating a series of malfunctions; however, the onward propagation obtains predictions for subsequent behaviour corresponding to each of the hypothesized faults [9]. The qualitative values are just like the ones from the measured values, which is 0 for nominal, "+" for above nominal, and "-" for below nominal [147].

The TCG will be used in this thesis. This includes the TCG construction from the ACIM BG model and then using it for electrical fault detection, see Chapter 9.

5.6. An Example for Building Bond Graph Model of a Simple Electrical Circuit and Generating Equations from Bond Graphs

To enhance the understanding of BG models, this section gives an example on building BG model of the simple electric circuit shown in Figure 5-11 (a). The circuit is consists of voltage source E (t), resistor (R), inductance (L) and capacitor (C). As seen in the figure the circuit is connected in series. Thus the variable are connected using 1- junction as is shown in (b). The bond graph equations are as in Figure 5-11 (c). Thus the flow from these components will be equal and the effort sums to zero as can be seen in the Figure 5-11 (c).

The I- and C-elements are called state variable because they are utilized to construct the state-space equations often associated with BGs. When the causality algorithm has been completed and causality assigned to all the elements in the BG model, the BG models can be converted into equations. The I- and C- storage elements, which have integral causality, identify the state variables of the differential equations [145].

The figure contains three parts:

(a) Electrical circuit

(b) A bond graph model of the electrical circuit illustrated in (a)

(c) The bond graph equations

$$e_1 + e_2 + e_3 + e_4 = 0$$

$$f_1 = f_2 = f_3 = f_4 = f$$

$$e_1 = E(t)$$

$$e_2 = Rf_2$$

$$\dot{f_3} = \frac{1}{L}e_3$$

$$\dot{e_4} = \frac{1}{C}f_4$$

$$E(t) + Rf + e_3 + e_4 = 0$$

$$\acute{f} = -\frac{1}{L}Rf - \frac{1}{L}e_4 - \frac{1}{L}E(t)$$

$$\dot{e_4} = \frac{1}{C}f$$

$$\begin{bmatrix} \dot{f} \\ \dot{e_e} \end{bmatrix} = \begin{bmatrix} -\frac{R}{L} & -\frac{1}{L} \\ \frac{1}{C} & 0 \end{bmatrix} \begin{bmatrix} f \\ e_4 \end{bmatrix} + \begin{bmatrix} -\frac{1}{L} \\ 0 \end{bmatrix} E(t)$$
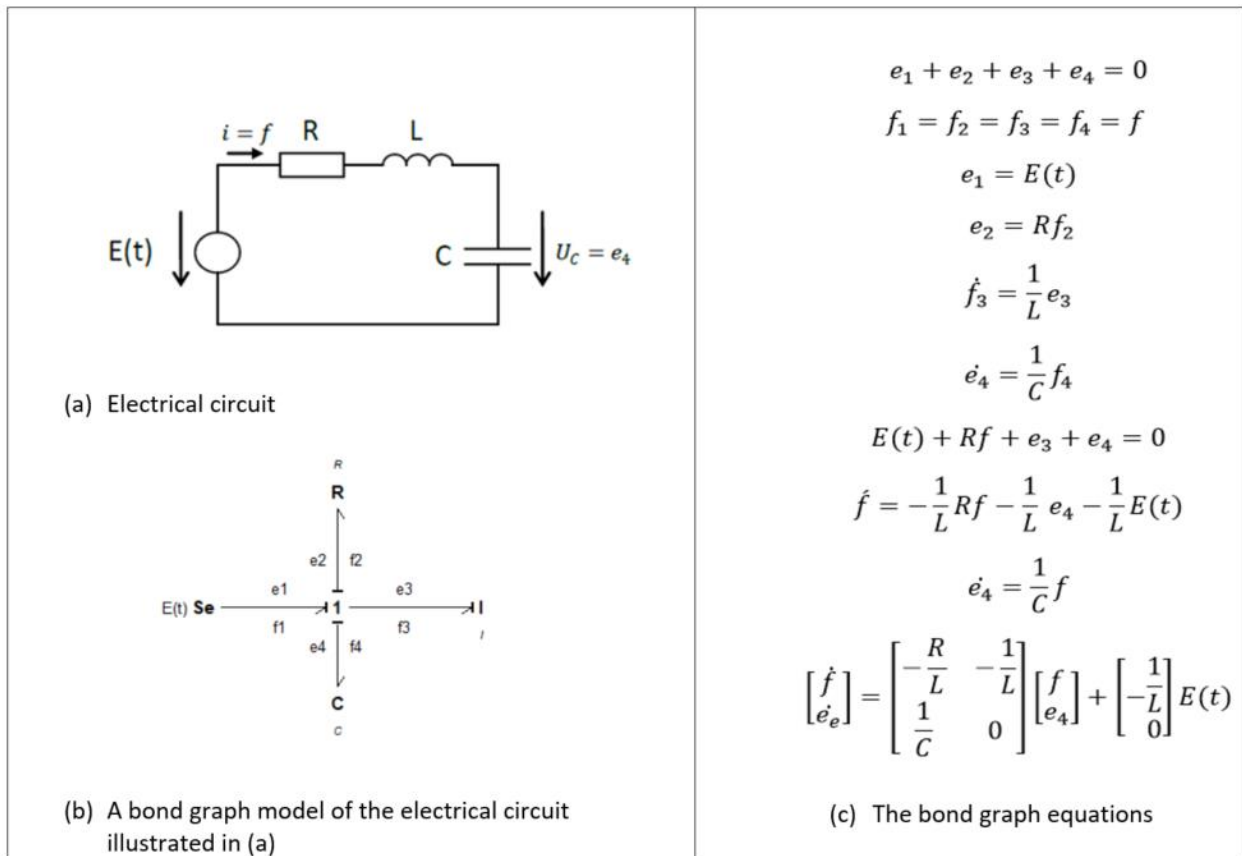
Figure 5-11 Example for building bond graph model of a simple electrical circuit and Generating Equations from Bond Graphs

5.7. Bond Graph for Fault Detection

The BG is a unified tool not only for modelling process engineering systems. It is also suitable for fault diagnosis, where the physical control properties can be derived by analyzing the causality relations on the BG model [148]. The model equations' principles can be investigated by analysing the causal paths where the causal components of the BG model are actually utilized to define the source and the effects of faults [78]. Additionally, it can be used for generating analytical redundancy relations (ARR) [149].

Many studies have been conducted using BGs for fault diagnosis [6, 7, 9, 21, 94, 148-150]. A variety of techniques for designing Fault Detection and Isolation (FDI) approaches have been proposed concerning the type of information utilized to define the system functions. For example, in [148], a diagnostic BG, based on the ARR, was used for residual analysis, monitoring, and fault diagnosis in a three-tank system. Another study for fault estimation in [150] applied the ARR for fault detection, and utilized a fault matrix for fault isolation. A

combined BG and principle component analysis (PCA) approach has been developed by [151] for fault diagnosis of three-tank system.

Qualitative reasoning based on BG modelling was used by [73] as a fault detection strategy. A BG fault diagnosis method based on residual generation and thresholds has been presented by [152]. They simulated the proposed method on a three=tank system. A TCG procedure was proposed by (Mosterman and Biswas) [6] for the fault diagnosis of a continuous system. The simulated results for a bi-tank system were provided to show the efficiency of the proposed fault detection approach.

5.8. Proposed Fault Detection Approaches

5.8.1. Quantative Fault Detection

This study will use a bond graph mothed for the detection of two typical electrical faults, broken rotor bar and stator winding asymmetry, in AC induction motors. Firstly a BG model of a three-phase squirrel-cage Ac induction motor in the neutral reference frame (A-B-C) was illustrated in chapter Seven. Second, the model is implemented using 20-SIM [153]. Then it investigates the effects of the BRB and stator IM faults-based motor current spectrum using a FFT signal processing technique. The results are validated by experiment; see Chapter Eight.

5.8.2. Qualitative Fault Detection

This study builds a qualitative simulation fault detection approach for ACIM condition monitoring based on the bond graph model developed in chapter Seven. The approach is based on qualitative reasoning. An illustration of the qualitative fault detection procedure is shown in Figure 5-12. First, it constructs the temporal causal graph based on the sequential causality assignment procedure. Then, it uses forward propagation to detect the effects of the fault (parameter deviations - increase) on the system behaviour. This qualitative approach will be used for qualitative fault detection of broken rotor bar and stator imbalance in a three-phase induction motor, see Chapter Nine.
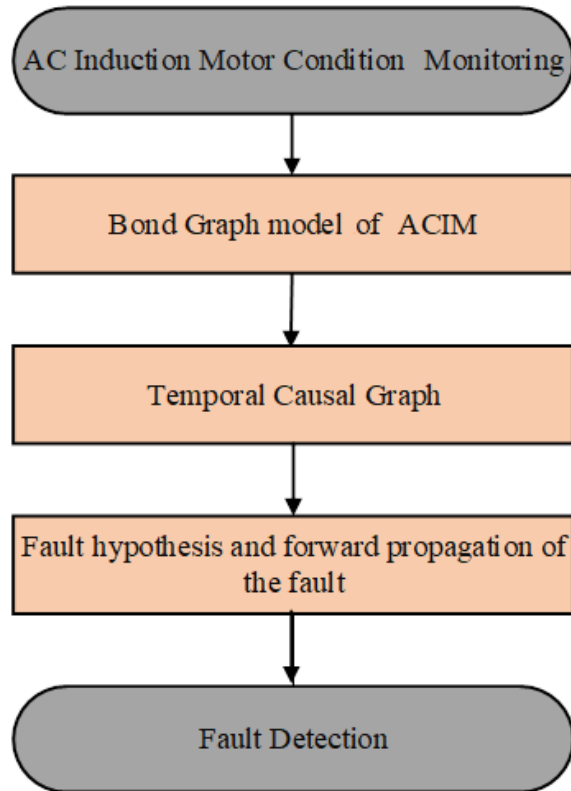
Figure 5-12 Flowchart of the qualitative fault detection procedure for fault detection in an ACIM

5.9. Summary

This chapter has provided the proposed fault detection procedure. First, it described BG modelling principles, including energy variables, standard BG elements and causality, and a brief distribution of the sequential assignment procedure and the TCG. Then, it provided an example of a simple electrical circuit to illustrate the construction of a bond graph model with qualitative equations. It also reviewed fault diagnosis methods based on BG modelling. Finally, the proposed quantitative and qualitative bond graph approaches are described.

Chapter 6 Test Rig Facilities & Experimental Results

This chapter represents the test bench utilized in this research. The test procedure was to introduce a fault into the AC induction motor and then detect its presence using the measured data. Details of the measuring devices, the data acquiring equipment, and application software are provided. Next, it discusses the considered simulated faults. Then, it reports the condition monitoring of ACIMs based on motor current analysis. Firstly, one and two broken rotor bars were effectively simulated by drilling holes in the bars (see Figure 6-9). Secondly, the stator winding imbalance was simulated by adding extra resistance in one phase only (see Figure 6-10). Then, MCSA analysis of the current signals for different severities of a broken rotor bar and stator imbalance faults showed that the two faults' different severities could be identified by considering the frequency and amplitude features.

6.1. Introduction

Experimental investigations play a crucial part in machine condition monitoring. An experimental study was conducted to evaluate the analysis of the results obtained from the BG model. The explanation of the test rig equipment's is represented in the following sections. The test rig utilized in this study allows the operator to perform a set of tests to acquire the data for diverse faults seeded into the system, changeable load conditions and different severities of each fault. Further, the test is repeatable for normal and abnormal behaviour of the AC motor.

6.2. The Structure of Test Platform

The test rig utilized in this research, see Figure 6-1 comprises a Clarke three-phase, AC induction motor under open loop control (V/Hz). The ACIM and the DC generator are coupled using a flexible coupling, as shown in Figure 6-1. The DC generator was used to apply different loads to the ACIM, as appropriate. The motor speed and load were adjusted using a touch screen on the control panel. A Hall Effect current transducers have been utilized to measure current signals. Further, a 16 channel YE6232B high-speed data acquisition system was used to record the experimental data.
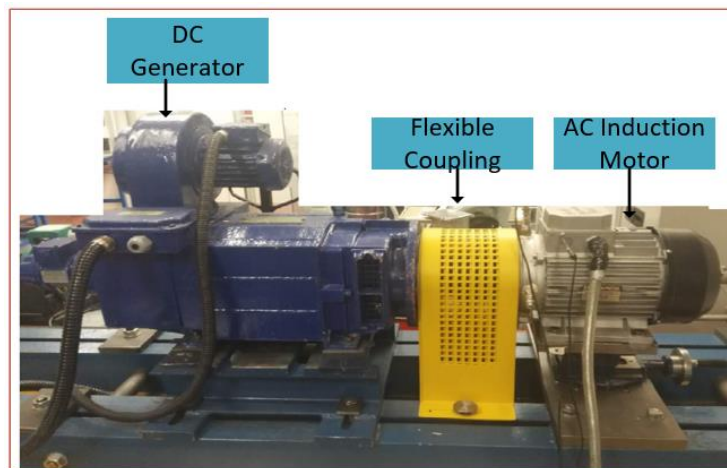
Figure 6-1 Photograph of the test bench

6.2.1. AC Induction Motor

The ACIMs used in this work were three phase squirrel-cage, rated at 4 kW at speed 1420 rpm (two-pole pairs). The specifications of the motors are presented in Table 6-1. Three identical motors were purchased. These motors were individually identified; hence the source of any collected data could be recognized. A photograph of the ACIM utilized in the test bench is displayed in Figure 6-2.

Table 6-1 ACIM specification

Parameter	Value
Rated Motor power	4 kW
Motor Speed	1420 rpm
Rated Voltage (Δ/Y)	230/400 V
Rated Current (Δ/Y)	15.9/9.2 A
Number of poles pair	2 pairs/phase
Supply frequency	50 Hz
Number of Phases	3
Number of rotor bars	28
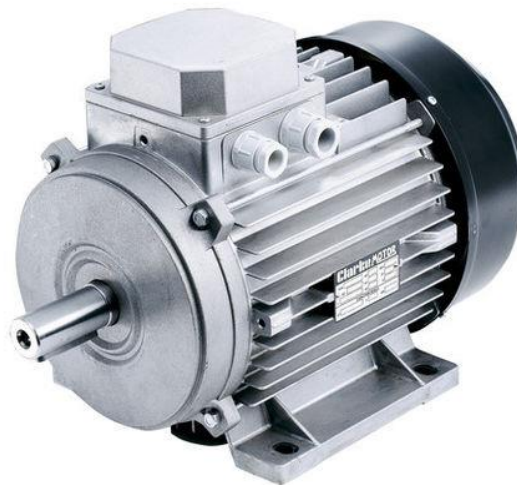
Figure 6-2 ACIM used in the test bench

6.2.2. Spider Flexible Coupling

The flexible spider coupling is shown in Figure 6-3. This coupling connected the drive shaft of the ACIM with the DC motor. This item of equipment is necessary for the alignment between rotation shafts as a way to eliminate shaft imbalance (misalignment), which could definitely lead to a malfunction and increase the need for maintenance. The description of the flexible coupling is in Table 6-2.

Figure 6-3 Flexible coupling (see also

Table 6-2)

Table 6-2 The specification of the Coupling

Sinocera Flexible Spider Coupling	
Outer diameter	130 mm
Border diameter	14-42 mm
Type	Fenner
Rubber width	36 mm
Hub length	18 mm
Hub diameter	105 mm
Taper lock bush size code	1610

6.2.3. DC Generator

A Siemens DC generator was used in this experimental study to make it easier to control the torque loads. It is a 10 Kw power at a 1720 rpm speed, current of 35 (A), and the voltage is 350 (V).

6.2.4. Speed and Torque Controller

To successfully operate the test rig at the selected speed and under various torque load conditions, a speed and torque controller is mandatory. The Siemens Micro Master Controller has been linked to the test bench to control speed and torque accurately. Figure 6-4 shows the controller.
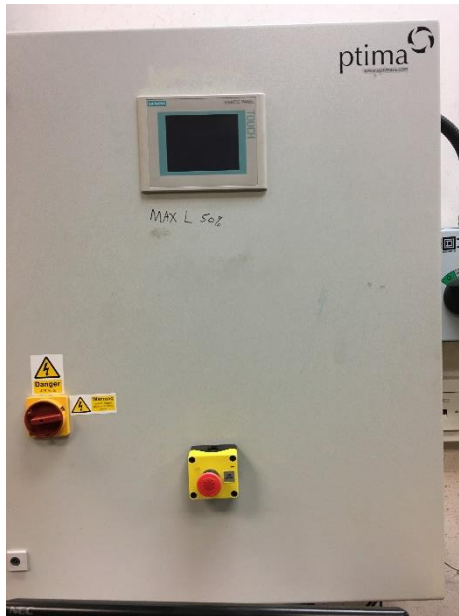
Figure 6-4 Touch screen of the torque and speed controller

The LCD touch screen of the controller is used to control the desired test profile. The block diagram in Figure 6-5 displays the characteristics of the control system.
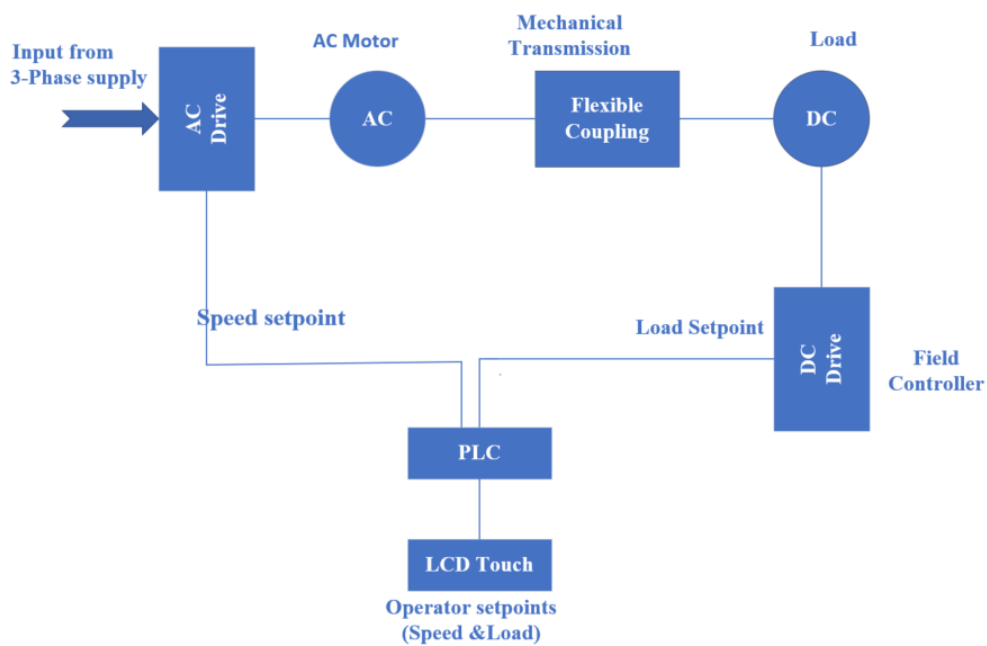
Figure 6-5 Block diagram of the speed and torque controller

6.2.5. Data Acquisition System

A data acquisition system (DAQS) was utilized to save the data from tests. The DAQS used in this work was a Sinocera YE6232B, as shown in Figure 6-6. This is equipped with 16 channels,

where every channel has a 24 bit A/D converter and a sampling frequency of 96 kHz. The specification of the DAQS is given in Table 6-3. The data acquisition device is controlled by software that enables the operators to set the parameters for data acquisition. Further, the DAQS converts the collected data to a form acceptable to MATLAB so it could be examined using a MATLAB code.

In this test facility, the parameters collected were the current of each phase of the stator and two encoder speeds to be used to investigate the system behaviour. In every test, the raw data was obtained and presented on a computer screen as graphs. This makes it possible for the data to be checked prior to being saved.

Figure 6-6 Data acquisition system (see also Table 6-3)

Table 6-3 Details of DACQS

Specification of YE6232B DAQS	
A/D Conversion resolution	24 bit
Sampling rate (Max)	96 kHz/ channel
Number of Channels	16
IEPE Power Supply	4 mA/+24VDC
Interface	USB 2.0
Input range	±10 V
Filter	Anti-aliasing
Gain	Selectable 1, 10 or 100

6.2.6. Three Phase Measurement Device

Hall Effect voltage and current transducers were used to measure the instantaneous three-phase currents. The Hall Effect transducer was connected to the DACQS. Figure 6-7 shows a photo of the measuring device, and Table 6-4 presents the specifications of the current transducers.

Table 6-4 Specification of Hall Effect current transducer

Specification ABB Hall Effect EL55P2 Current Transducer	
Bandwidth (-1 dB)	0:200 kHz
Primary nominal current (Ipn) rms	50 A
Secondary nominal current (Isn) rms	25 mA
Measuring range @ Va	0 : ±80 A
Accuracy	±0.5% @ (Ipn , 0:70oC and ±15V)
Supply voltage (Va)	±(11:15.7) V
Linearity	Better than 10^{-3}
No load current consumption	1 6 mA (@±15V Va)

Figure 6-7 Photograph of the unit for three phase current measurements

6.2.7. Shaft Encoder

The Hengstler speed encoder RI 32 was placed over the shaft of the ACIM to gauge its angular speed. As shown in Figure 6-8, the speed encoder is attached to the fan cover of the ACIM. It gives two outputs, 1 pulse every revolution, and 100 pulses per revolution. The encoder is linked to the DACQS directly through channels 1 and 2.
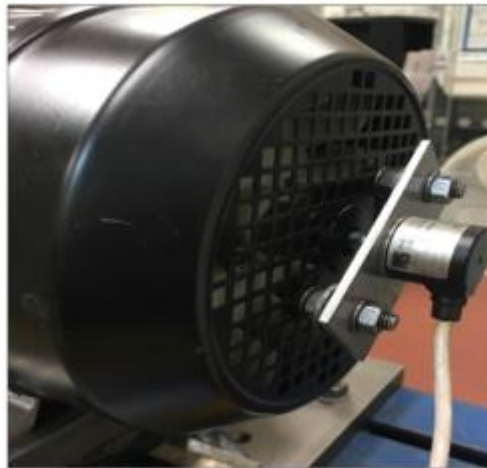
Figure 6-8 Hengstler speed encoder

6.3. Simulated Faults

Two of the most common electrical faults that occur in electromechanical systems have been investigated; broken rotor bar(s) and imbalance in the stator winding.

6.3.1. Broken Rotor Bar Fault

The main causes of rotor bar breakage are due to external factors such as thermal and magnetic stresses caused by electromagnetic forces, mechanical stress due to bearing failure, dynamic stresses due to shaft torque, and manufacturing problems (i.e., weak joints into the end ring) and metal fatigue [112, 154]. When a bar is partially or completely broken (see Figure 6-9), its resistance increases, so the current it carries decreases or falls to zero.

The broken rotor bar causes an increase of the rotor resistance that results in the asymmetry of the rotating electromagnetic field in the air gap between the stator and rotor. This leads to fluctuations and reduction of the speed and torque, and an unbalanced stator current due to harmonic components around the fundamental supply being induced [120, 154]. These effects can lead to a decrease in motor efficiency or even breakdown. Thus a broken rotor bar should be detected in its initial stage to prevent motor damage.

In the experiments, two broken rotor bar severities were addressed by using three motors with different degrees of broken bar fault. The first was a healthy motor, and the second had one broken bar and the third two broken bars. The BRB fault was achieved by simply drilling a hole through the bar, as shown in Figure 6-9. The tests were undertaken at different loads, though full load was avoided to protect the test motor from probable damage. The collected data were classified based on the conditions and different severity of faulty motors.

The broken rotor bar test procedure is done as follows:

In this study, to investigate the current signals under the defect of a broken rotor bar(s), three motors were used. In each case, the current signals were analysed for baseline motor (BL), the motor with one broken bar (1BRB), and motor with two broken bars (2BRB). Each of the three motors was run under five various torque loads: 0%, 20% 40%, 60% and 80% of full load, and this procedure was repeated three times. The full load was avoided to protect the test equipment from possible damage particularly on account of defected motors. The collected data was labelled with a test number specifying motor condition and load, which helped to organize the examinations of the acquired data. All tests were carried out at full speed.
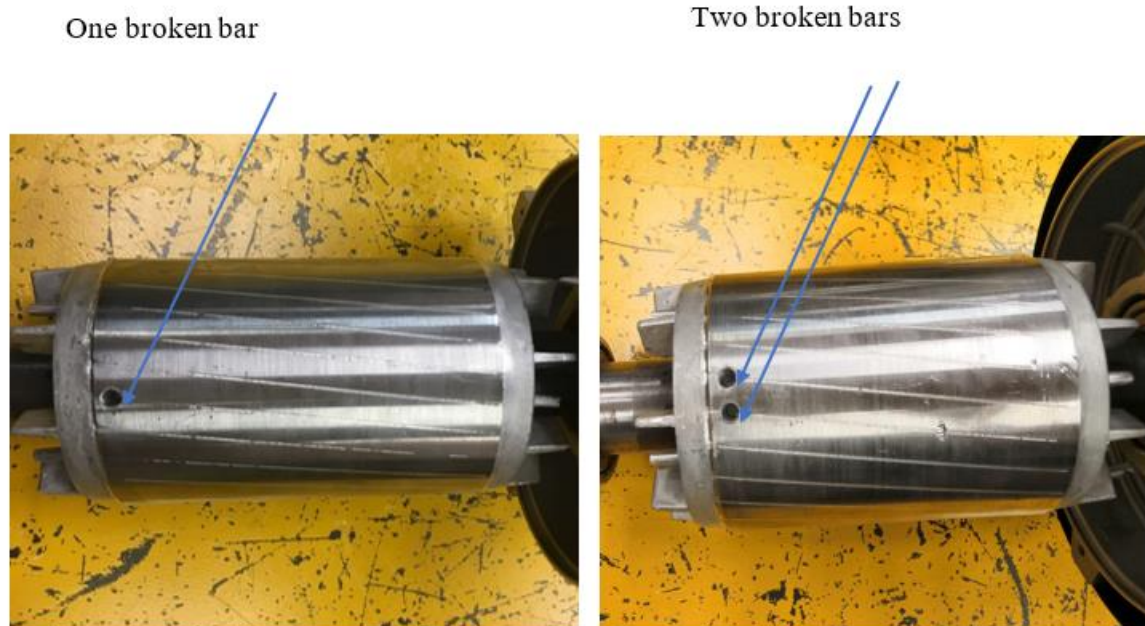
Figure 6-9 Photographs of rotor with one and two broken bars

6.3.2. Stator Winding Imbalance

Unbalanced stator winding, causes significant problems including a highly unbalanced stator current, a significant and even substantial increase in the motor temperature, unbalanced electromagnetic torque and reduction of the motor efficiency and shortening of the machine's lifetime [112, 155, 156].

The winding asymmetry was simulated by increasing of the resistance in the winding of one phase, see Figure 6-10. The resistance from the drive to the ACIM is 0.3 Ohm for each of the three phases. In this work, two resistances were introduced, 0.4 Ohm and 0.2 Ohm to simulate imbalanced stator winding; see Figure 6-10 so that the faulty phase's total resistance be increased to either 0.7 Ohm or 0.5 Ohm. An external resistor bank shown in Figure 6-11 is connected to one of the three phases to implement the stator winding imbalance. To evaluate the motor's performance, the current signals were acquired for three conditions healthy motor (BL), the motor with an increase in a phase resistance by (Rs=0.4 Ohm), then a further experiment with an increase in the phase resistance by (Rs=0.2 Ohm). The tests for each condition were repeated three times, and each test was run with five loads; 0%, 20%, 40%, 60%, and 80% of full load and at full speed. The collected data was labelled and saved with a file name that indicates the experiment configuration to make it easier for data analysis later.
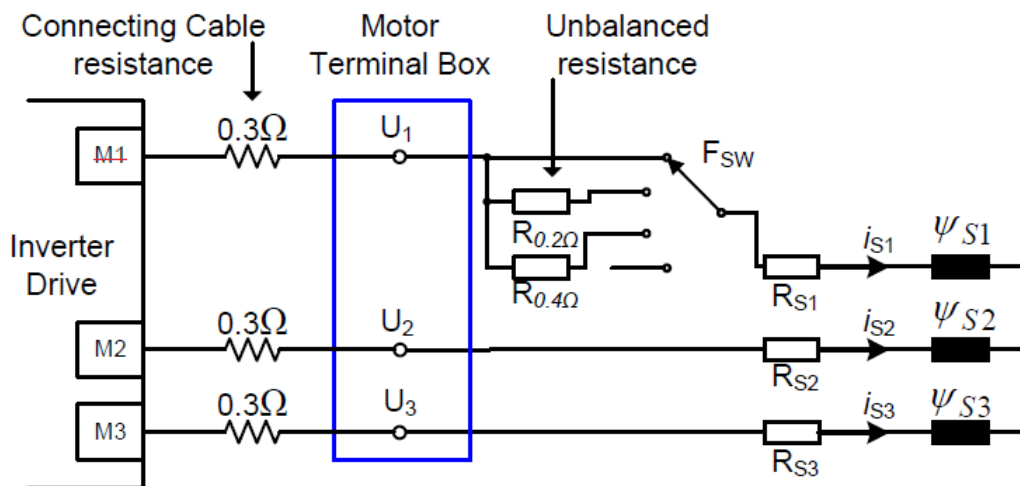
Figure 6-10 Stator winding imbalance [118]

Figure 6-11 External resistor bank

6.4. Experimental Results

The results obtained from the experimental procedures described are presented and discussed in the following sections. The analysis is made based on the harmonic components and peak amplitudes present in the current spectrum. A photo of the test rig was presented in Figure 6-1, and the ACIM specification is as in Table 6-1. The motor was operated under fixed v/Hz so there was no feedback from the driver. Each test was repeated three times, in each test, the motor ran under five different load conditions: 0% 20% 40% 60% and 80% of full load Figure 6-12 shows the motor speed under different load conditions. The response to an increase in load rise was a decrease in motor speed because of the increased load torque. The phase current-load plot is shown in Figure 6-13.
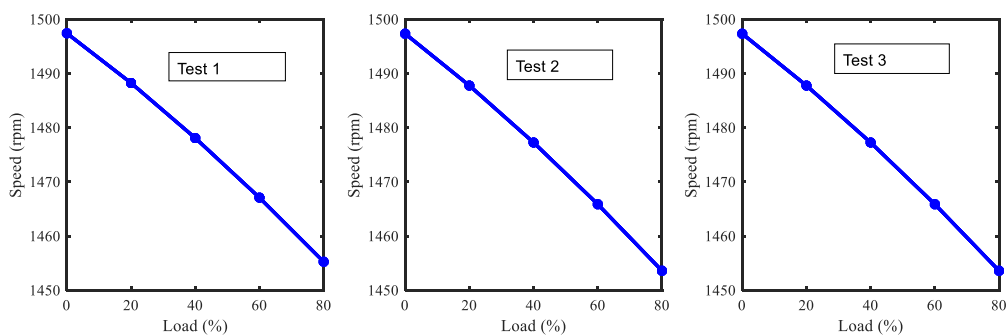
Figure 6-12 Motor speed under five different load sittings for three test runs
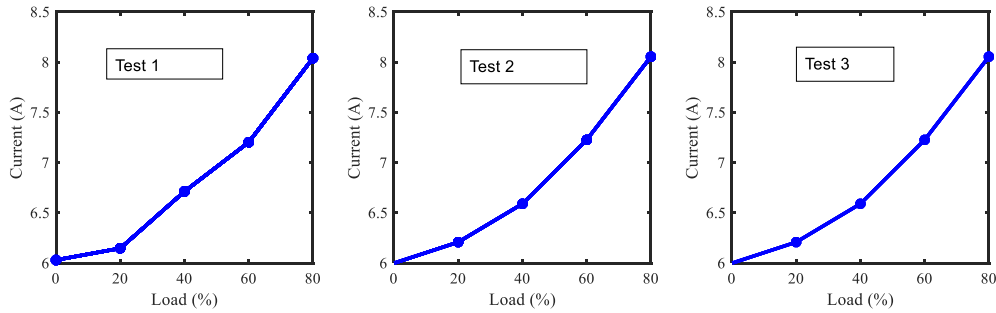
Figure 6-13 Motor phase current under five different load sittings for the three test runs

The advantages of using motor current for fault detection are: first, the current signals can be measured without accessing the motor because the current measurement can be carried out away from the motor; second, the influence of the motor faults are represented directly in the current signal; and third, that the fault manners in the current signal are distinctive for some electrical faults such as a broken rotor bar and imbalanced stator winding.

6.5. Results and Discussion

Generally, ACIM faults caused the current spectra of a healthy motor to be modified by increasing the amplitude of specific harmonic components related to the fault. With a broken rotor bar fault, changes occur in the harmonic components at $(f_s - 2sf_s)$ and $(f_s + 2sf_s)$ as explained in Section 4.4.1. The effect of a stator winding fault is seen in the spectral peak at $3f_s$, where f_s the supply frequency as explained in Section 4.4.2. This section provides spectrum analysis for the experimental detection and diagnosis of BRB and stator imbalance faults under different loads and different fault severities.

6.5.1. An Investigation of BRB Fault based on Current Signal Spectrum Analysis

In this study, to investigate the current signals under the defect of broken rotor bar(s), three motors were used. In each case, the current signals were analysed for baseline motor (BL), the motor with one broken bar (1BRB), and motor with two broken bars (2BRB). As stated in Section 6.4, each of the three motors was run under loads: 0%, 20% 40%, 60%, and 80% of full load, and this procedure was repeated three times. The full load was avoided to protect the test equipment from possible damage especially in the case of faulty motors. Each load is placed for a duration of two minutes and data recording was for 30 seconds. The collected data was labelled with a test number specifying motor condition and load, which helped to organise the examinations of the acquired data. All test were carried out at full speed. Table 6-5 details the test conditions; fault severity, load and motor speed under which data was recoding.

Table 6-5 Test procedure for broken rotor bar faults

Experiment No.	Severity of Broken Rotor Bar Fault	Load Conditions (Torque Load (N.m))	Data Recording for Each Load Condition.	Speed RPM
1	Healthy Motor (BL)	0%, 20%, 40%, 60% and 80% full load	30 (sec)	100%
2	Motor with 1 BRB	0%, 20%, 40%, 60% and 80% full load	30(sec)	100%
3	Motor with 2 BRBs	0%, 20%, 40%, 60% and 80% full load	30 (sec)	100%

Typical current spectra for the baseline motor under different loads are shown in Figure 6-14. It is obvious that the changes in load do not produce significant changes in the current spectrum (except at 80% full load), so any changes in the current spectrum are caused by other factors such as a BRB.
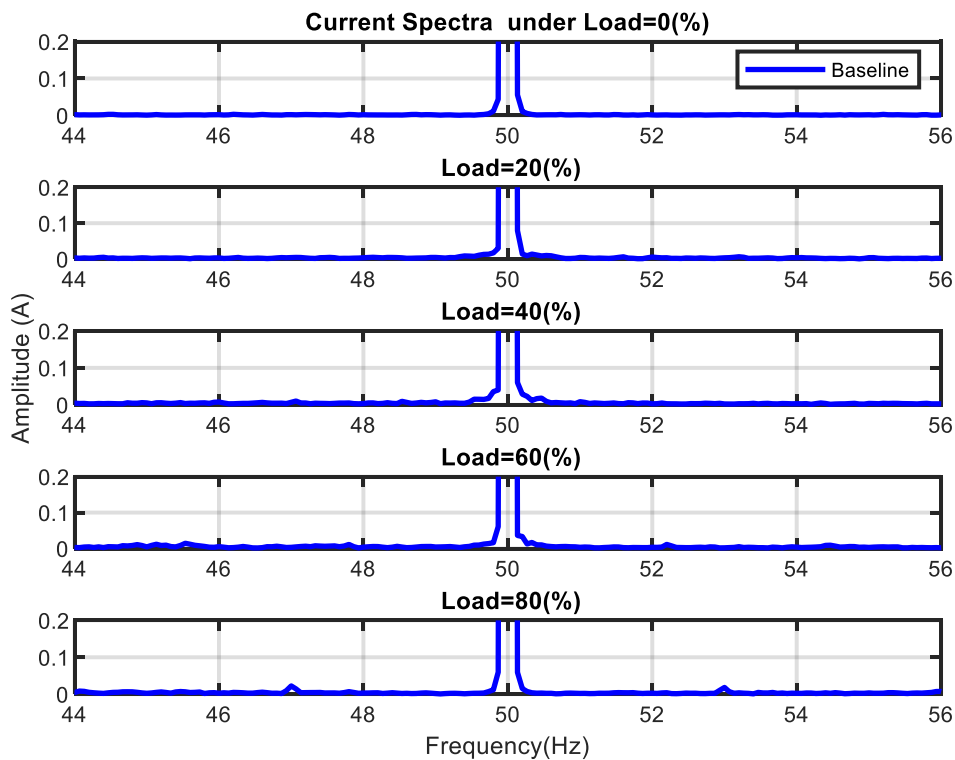
Figure 6-14 Motor phase current spectra for baseline conditions under different loads

A broken BRB fault causes an increase of the resistance of the bar(s), so the current that would normally pass through the broken bar(s) travels through the remaining bars, causing an unbalanced magnetic field in the air gap with consequent torque pulsations that modulate the current and induce harmonic components around the supply frequency. Figure 6-15 depicts the current spectra of a motor with one broken bar under 0%, 20%, 40%, 60%, and 80% of full

load and at full speed. Harmonic components and sidebands around the 1st harmonic f_s can be seen clearly. The sidebands amplitude increase with the load. It is obvious that the sidebands, as a diagnostic indicator, can be seen much more clearly under higher loads, from 40% to 80%. As expected, the value of s (slip) changed slightly with load, so the precise frequency of the sidebands increased as load increased.
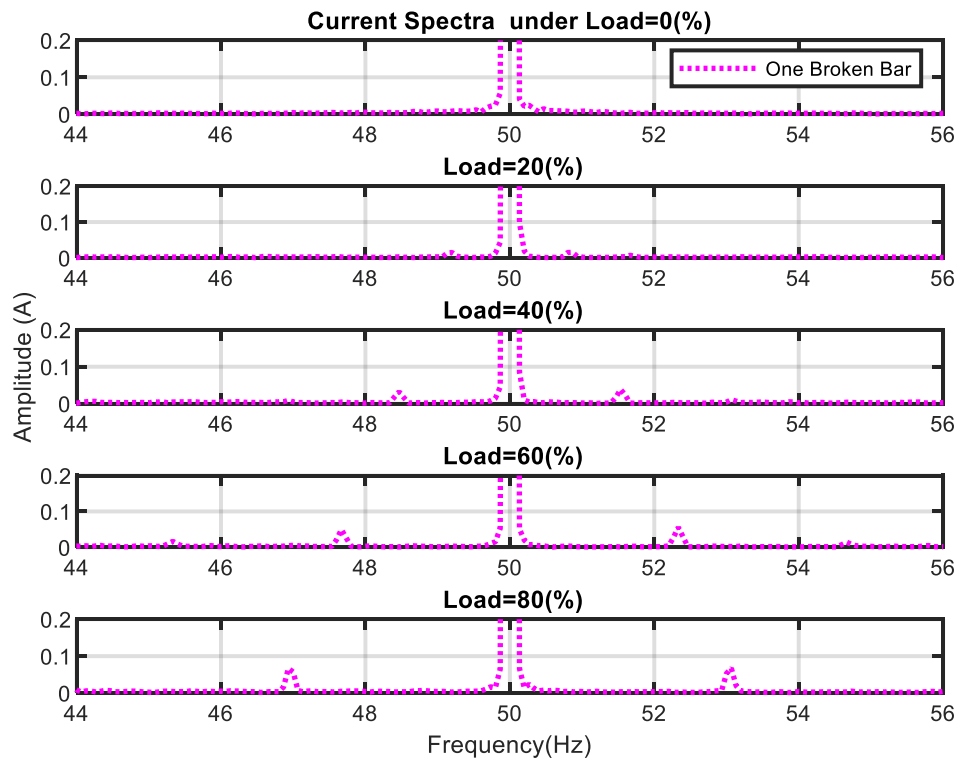
Figure 6-15 Motor phase current spectra for one BRB under different loads, sidebands at (fs±2sfs)

A similar observation can be made from Figure 6-16. The rise in amplitude of the sidebands at (fs±2sfs), due to two BRBs is greater than those occurring for 1 BRB and the BL condition, compared to results in Figure 6-14 and Figure 6-15. As with the single BRB fault, the sidebands around the supply frequency are shifted away from the fundamental frequency with an increase of torque load.
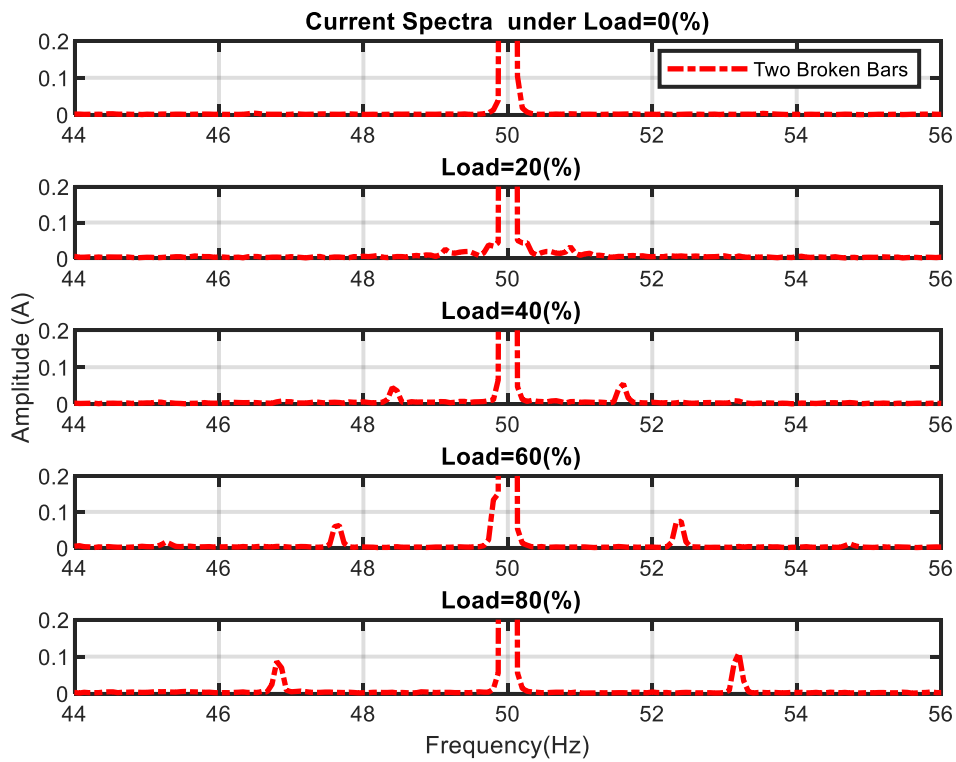
Figure 6-16 Motor phase current spectra for two BRBs under different loads, sidebands at (fs±2sfs)
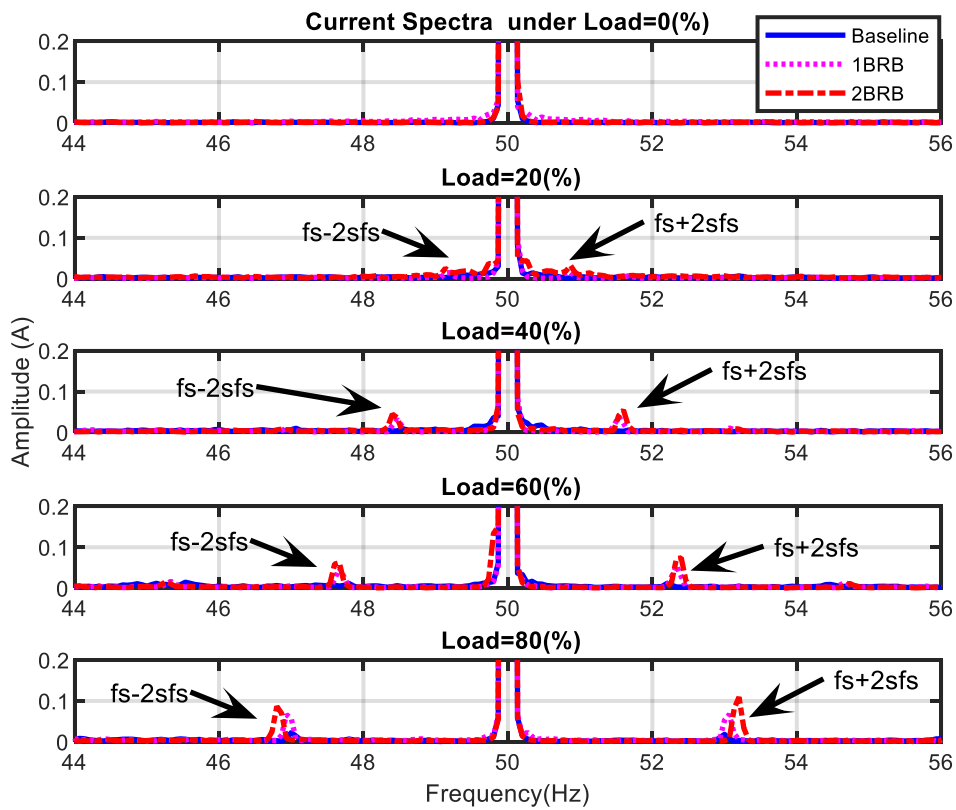
Figure 6-17 Motor phase current spectra for different severities of BRB fault, under different loads

Figure 6-17 presents a comparison of the stator current spectra for baseline and two levels of BRB faults (1BRB and 2 BRB) at different loads and shows the relevant diagnostic features. It is clear that a broken rotor bar fault generates twofold sidebands around the first harmonic in the current spectrum. No sidebands are visible for one or two broken bars under 0% load, for the reason that the slip has little influence since it is very small. It is seen clearly that the amplitude of the sideband increased with load, which means this fault can be detected more easily under high load.
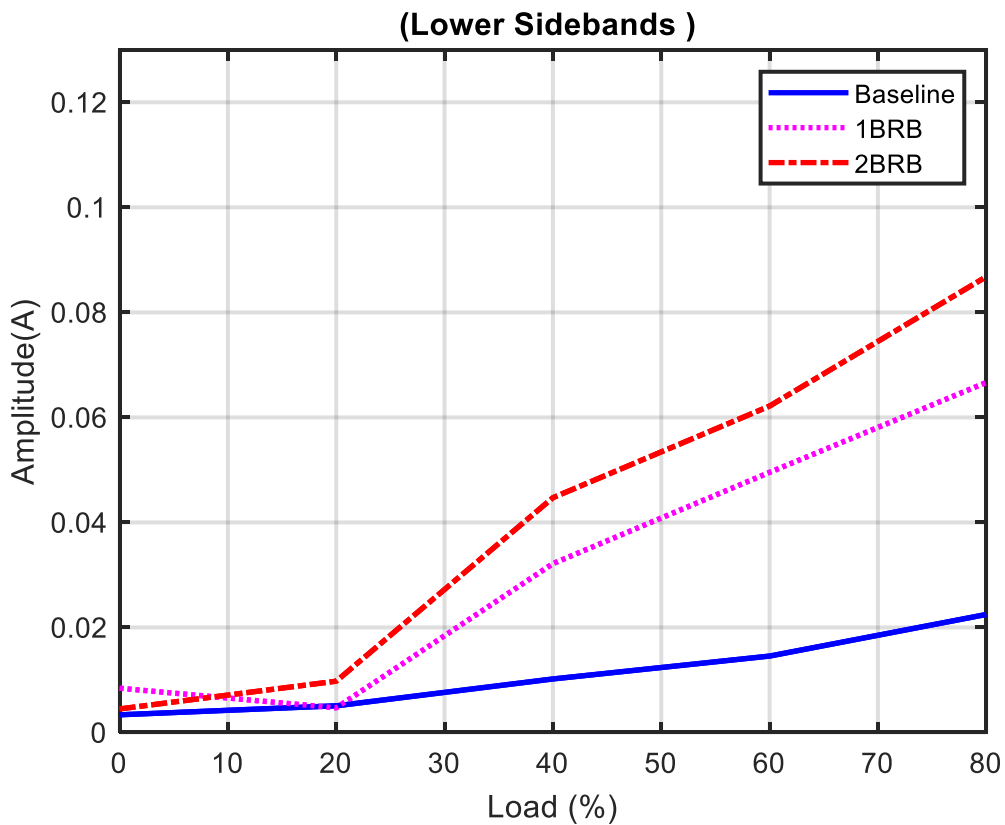
Figure 6-18 Comparison of the trends in amplitude of the lower side bands (fs - 2sfs) with increase in load
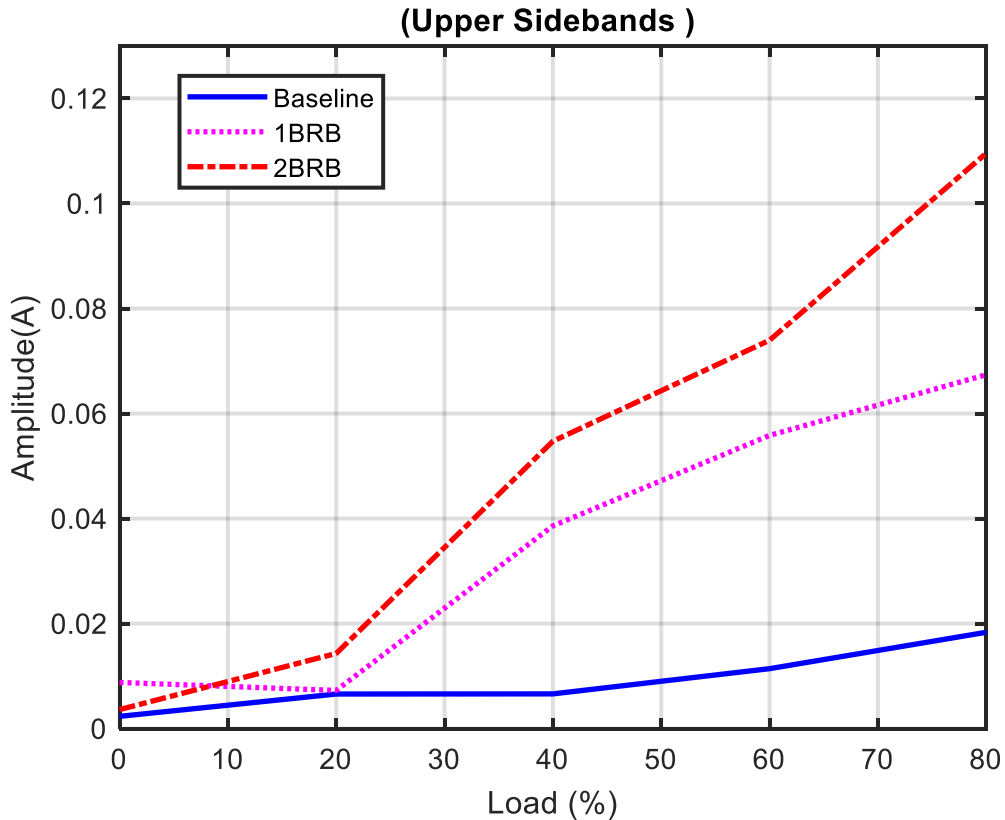
Figure 6-19 Comparison of the trends in amplitude of the upper side bands (fs + 2sfs) with increase in load

Figure 6-18 and Figure 6-19 detail the increase in the amplitude of the lower sidebands ($f_s - 2sf_s$) and upper sidebands ($f_s + 2sf_s$) for baseline and two levels of BRB fault under various load conditions. It can be seen that the amplitude of the sidebands ($f_s \mp 2sf_s$) increases with the severity of the BRB fault and load, i.e., the amplitude of the sidebands in the case of one BRB is less than the amplitude in the case of two BRBs. This shows that the spectrum analysis provides a clear indication of the BRB fault's presence and magnitude. It is also demonstrates that the motor slip increased as the load increased, so that the sidebands around the supply frequency shift away from the fundamental frequency with the increase of load.

To conclude, the results produced by both the bond graph model and experiment show that a broken rotor bar fault can induce detectable increases in motor current spectral amplitude presented as twofold sidebands at ($f_s \pm 2sf_s$) around the fundamental frequency. These outcomes are in great concurrence with the outcomes acquired by Sharma, et al., [157], Chen and Živanović, [120] and Nemec, et al., [66].

6.5.2. Investigation of Stator Winding Asymmetry

To examine the effects of various degrees of stator imbalance defect on the motor current spectrum, the current signals from the three motors were analysed. In each case, baseline motor, the motor with stator imbalance of Rfs, = 0.2 Ω, and motor with stator imbalance Rfs = 0.4 Ω were tested. Again, for each case of these three fault levels, the test was repeated three times, and the motor was run under different load conditions 0%, 20% 40%, 60%, and 80% of full load. Thus there were 15 data points for each of the three tests for each of the three motors. Again full load was avoided to protect from possible damage under the fault effects. Once again, each load is placed for a duration of two minutes, and the data recording was for 30 seconds. The collected data was labelled with test number, motor, motor condition and load condition. This labelling helped in the examinations of the data. All test were run under 100% full speed.

To examine the response of the system with imbalanced stator winding, spectral analyses of the collected data are presented in Figure 6-20 to Figure 6-24. It is obvious that the amplitude of the harmonic component at 150 Hz increased with an increase in fault severity for all load conditions.
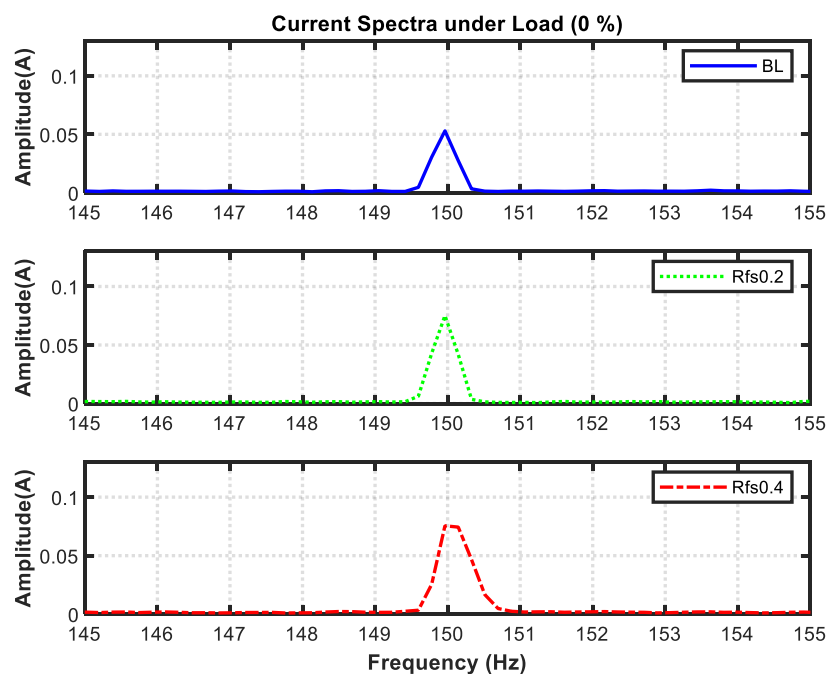
Figure 6-20 Current spectrum of the ACIM, healthy and with two levels of fault imbalance in the winding (Rfs = 0.2 Ω and 0.4 Ω) under 0% load
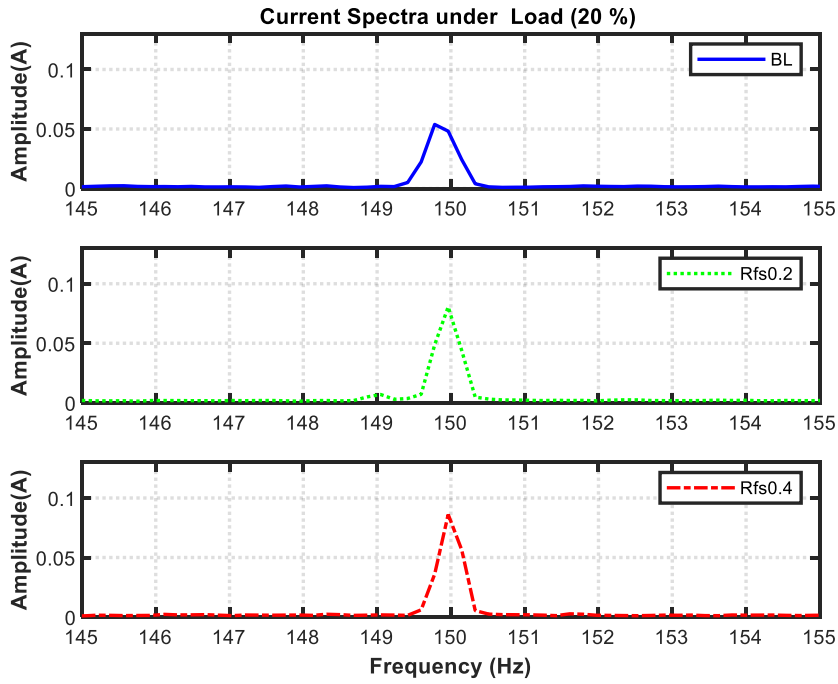
Figure 6-21 Current spectrum comparison of the ACIM, healthy and with two levels of fault imbalance in the winding (Rfs = 0.2 Ω and 0.4 Ω) under 20% load
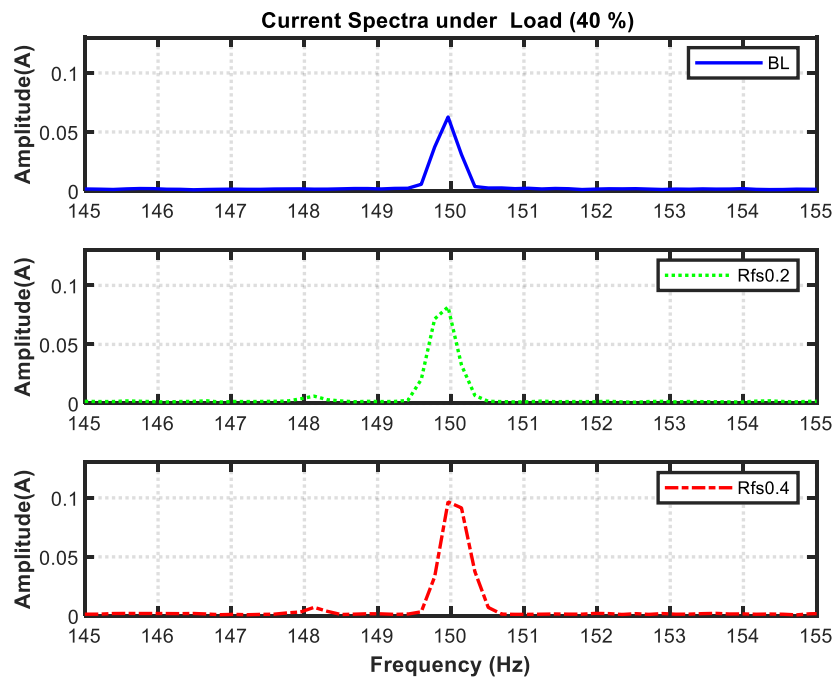
Figure 6-22 Current spectrum comparison of the ACIM, healthy and with two levels of fault imbalance in the winding (Rfs = 0.2 Ω and 0.4 Ω) under 40% load
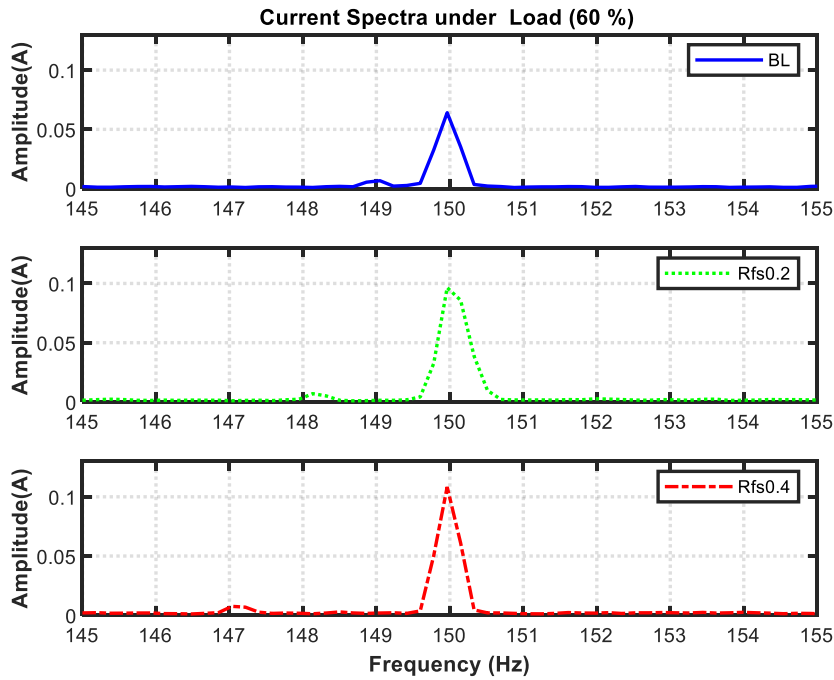
Figure 6-23 Current spectrum for the ACIM, healthy and with two levels of fault imbalance in the winding (Rfs = 0.2 Ω and 0.4 Ω) under 60% load
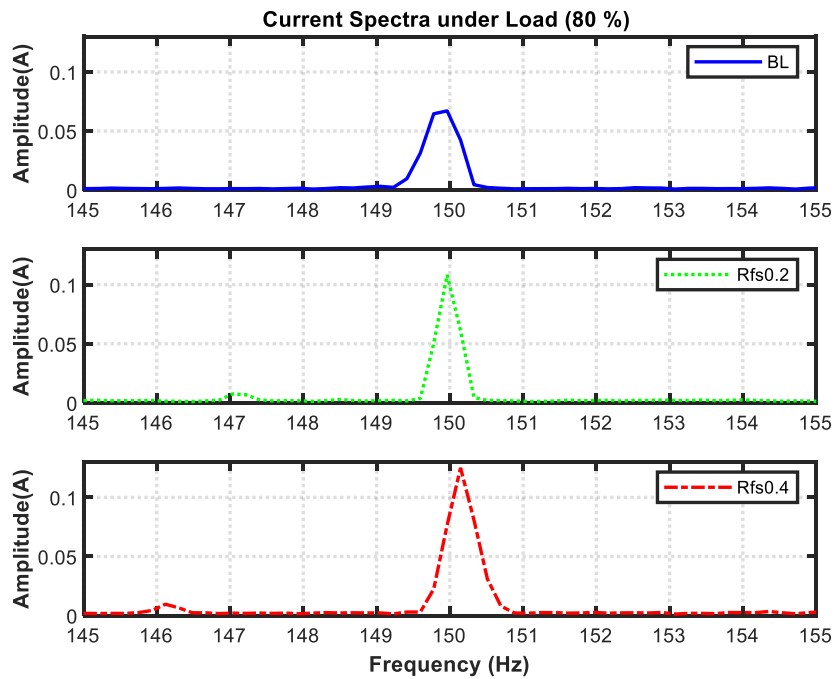
Figure 6-24 Current spectrum comparison for the ACIM, healthy and with two levels of fault imbalance in the winding (Rfs = 0.2 Ω and 0.4 Ω) under 80% load

The combined depiction of the current spectrum results for baseline motor and the motor with two fault levels for stator imbalance, at full speed and under 0%, 20%, 40%, 60% and 80% full load is shown in Figure 6-25. Obviously, the amplitude of the 150 Hz peak increased with an increase in the severity of the fault no matter what the load.
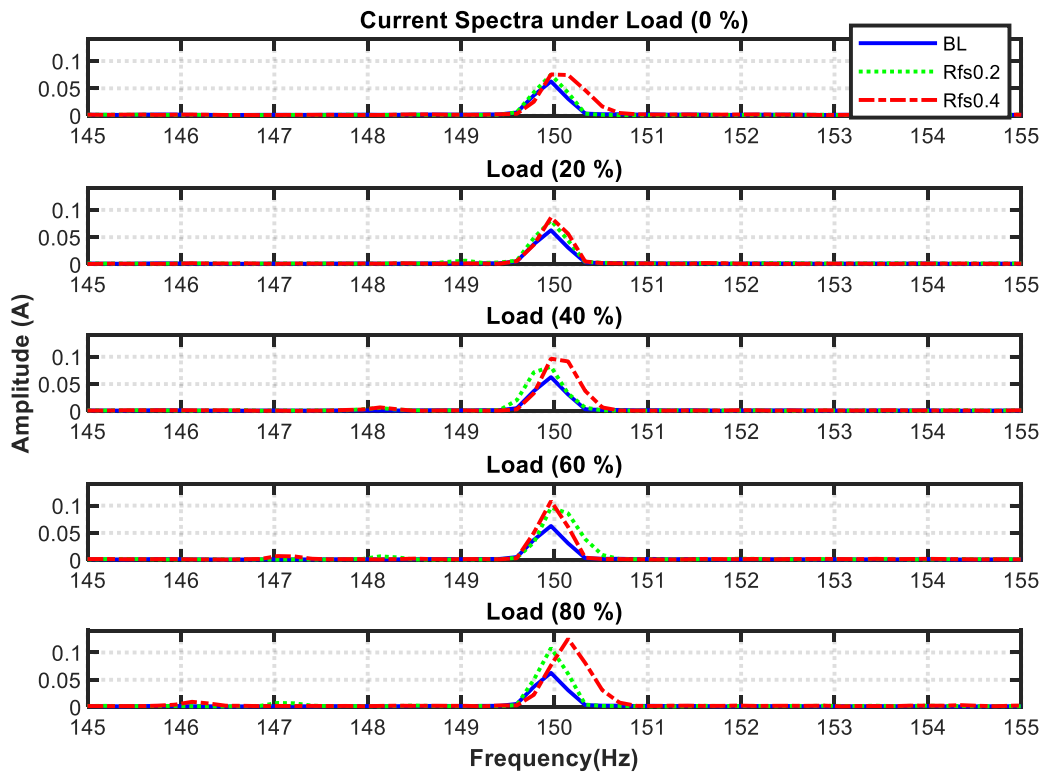
Figure 6-25 Current spectra for different levels of stator imbalance for full speed at 0%, 20%, 40%, 60% and 80% full load

A similar observation can be made from Figure 6-26, which again shows the amplitude of the peak at $3f_s$ increased significantly with level of fault whatever the load, and this can be considered as an indicator of the stator winding asymmetry [158].
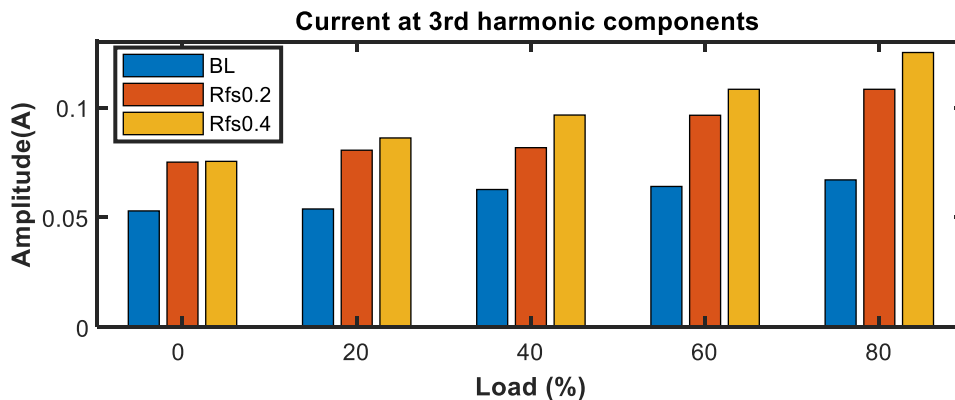
Figure 6-26 Amplitudes of 3rd harmonic components of current spectra for different levels of stator imbalance (BL and Rfs = 0.2 Ω and 0.4 Ω) for full speed at 0%, 20%, 40%, 60% and 80% full load

To conclude, the results produced by both the bond graph model and experiment show that a stator winding imbalance fault can induce detectable increases in motor current spectral

amplitude at the distinctive frequency of $3f_s$ (150 Hz). This is in good agreement with the results obtained by [159], [117], and [158].

6.6. Summary

This chapter describes the test bench equipment. It includes the structure of the test bench and the specification of test components. Further, it presents the data acquisition equipment and the measuring devices, including the three phase current measurements and shaft speed encoder. It also presents an explanation of the investigated faults (broken rotor bar and stator winding imbalance) and the procedure for collecting the data. Then it presents the practical implementations of the developed system for the detection and diagnosis of broken rotor bar and stator winding imbalance faults in an ACIM.

On the basis of the experimental results obtained:

The effects of the given faults on the current signals show that the experimental results obtained are in good agreement with the predicted signals, as described in Chapter Eight, as well as the results reported in the literature. The result presented in Figure 6-14 to Figure 6-19 are in good agreement with the result obtained by Sharma et al. [157], Chen and Živanović [120], and Nemec, et al. [66].

It is also seen from the results presented that changes in the current spectrum vary significantly with load and motor fault. A broken rotor bar fault changes the stator current spectrum of the healthy machine by increasing the amplitude of the sidebands around the fundamental supply in the current spectra.

It can be seen from Figure 6-20 to Figure 6-26 that the amplitude of the third harmonic of the supply frequency at (150 Hz) increased significantly with the level of fault for all loads tested for stator winding imbalance. The results presented are in good agreement with those obtained by Benbouzid and Kliman [159], Joksimovic and Penman [117] and Babaa, et al. [158].

The increase of spectral amplitude at $(f_s \pm 2sf_s)$ and at $3f_s$, caused by broken rotor bar and stator imbalance respectively, will be considered when developing a qualitative simulation technique in Chapter Nine, with emphasis on qualitative reasoning for the detection of broken rotor bar and imbalanced stator winding faults.

Chapter 7 Bond Graph Modelling for ACIM Condition Monitoring

This chapter addresses the bond graph methodology as a pictographic approach for modelling an AC induction motor. First, it gives a brief introduction, next, the mathematical model of the healthy motor, then motor with broken rotor bar and motor with stator imbalance fault. Next, it introduces the bond graph model of the ACIM in order to highlight and present the predicted effects of electrical faults on the ACIM behaviour based on motor current signature analysis.

7.1. Introduction

Various models have been presented for the simulation of electric machines [3, 9]. However, most of these are based on mathematical models, not a structured presentation of the system. Bond graphs are considered more efficient as they can model the dynamics of the system's behaviour based on the combination of three different aspects; physical structure, causality, and mathematics. This approach has been used widely for the modelling of engineering systems [67, 160]. The development of a bond graph model for ACIMs could provide vital information for fault diagnosis.

A powerful and simple modelling technique, the BG, is a pictorial representation of a dynamic physical system, which allows the complicated flows of energy in the physical domain to be determined, and has been shown to be effective for quantitative and qualitative based fault diagnosis. The BG works as a mediator between the physical system and the analytical models related to it [135].

7.2. Model of a Healthy ACIM

Mathematical models of ACIMs have been presented many times in publications [161]. There are two general frameworks for such models: one using the orthogonal (Park) reference frame, and the other using the natural reference frame (three sinusoidal waveforms) [162, 163]. The mathematical model of ACIM applied in this study follows, in principle, that developed by [1]: the rotor windings are symmetrically distributed around the rotor axis; there is a smooth air gap; and the stator windings are symmetrically aligned alongside the stator axis. Figure 7-1 represents the equivalent circuit of the AC induction motor.
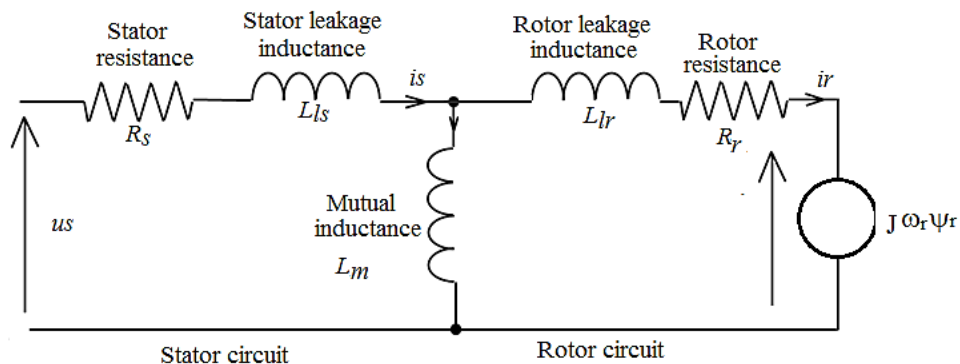
Figure 7-1 Representation of the equivalent circuit of an ACIM

The ACIM mathematical model is obtained by presenting the stator and rotor electrical circuits equations. The voltage and flux equations of a three-phase ACIM in (a-b-c) axes are [101, 163]:

$$u_s = R_s I_s + \frac{d\Psi_s}{dt} \tag{7-1}$$

$$u_r = R_r I_r + \frac{d\Psi_r}{dt} \tag{7-2}$$

$$\Psi_s = L_{ss} I_s + L_{sr} I_r \tag{7-3}$$

$$\Psi_r = L_{rr} I_r + L_{rs} I_s \tag{7-4}$$

The notations $u_s, I_s, \Psi_s, u_r, I_r$ and Ψ_r are columns vectors representing the voltage, current, and flux of the stator and rotor respectively. R_s, R_r, are the diagonal matrices for one phase equivalent resistance of stator and rotor, because the resistance in each rotor or stator phase is assumed to be equal in an ideal induction motor.

$$R_s = \begin{bmatrix} r_s & 0 & 0 \\ 0 & r_s & 0 \\ 0 & 0 & r_s \end{bmatrix} \tag{7-5}$$

$$R_r = \begin{bmatrix} r_r & 0 & 0 \\ 0 & r_r & 0 \\ 0 & 0 & r_r \end{bmatrix} \tag{7-6}$$

The notations L_{ss} and L_{rr} are matrices of the stator and rotor windings 'self-inductance respectively, while L_{sr}, L_{rs} are matrices of the stator to rotor inductance and the rotor to stator inductance, respectively. The inductance matrices are formed as [64, 163]:

$$L_{ss} = \begin{bmatrix} L_s & -0.5L_m & -0.5L_m \\ -0.5L_m & L_s & -0.5L_m \\ -0.5L_m & -0.5L_m 0 & L_s \end{bmatrix} \tag{7-7}$$

$$L_{rr} = \begin{bmatrix} L_r & -0.5L_m & -0.5L_m \\ -0.5L_m & L_r & -0.5L_m \\ -0.5L_m & -0.5L_m 0 & L_r \end{bmatrix} \tag{7-8}$$

$L_s = L_{ls} + L_m$, $L_r = L_{lr} + L_m$. The notations L_{ls}, L_{lr} are the stator and rotor winding leakage inductances respectively, L_m is the mutual inductance.

The stator to rotor inductance and rotor to stator inductance L_{sr}, L_{rs} are expressed as follows [64]

$$L_{sr} = [L_{rs}]^T = L_m \begin{bmatrix} \cos\theta_r & \cos(\theta_r + \frac{2\pi}{3}) & \cos(\theta_r - \frac{2\pi}{3}) \\ \cos(\theta_r - \frac{2\pi}{3}) & \cos\theta_r & \cos(\theta_r + \frac{2\pi}{3}) \\ \cos(\theta_r + \frac{2\pi}{3}) & \cos(\theta_r - \frac{2\pi}{3}) & \cos\theta_r \end{bmatrix} \tag{7-9}$$

$$L = \begin{bmatrix} dL_{ss} & dL_{sr} \\ dL_{sr} & dL_{rr} \end{bmatrix} \tag{7-10}$$

$$\frac{dL_{sr}}{d\theta} = \begin{bmatrix} 0s & dL_{sr} \\ dL_{sr} & 0s \end{bmatrix} \tag{7-11}$$

$$dL_{sr} = -L_m \begin{bmatrix} 0 & 0 & 0 & \sin\theta_r & \cos(\theta_r + \frac{2\pi}{3}) & \cos(\theta_r - \frac{2\pi}{3}) \\ 0 & 0 & 0 & \sin(\theta_r - \frac{2\pi}{3}) & \sin\theta_r & \sin(\theta_r + \frac{2\pi}{3}) \\ 0 & 0 & 0 & \sin(\theta_r + \frac{2\pi}{3}) & \sin(\theta_r - \frac{2\pi}{3}) & \sin\theta_r \\ \sin\theta_r & \sin(\theta_r + \frac{2\pi}{3}) & \sin(\theta_r - \frac{2\pi}{3}) & 0 & 0 & 0 \\ \sin(\theta_r - \frac{2\pi}{3}) & \sin\theta_r & \sin(\theta_r + \frac{2\pi}{3}) & 0 & 0 & 0 \\ \sin(\theta_r + \frac{2\pi}{3}) & \sin(\theta_r - \frac{2\pi}{3}) & \sin\theta_r & 0 & 0 & 0 \end{bmatrix} \tag{7-12}$$

L_{sr}, L_{rs} are the stator to rotor inductance and the rotor to stator inductance respectively and θ_r is the rotor angle.

To complete the model, the torque equation is required to describe the mechanical dynamics of the ACIM, it can be expressed as [164-166]:

$$\frac{d\omega_r}{dt} = \frac{1}{Jm}(T_e - T_l) \tag{7-13}$$

Where ω_r is the rotor's mechanical angular speed, T_e and T_l are the electromagnetic torque and load torque respectively, Jm is the machine's inertia

In this ACIM model the voltage equations can be written as follows:

$$U_s = \left(R_s + \frac{dL}{dt}\right).I_s + L.\frac{di}{dt} \tag{7-14}$$

$$U_r = \left(R_r + \frac{dL}{dt}\right).I_r + L.\frac{di}{dt} \tag{7-15}$$

Then the current equation is [64]

$$\frac{di}{dt} = -L^{-1}\left(R_s + \frac{dL}{dt}\right).I_s + L^{-1}.U_s \tag{7-16}$$

$$\frac{di}{dt} = -L^{-1}\left(R_r + \frac{dL}{dt}\right).I_r + L^{-1}.U_r \tag{7-17}$$

$$U_s = \begin{bmatrix} u_{sa} \\ u_{sb} \\ u_{sc} \end{bmatrix}, u_r = \begin{bmatrix} u_{ra} \\ u_{rb} \\ u_{rc} \end{bmatrix}, I_s = \begin{bmatrix} i_{sa} \\ i_{sb} \\ i_{sc} \end{bmatrix}, I_r = \begin{bmatrix} i_{ra} \\ i_{rb} \\ i_{rc} \end{bmatrix} \tag{7-18}$$

7.3. ACIM Model with Broken Rotor Bar

Abnormal operating conditions will affect the system symmetry of an ACIM. The electrical fault generated by a rotor broken caused an increase of rotor resistance, such that the electromagnetic field rotating between rotor and stator ceases to be symmetrical. This will induce harmonic components into the stator current. It is possible to simulate the results produced by a BRB simply by adding resistance to the particular rotor phase containing the BRB [165-168]. Thus, the rotor resistance matrix R_r in Equation (7-6) must be modified as:

$$R_r^* = \begin{bmatrix} r_r + \Delta r_{ra} & 0 & 0 \\ 0 & r_r + \Delta r_{rb} & 0 \\ 0 & 0 & r_r + \Delta r_{rc} \end{bmatrix} \tag{7-19}$$

The resistance changes of the three rotor phases are expressed as $\Delta r_{ra}, \Delta r_{rb}, \Delta r_{rc}$ which are defined as [169]:

$$\Delta r_{ra,b,c} = \frac{3n_{brb}}{N_b - 3n_{brb}} r_r \tag{7-20}$$

N_b is the total number of rotor bars, n_{brb} the number of broken rotor bars, r_r is the resistance of the healthy rotor.

The squirrel cage motor is a three-phase circuit where the bars of each phase are N/3 series connected conductors, so the rotor resistance is [169]:

$$r_r = \frac{(2N_1)^2}{N/3} r_b \tag{7-21}$$

Where r_b the rotor bar resistance and N_1 the number of equivalent stator turns. However, if n rotor bars are broken, the number of conductors for the faulty phase become (N/3 - n) and its resistance, according to [167, 169] is:

$$r_r^* = \frac{(2N_1)^2}{\frac{N}{3} - n_{brb}} r_b \tag{7-22}$$

Thus, the resistance increment with n broken bars, Δr, is obtained as a simple difference:

$$\Delta r = r_r^* - r_r = \frac{3n_{brb}}{N_b - 3n_{brb}} r_r \tag{7-23}$$

7.4. Model with Stator Winding Imbalance Fault

Motor winding failure and an unbalanced stator will cause significant problems such as magnetic field asymmetry the unbalanced stator current, torque pulsation, increased motor

temperature, vibrations, reduction of machine efficiency and shortening of machine life [112, 155, 156, 170].

To investigate the effects of the unbalanced stator winding, this study used an external resistance bank as described in Section 6.3.2, to increase the resistance in one phase of the stator. In the same way, winding asymmetry was simulated in the BG model by an increase of the resistance in one phase.

The additional resistance inserted will be referred to as R_{fs}. The effect of the additional resistance in the stator equivalent circuit on the voltage will be:

$$u_{sa} = (R_{fs} + R_s)I_s + \frac{d\Psi_s}{dt} \tag{7-24}$$

By inserting this change in Equation (7-14) the stator winding asymmetry can be simulated.

7.5. Bond Graph of an AC Induction Motor

In BG modelling the systems are modelled as a set of elements which exchange energy in a manner that conserves power. In this research, a BG model of a three-phase ACIM using the natural reference frame has been produced to examine the effects of electrical faults on an ACIM. The BG model is depicted in Figure 7-2. This model is used to address the influence of a broken rotor bar and stator imbalance on the behaviour of the electromechanical system and includes both electrical and mechanical components. Typically, the start point when constructing a dynamic system such as a BG diagram are the power sources. In the ACIM, the (supply voltages) for the three phases u_{sa}, u_{sb} and u_{sc}, corresponding to the stator phase voltages $(a, b, \text{and } c)$. The effort source that simulates the rotor voltage, u_r is equal to zero because the simulated machine is a squirrel cage motor. It can be seen from the BG model that the stator and rotor winding resistances are shown using the R-field which are $(R_{sa}, R_{sb}, R_{sc}, R_{ra}, R_{rb}, R_{rc})$. Where $R_{sa,sb,sc}$ and $R_{ra,rb,rc}$ are, respectively, the resistances of the three stator and rotor phases.

The IC-field shown in Figure 7-2 combines I- and C- multiport to model the energy exchange and air gap flux that takes place between components of the system, as Equation (7-26) [101]:

$$\begin{bmatrix} \Psi_{sa,sb,sc} \\ \Psi_{ra,rb,rc} \end{bmatrix} = \begin{bmatrix} L_{ss} & L_{sr} \\ L_{sr} & L_{rr} \end{bmatrix} \cdot \begin{bmatrix} i_{sa,sb,sc} \\ i_{ra,rb,rc} \end{bmatrix} \tag{7-25}$$

The output effort from the IC port will be T_e, the generated electromagnetic torque. This will depend on rotor and stator currents and the phase angle between them, see bond number 13. The T_e will be consumed in overcoming J_m, the inertia of the machine and T_l, the mechanical torque (load) at the 1-junction (J7) that connected bonds (13-14 and 15) as shown in Figure 7-2. Such a representation enables the rotor speed to be calculated as a common flow of the (J7) junction. Consequently, using a BG approach enables diverse domains to be portrayed in one, single depiction based on the system structure, and causality relations between its components. This is the major benefit of using the BG method.
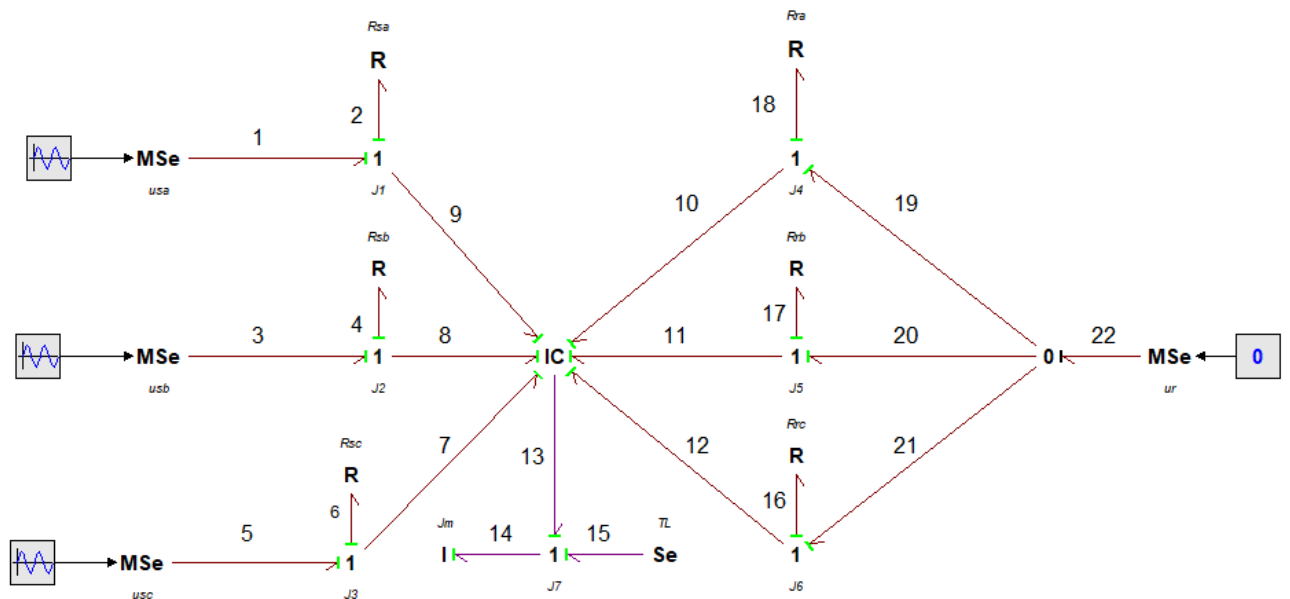
Figure 7-2 Presentation of Bond Graph for ACIM

The IC–port is used because Equations (7-9) and (7-12) contain the cosine and sine terms used to determine the angle θ_r which determines the position of the rotor, Equation (7-27). Concerning the shaft, the electromagnetic torque developed will be a function of both rotor and stator currents, and the angle separating them. This is shown as output E_{13} from the IC-port, see Equation (7-27). The electromagnetic torque, E_{13} is consumed into the 1-junction (J7) by the mechanical torque (T_l) and inertial moment (J_m). Equation (7-28) represents the mechanical expression.

$$T_e = E13 = \frac{p1}{2} \begin{bmatrix} F9 & F8 & F7 & F10 & F11 & F12 \end{bmatrix}. dL_{sr}. \begin{bmatrix} F9 \\ F8 \\ F7 \\ F10 \\ F11 \\ F12 \end{bmatrix} \qquad (7\text{-}26)$$

$$J_m \frac{d\omega}{dt} = T_e - T_l \qquad\qquad (7\text{-}27)$$

7.6. Summary

This chapter presented the development of the pictorial model that simulated the ACIM under different conditions, including broken rotor bar and stator imbalance. It started with the mathematical model of the healthy motor, then motor with broken rotor bar and motor with stator imbalance fault. Next, it introduced the bond graph model of the ACIM that simulate the ACIM in the natural reference frame using the IC-filed that coupled the electrical and mechanical components of the electro-mechanical system in order to highlight and present the predicted effects of electrical faults on the ACIM behaviour based on motor current analysis. The implementation and the result discussions and evaluation of this developed BG model would be introduced in the next chapter (see Chapter Eight). Additionally, this bond graph model will be used later in the qualitative simulation approach, see Chapter Nine.

Chapter 8 Implementation and Simulation Result of the Bond Graph Model

This chapter presents an assessment of the implementation of the bond graph model of the ACIM developed in the previous chapter and the simulation results obtained. Using the given system parameters the BG model was implemented in 20-SIM software. The model was used to simulate the dynamic behaviour of the squirrel cage ACIM under three different operating conditions: normal, broken rotor bar, and stator winding fault. Finally, the result obtained from predicted signals were evaluated against experimental data.

8.1. Introduction

To enhance the understanding of the effects of electrical faults on the behaviour of the ACIM, a BG dynamic model of a squirrel cage ACIM was developed. By using this model, it was possible to predict the behaviour of the current signature for the healthy condition and ACIM with two seeded electrical faults. The results obtained were assessed as to whether they could be used as a diagnosis rule and a benchmark for a qualitative simulation approach.

The BG model of the ACIM was implemented using 20-SIM software. The parameters of the motor used in the test bench are presented in Table 8-1. The model is initiated with 0% load at full speed for 0.6 seconds; the three-phase current are depicted in Figure 8-1. Figure 8-2 shows the motor speed for a healthy motor.

Table 8-1 ACIM parameters

MOTOR PARAMETER	Value
Voltage Vs	240 V
Supply Frequency	$F_s = 50$ Hz
Stator Resistance	1.2 Ω
Stator Leakage Inductance	0.0784 H
Rotor Resistance	1.87 Ω
Rotor Leakage Inductance	0.0784 H
Mutual Inductance	0.0709 H
Inertia	0.08 Kg.m^2
Number of pole pairs	P=2
Power Factor	0.84
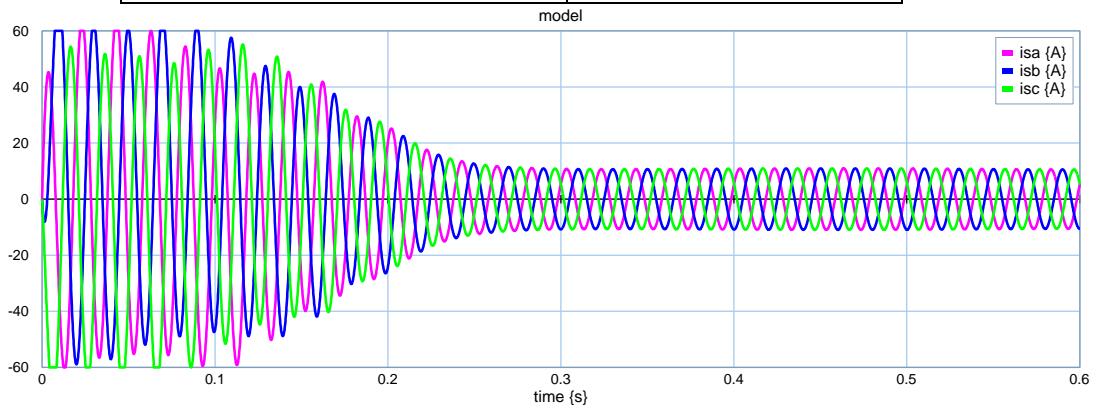
Figure 8-1 Stator currents predicted by BG model
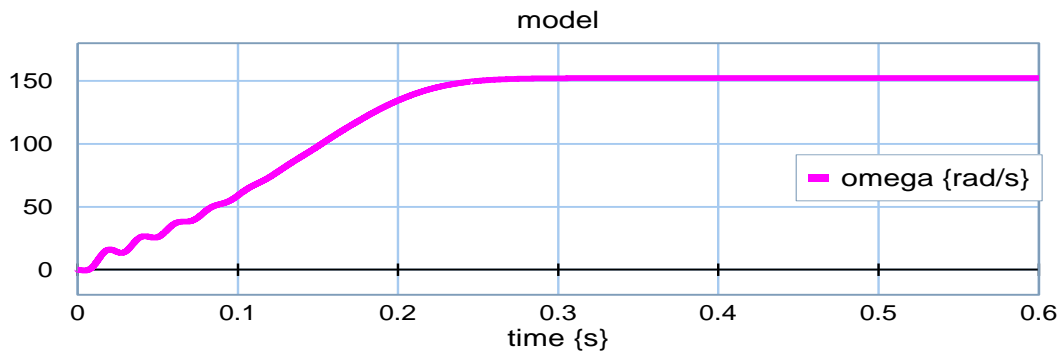
Figure 8-2 motor speed predicted by BG model

8.2. Model Validation against Experimental Data

Many monitoring techniques have been used for detecting ACIM faults. MCSA is a widely used technique, which detects faults using spectral analysis of the motor current signals. One of the most used spectrum analyses is FFT. In this study, the current signals generated from BG model were analysed and the frequency signature of the BRB and stator imbalance are identified using the FFT signal processing technique. This technique has been found to be an efficient method for the detection of electrical faults such as BRB and imbalanced stator winding [119].

8.2.1. Measured and Simulated Motor Current under Baseline (Healthy) Conditions

Figure 8-3 illustrates the current spectrum of a healthy motor for both simulated and measured data under full speed and various load conditions range between 0% and 80% of full load, with increments of 20%. It is clear from this figure that the simulated current spectrum closely matches the measured experimental spectrum.
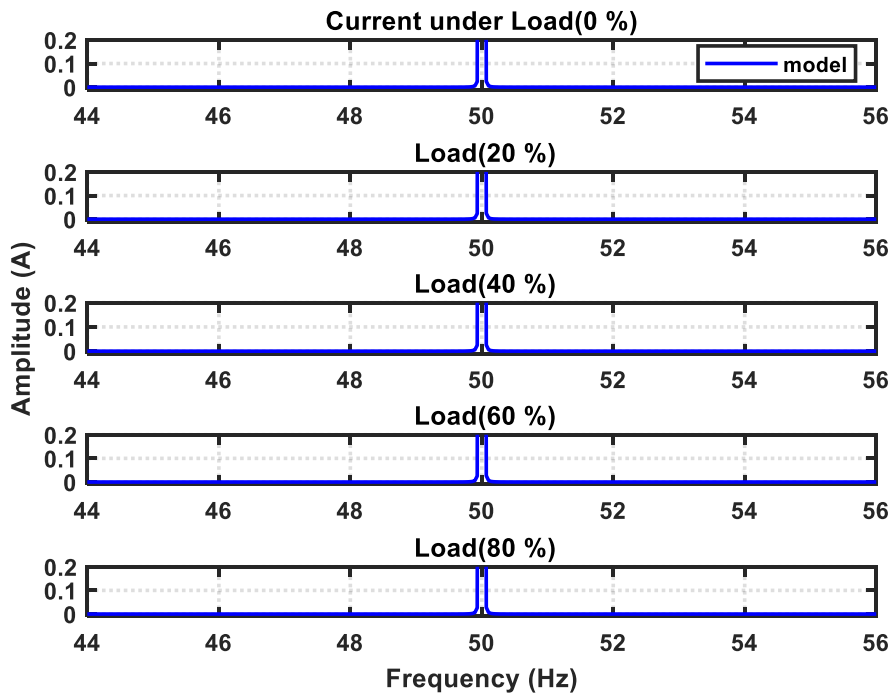
(a)
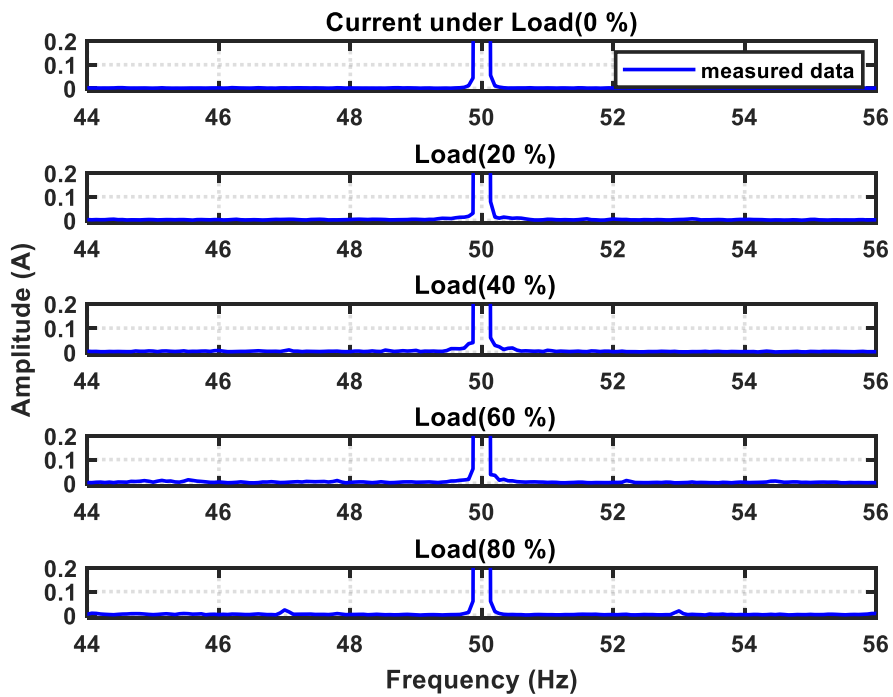
(b)

Figure 8-3 Simulated and measured current spectra of baseline motor under various load conditions

(a)   Predicted current spectrum of the Baseline ACIM,

(b)   Measured current spectrum of the Baseline ACIM

8.2.2. Measured and Simulated Motor Current with BRB

Generally, an electrical motor fault introduces changes to the spectral components of the healthy stator current [171]. With the occurrences of a broken rotor bar, the asymmetric magnetic field will generate frequency components at twice the slip frequency, $2sf_s$, around the supply frequency, f_s, in the stator current. These distinctive features of BRB fault are explained in Section 4.4.1.

Figure 8-4 and Figure 8-5, present the predicted and measured current spectrum of the ACIM with 1 and 2 BRBs at full speed, under zero load, and 20%, 40%, 60%, and 80% of full load. It is clear that the current spectrum of ACIM with a broken rotor bar fault shows as sidebands around the first harmonic of the current spectrum. It can be seen that the signals obtained from the bond graph model show the same behaviour of the signals acquired from the experimental study.
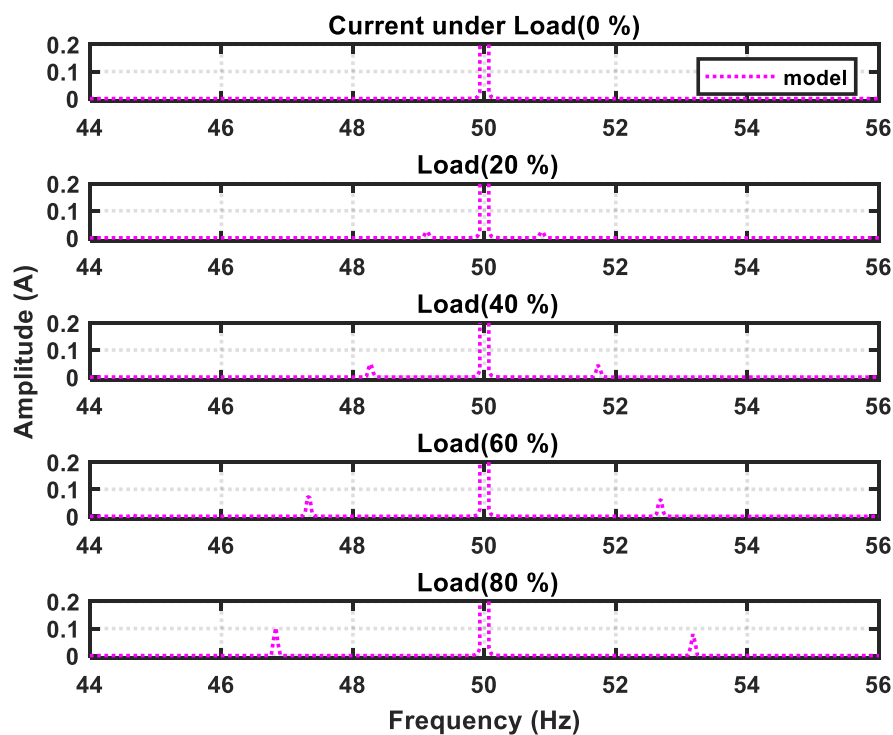
(a)   Predicted current spectrum of the ACIM with 1 BRB
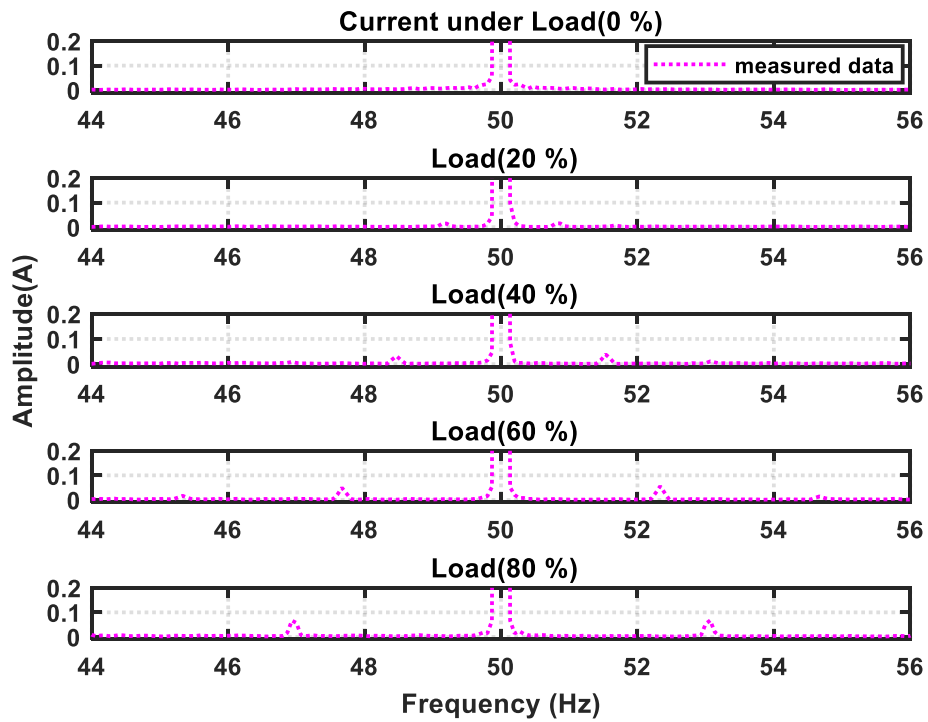
(b)Measured current spectrum of the ACIM with 1 BRB

Figure 8-4 Predicted and measured current spectrum of the ACIM with 1 BRB at full speed under zero load and 20%, 40%, 60% and 80% of full load (a) Predicted current spectrum of the ACIM with 1 BRB (b) measured current spectrum of the ACIM with 1 BRB

It is obvious that the value of 2sfs will change with the load as the value of the slip will increase. So the width of (fs ± 2sfs) will spread. Thus, with 20% of full load, the slip is small and |fs ± 2sfs| is about 1 Hz, but at 80% of full load the slip is much larger, and |fs ± 2sfs| is more than 3 Hz.
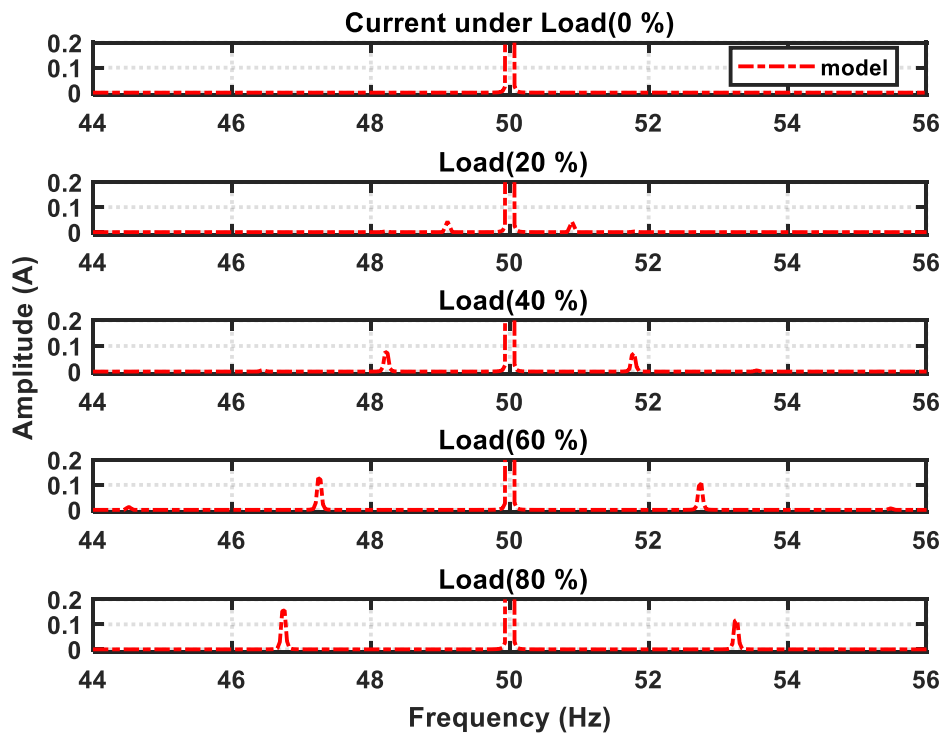
Predicted current spectrum of the ACIM with 2 BRB
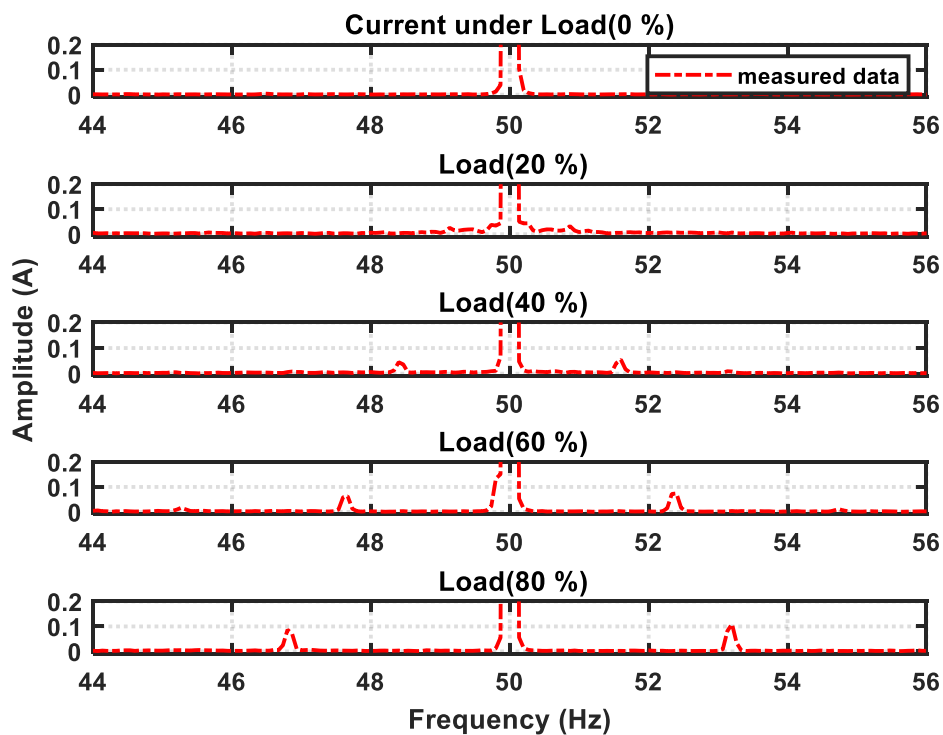
Measured current spectrum of the ACIM with 2 BRB

Figure 8-5 Current spectrum of the ACIM with 2 BRBs at full speed under zero load, and 20%, 40%, 60% and 80% of full load (a) Predicted current spectrum of the ACIM with 2 BRB , (b) Measured current spectrum of the ACIM with 2 BRB

8.2.3. Measured and Simulated Motor Current with Stator Winding Imbalance

Stator winding asymmetry caused changes in the dynamics of the current. Previous studies stated that the amplitudes at higher orders of the supply frequency components, particularly at 150 Hz, is increased under the effects of stator winding imbalance [117, 159]. To examine the response of the system and BG model under an unbalanced stator winding, current spectrums for the measured and predicted signals are presented in Figure 8-6, Figure 8-7, and Figure 8-8, which represent the spectrum comparison of the baseline motor and two deferent levels of winding imbalance Rfs0.2Ω and Rfs0.4Ω respectively. It is obvious that from these three figures, the measured and predicted signals behave similarly. The amplitude of the spectral peak at $3f_s$ is increased considerably, whatever the load. This is an indicator of stator winding asymmetry. The amplitude at the 3rd harmonic component 150 Hz under the effect of winding imbalance where (Rfs=0.4) is higher than the amplitude of the 3rd harmonic component 150Hz with Rfs=0.2 Ω
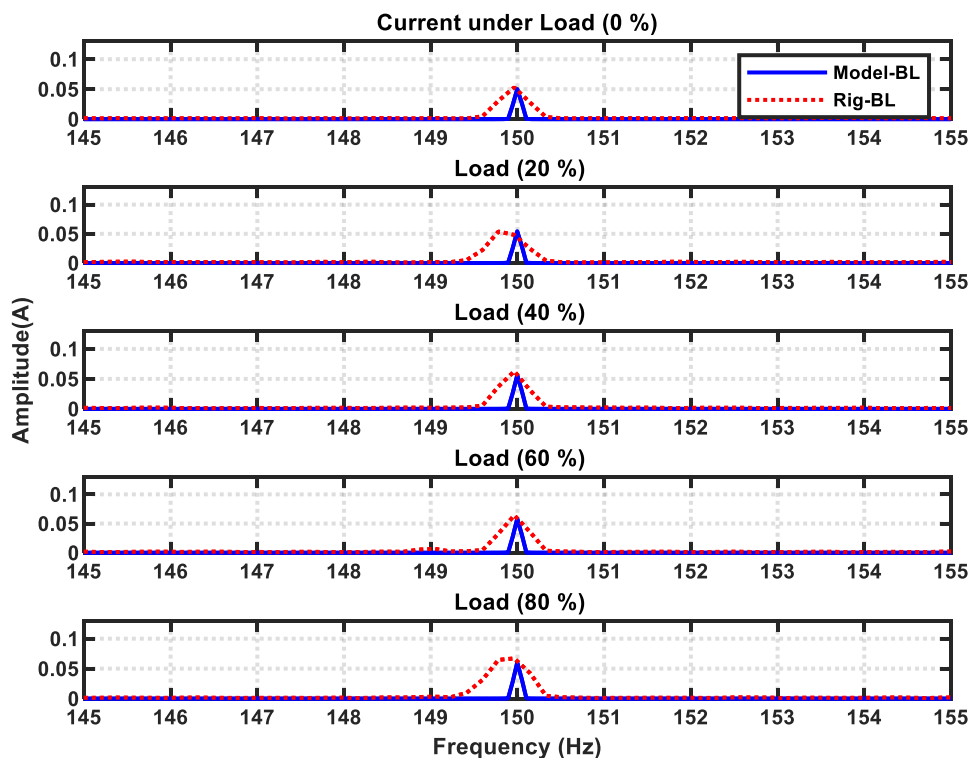
Figure 8-6 Predicted and measured current spectrum of the baseline ACIM at full speed under zero load and 20%, 40%, 60% and 80% of full load
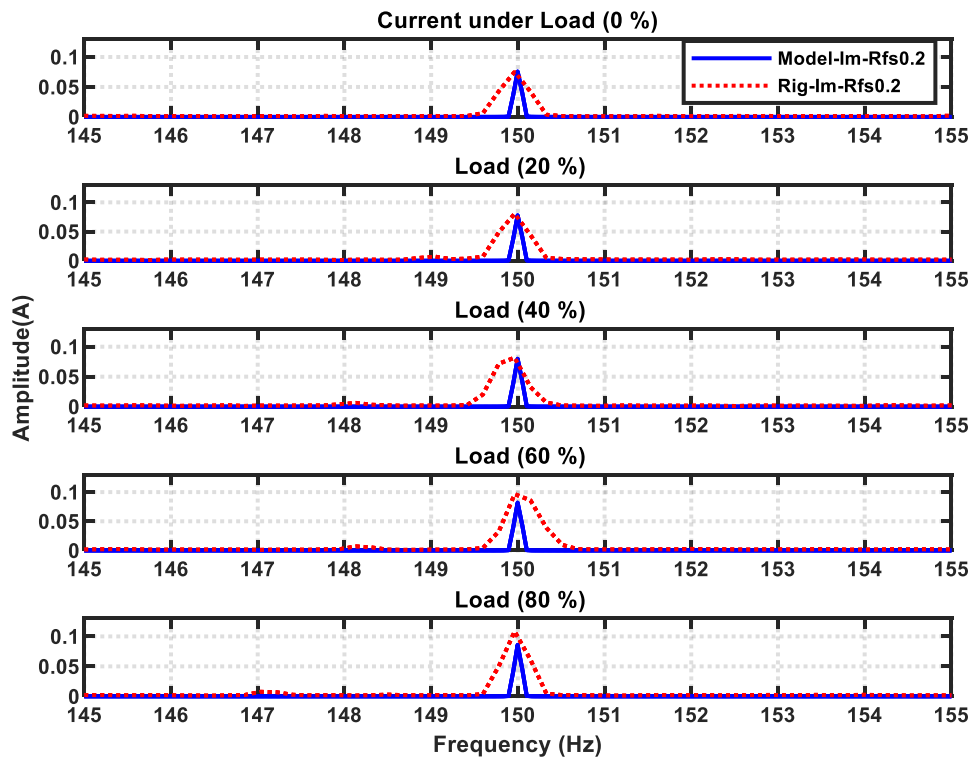
Figure 8-7 Predicted and measured current spectrum of the ACIM with stator winding asymmetry (Rfs 0.2) at full speed under zero load and 20%, 40%, 60% and 80% of full load
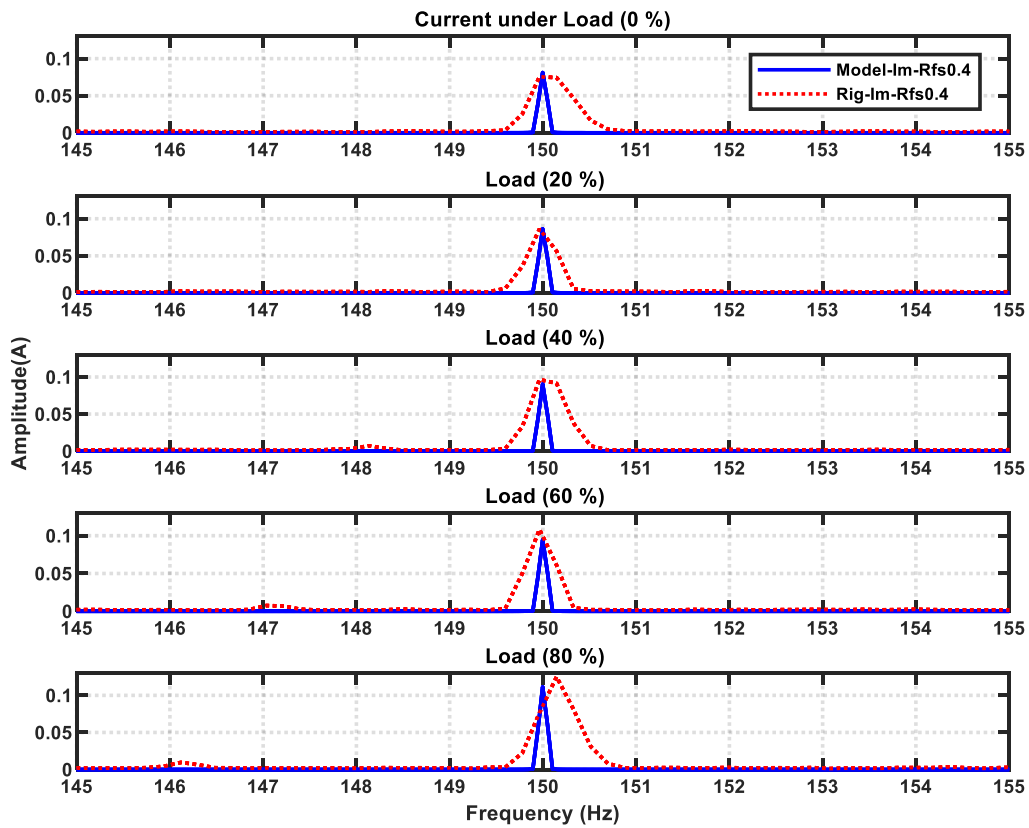
Figure 8-8 Predicted and measured current spectrum of the ACIM with stator winding asymmetry (Rfs 0.4) at full speed under zero load and 20%, 40%, 60% and 80% of full load

8.3. Results

Generally, ACIM faults caused the current spectra of a healthy motor to be modified by increasing the amplitude of specific harmonic components related to the fault. With a broken rotor bar fault, changes occur in the harmonic components f_s, $(f_s - 2sf_s)$ and $(f_s + 2sf_s)$. The effect of a stator winding fault is seen in the spectral peak at $3f_s$. This section provides a spectrum investigation for the detection and identification of BRB and stator imbalance faults under various load conditions and diverse fault severities.

8.3.1. Broken Rotor Bar

As stated in the literature [50, 66, 120, 171], a BRB modifies the current spectra by increasing the amplitude of the sidebands around the supply frequency at $(f_s \pm 2sf_s)$. This effect is shown clearly in simulated spectra seen in Figure 8-9. The figure shows the current spectra of the simulated signals for three different degrees of broken bar severity; baseline, 1 BRB and 2 BRB, under different loads. It is clear from this figure the amplitude of the sidebands vary significantly with both fault degree and torque load. The sidebands rise in amplitude with the rise of torque load. It can be seen that the value of 2sfs will change with the load as the value of the slip increases. This demonstrates that the appearance of a peak at $(f_s \pm 2sf_s)$ in the spectrum of the current signals provides a reasonable indication of the occurrence of a rotor breakage fault.

The results represented in the above-mentioned figure are in good agreement with those found by [50, 66, 120].

Figure 8-10 and Figure 8-11 present the trends of the lower $(f_s - 2sf_s)$ and upper $(f_s + 2sf_s)$ sidebands under various condition and different loads.
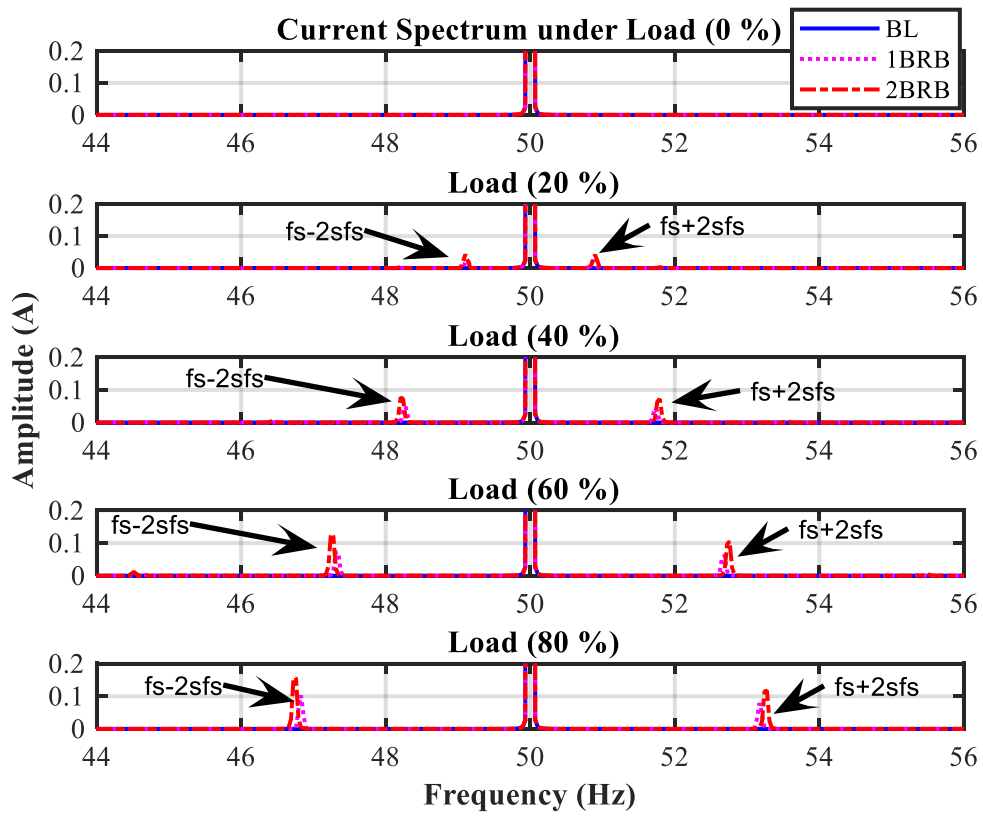
Figure 8-9 Predicted current spectra under different loads and different levels of BRB fault
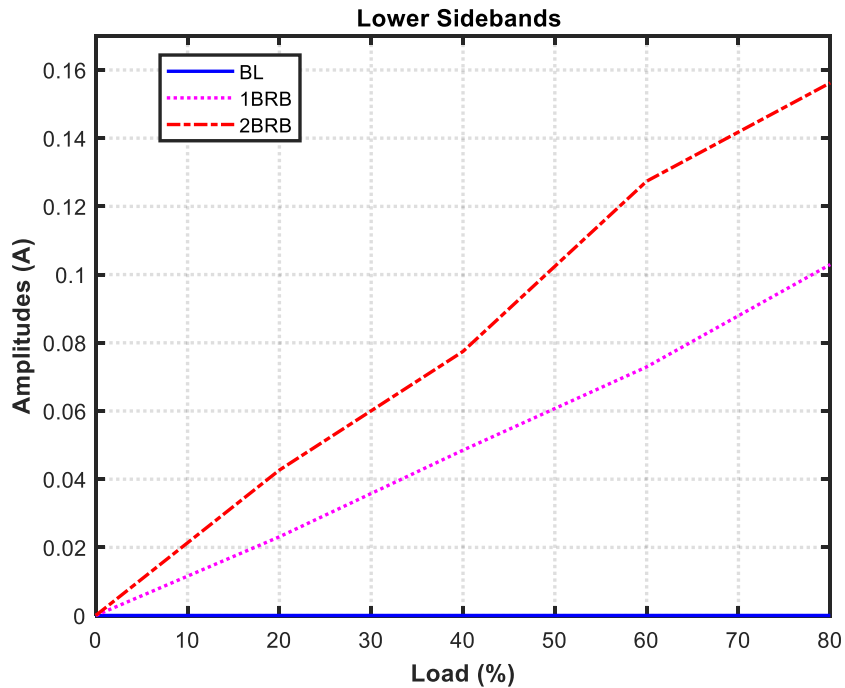
Figure 8-10 Comparison of the trends in amplitude of the lower side bands (fs - 2sfs) with increase in load
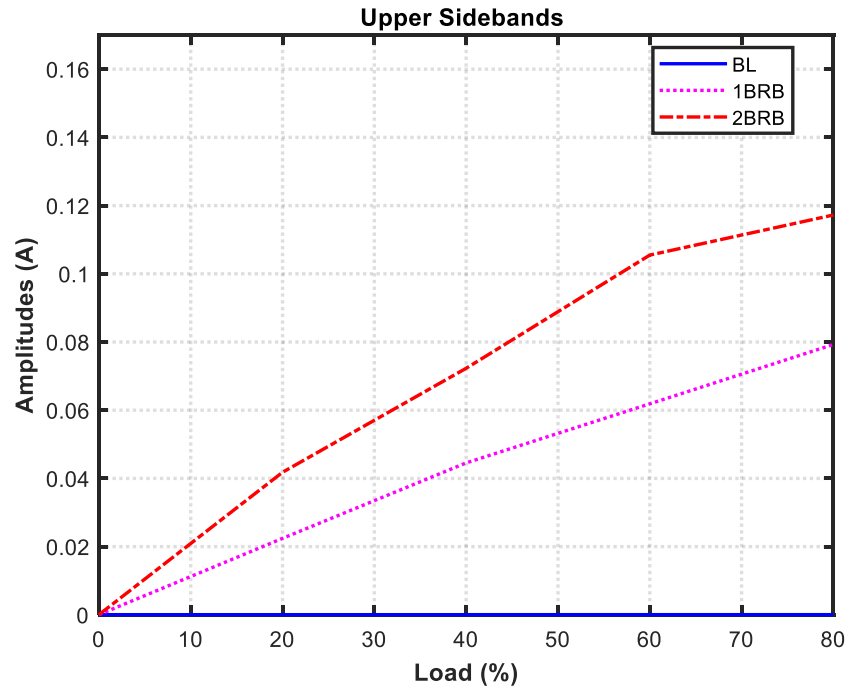
Figure 8-11 Comparison of the trends in amplitude of the upper side bands (fs + 2sfs) with increase in load

8.3.2. Stator Winding Asymmetry

It has been mentioned that the effects of stator imbalance is the harmonic frequency component at $3f_s$ in the stator current spectrum [172]. To examine the response of the system with an unbalanced stator winding, the simulated current spectra for the signals generated using the BG model are presented in Figure 8-12. It shows the current spectrum for ACIM, baseline and motor with two levels of winding imbalance under various load conditions at full speed. It is obvious that the amplitude of the harmonic components at 150 Hz increased with an increase in fault severity for all load conditions.
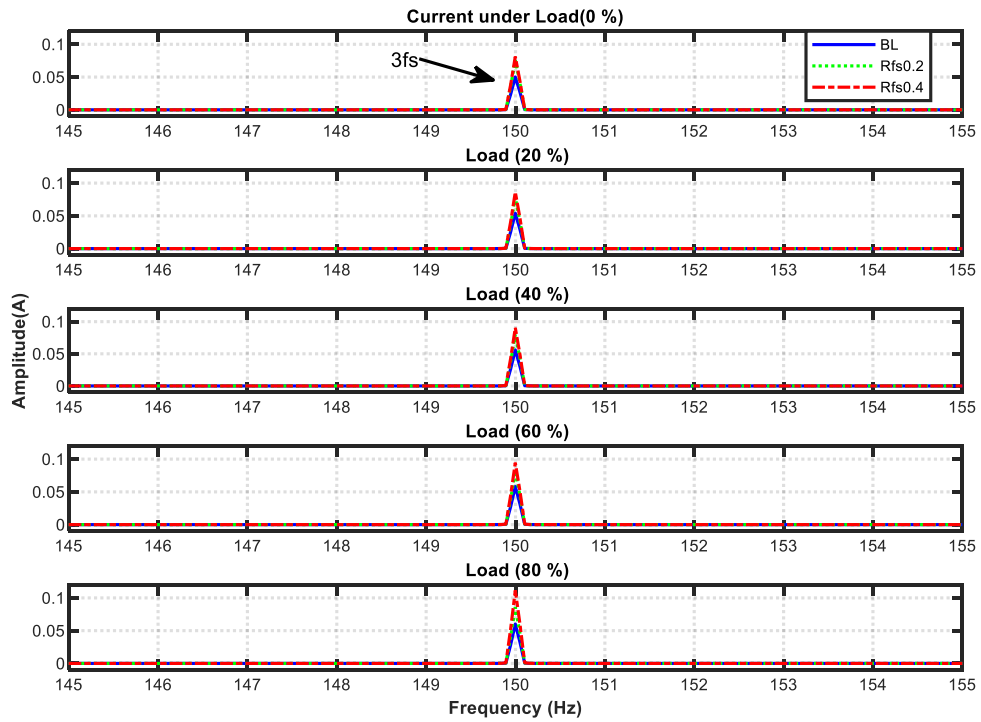
Figure 8-12 Predicted current spectra for different levels of stator imbalance for full speed at zero load and 20%, 40%, 60% and 80% full load

Figure 8-13 shows the simulated current at 3rd harmonics under different conditions, healthy and with two fault levels for stator imbalance, at full speed for 0, 20%, 40% 60%, and 80% of full load. The third harmonic at 150 Hz current component increased with the severity of the imbalance condition whatever the load.
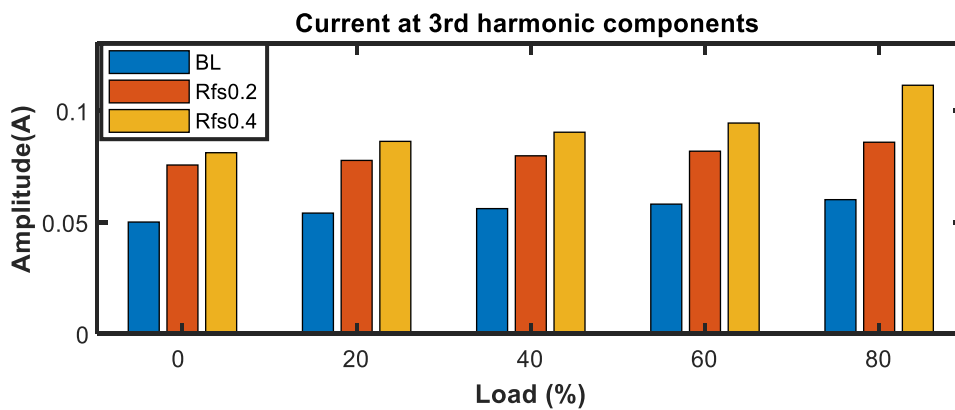
Figure 8-13 Simulated third harmonic components at different loads and levels of imbalance fault

8.4. Summary

This chapter presents the outcomes acquired using the BG model of an ACIM motor for the detection and diagnosis of a broken rotor bar and imbalanced stator winding based on the analysis of motor current. The figures presented to illustrate the effects of the given electrical faults on the current signals and the experimental results obtained validate the model predictions. Figure 8-3 to Figure 8-5 show that the predicted signals agree well with the measured signals for both healthy motor and motor with one/two broken rotor bars. It is shown that changes in the current spectrum vary significantly with load and motor fault. The broken rotor bar malfunction changes the stator current spectrum of the healthy machine by increasing the amplitude of the sidebands and the amplitude of the fundamental supply in the current spectrum.

Figure 8-7 and Figure 8-8 represent the current spectrum of the measured and predicted signals with stator winding imbalance. It can be seen from these figures that the amplitude of the third harmonic (150 Hz) increased significantly with the level of fault for all loads tested. These two figures show that the bond graph results are in good agreement with the corresponding results from the experiment.

The results represented in the above-mentioned Figure 8-9 are in good agreement with those found by [50, 66, 120].

Figure 8-12 and Figure 8-13 show an increase in the third harmonic amplitude with the fault level increase. These results are in good agreement with those obtained by Benbouzid and Kliman [159], Joksimovic and Penman [117] and Babaa, et al. [158]

To conclude, the model results introduced in this chapter give a good indication that the bond graph model could be applied for the condition monitoring of the ACIMs under the given faults. This model will be used later in Chapter Nine for the qualitative fault detection procedure.

Chapter 9 Qualitative Simulation Approach to ACIM Fault Detection

This chapter represents the implementation of the qualitative simulation (QS) approach, which is based on the construction of the Temporal Causal Graph (TCG) from the ACIM Bond Graph model developed in Chapter Seven.

First, this chapter provides a brief introduction to qualitative approaches, followed by the fault detection procedure. Next, it presents a novel TCG of the ACIM, forward fault propagation, and detection of the given electrical faults, broken rotor bar(s), and stator winding imbalance. It demonstrates the detection of the faults based on the TCG and forward propagation of the effects of parameter deviation on system behaviour. It also provides a simulation result for validation of the qualitative fault detection. Then, it presents a qualitative fault diagnosis based on the changes in amplitudes of the current signal spectrum at frequencies $(f_s + 2sf_s)$ and at $3f_s$, caused by BRB and stator IM, respectively. Finally, it evaluates the graphical causality based fault detection approach based on a comparison with a comparable work from the literature.

9.1. Introduction

In qualitative approaches, relations between the modelled system's inputs and outputs are simulated by qualitative expressions. Such an approach can be used to examine and enhance the understanding of ACIM behaviour under, say, the effect of electrical faults. Bond Graph modelling and QS approaches are potential for fault detection because qualitative models can be derived from numerical models, and simulation studies are less parameter-dependent and more computationally efficient. The choice of BG modelling is based on the use of causality relations to avoid spurious solutions that occur in most QS methods.

This chapter aims to develop the temporal causal graph and then use it for studying the effect of a broken rotor bar and stator winding imbalance on the system response. The results illustrate the behaviour of the ACIM in the presence of these two types of electrical faults.

9.2. Bond Graph Model of ACIM

To evaluate the performance of the qualitative fault detection approach, the BG model developed in Chapter Seven is again shown in Figure 9-1 to make it easier for the reader to follow the structure. The TCG is constructed based on the sequential assignment procedure as explained in Chapter Five; Section 5.5.1.
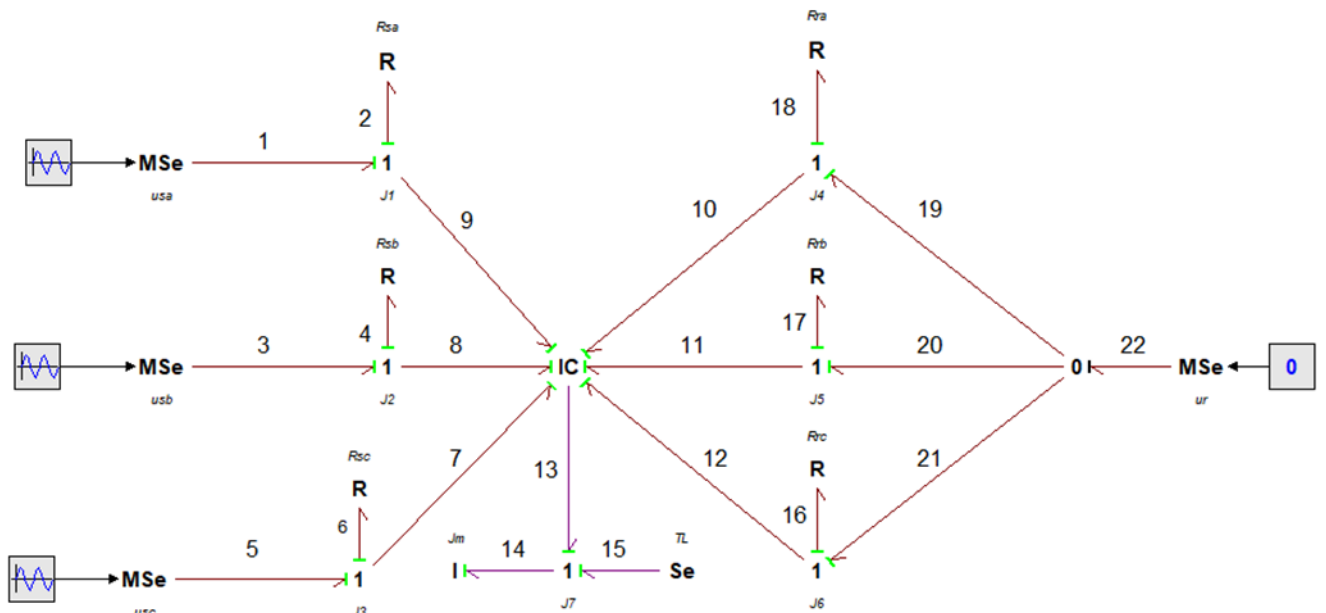
Figure 9-1 Depiction of a BG Model of ACIM in (A, B and C) reference frame
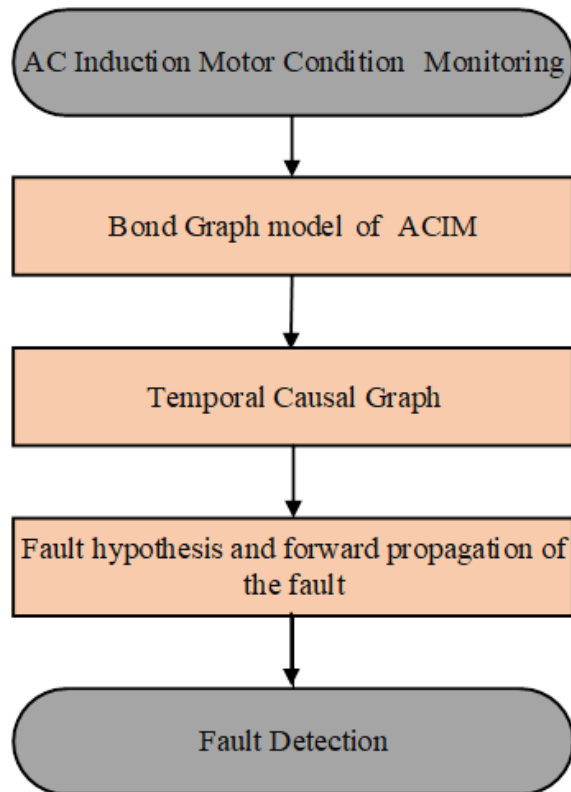
Figure 9-2 Flowchart of the qualitative fault detection procedure for fault detection in an ACIM

9.3. Qualitative Equations

The qualitative equations of AC induction motor are generated from the BG model shown in Table 9-1, which represent the associations between system components to derive the system behaviour.

In order to generate qualitative equations from the BG, a step by step approach is needed [173]. The effort and flow equations of the ACIM BG model are shown in Table 9-1, and the effort and flow variables are shown in Table 9-2.

Table 9-1 Qualitative equations from ACIM Bond Graph model

Effort Equations	Flow Equations
E1 = E2 + E9	F1 = F2 = F9
E2 = R2 ∗ F2	F3 = F4 = F8
E3 = E4 + E8	F5 = F6 = F7
E4 = R4 ∗ F8	F10 = F18 = F19
E6 = R6 ∗ F6	F11 = F17 = F20
E5 = E6 + E7	F12 = F16 = F21
E19 = E18 + E10	$(F9, F8, F7, F10, F11, F12)$ $$= L * \left(\int E9, \int E8, \int E7, \int E10, \int E11, \int E12 \right)$$
E19 = E21 = E20	$F15 = \dfrac{1}{Jm}(E13 - E15)$
E20 = E17 + E11	F13 = F15 = F14
E18 = R18 ∗ F18	
E20 = E17 + E11	
E17 = R17 ∗ F17	
E21 = E16 + E12	
E16 = R16 ∗ F16	
E13 $= (F9, F8, F7, F10, F11, F12)$ $∗ dl/d\theta$	

Table 9-2 Effort and flow variables in the qualitative equations and TCG

Effort	Meaning	Flow	Meaning
E1	Voltage source	F1	Phase A current flow
E2	Voltage drop across R_{sa}	F2	Current go through R_{sa}
E3	Voltage source	F3	Phase B current flow
E4	Voltage drop across R_{sb}	F4	Current go through R_{sb}
E5	Voltage source	F5	Phase C current flow
E6	Voltage drop across R_{sc}	F6	Current through R_{sc}
E7	Voltage drop across Inductance stator A	F7	Current flow through Inductance stator C
E8	Voltage drop across Inductance stator B	F8	Current flow through Inductance stator B
E9	Voltage drop across Inductance stator C	F9	Current flow through Inductance stator A
E10	Voltage drop across Inductance rotor A	F10	Current flow through Inductance rotor A
E11	Voltage drop across Inductance rotor B	F11	Current flow through Inductance rotor B
E12	Voltage drop across Inductance rotor C	F12	Current flow through Inductance rotor C
E13	Motor induced torque	F13	Rotor speed (flow)
E14	Inertia torque	F14	Rotor speed (flow)
E15	Load torque	F15	Rotor speed (flow)
E16	Voltage drop across R_{rc}	F16	Current go through R_{rc}
E17	Voltage drop across R_{rb}	F17	Current go through R_{rb}
E18	Voltage drop across R_{ra}	F18	Current go through R_{ra}
E19	Rotor phase A voltage	F19	Rotor current phase A
E20	Rotor phase B voltage	F20	Rotor current phase B
E21	Rotor phase C voltage	F21	Rotor current phase C

9.4. Temporal Causal Graph

The TCG is constructed from the ACIM BG model shown in Figure 9-1, see Chapter Five; Section 5.5 for more detail.

A TCG is certainly a graph that introduces the cause-effect relations involving the power variables within the BG model. The TCG of the ACIM, Figure 9-3 is derived from the BG model in Figure 9-1. The vertices in the TCG are the effort and flow variables, and the relations between them are the edges [3]. The behaviour of the system is modelled by the relationships

allocated to control junctions and to those between the components of the system. An edge allocated a "1" shows the variables are directly proportional, similarly a "-1" shows the flows are inversely proportional [6]. A graph edge assigned an "=" indicates the two variables linked by this edge are equal in value, for example $F2 \xrightarrow{=} F9$ in Figure 9-3. This is because bond No. 2 and bond No. 9 are connected with a 1-junction which it is a common flow junction. When an edge is linked to system elements, it illustrates the relation between them, so that for the simplest electrical circuit i.e. a resistor with effort causality, the edge linking the effort and flow has the value of the resistance (R). In bond No. 2 the relation between the effort E2 and the flow F2 is ($E_2 \xrightarrow{R2} F_2$). The relation that has deferential equations it has (int) which implies integration for example the relation $F_{15} \xrightarrow{1/jm(int)} E_{13} - E_{15}$).
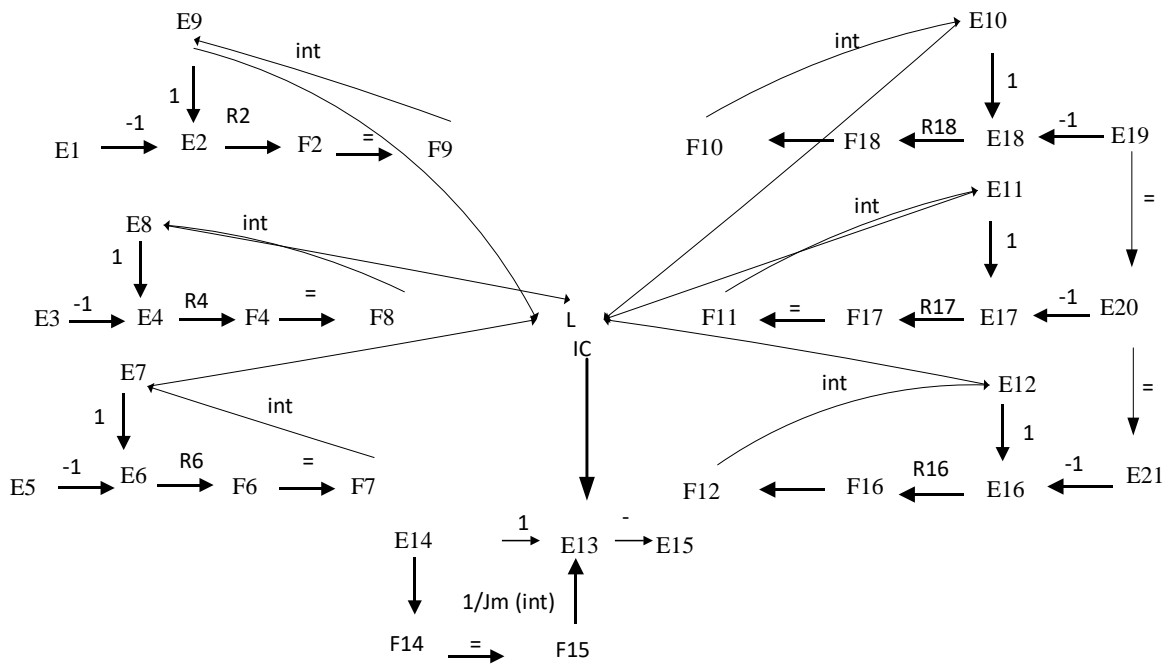
Figure 9-3 Depiction of the temporal casual graph of ACIM BG model

To detect the effects of the fault, TCG and forward propagation can be executed based on a fault hypothesis.

The notations $R2, R4, R6$ are the resistance of stator phases A, B, C in the TCG and $R18, R17, R16$ are the resistance of rotor phases A, B, C in the TCG. The effort and flow variables are tabulated as in Table 9-2.

9.5. Fault Detection Procedure

According to [174], "to find the correct parameter deviation, predictions of future behaviour are generated by forward propagation and continued monitoring of the predicted behaviour."

The QS approach applies qualitative investigation to identify the effects of changes (increases) in the various parameters on behaviour of the system. It is based on the analysis of steady state behaviour. Figure 9-2 represents the qualitative fault detection procedure.

Firstly, causality assignment is used to derive the TCG from the BG model. Then one or more of the relevant measured parameters are used to generate a fault hypothesis. Secondly, forward propagations is used to derive the future response of the system based on a fault hypothesis that will allow detection of the effect(s) of the fault.

Variations from nominal behaviour can be expressed qualitatively as; (-), (+), (0), and (.), where (-) implies decreasing, (+) implies increasing, (0) means steady conditions, and (.) represents unknown qualitatively, increasing and/or decreasing [175] [136]. This research assumes the unknown qualitatively as a fluctuating (unbalanced) condition.

9.5.1. Broken Rotor Bar Fault Detection Algorithm

The effects of a broken rotor bar is commonly modelled by calculating the increase of the rotor resistance phase/phases. Thus the algorithm starts by assuming the rotor resistance of phase A (R18 in the TCG see Figure 9-3) is increased. Then a forward propagation was carried out to detect system behaviour under the fault, using the TCG and its causality relations.

When $R18^+$, the resistance of phase A is exceeding its given value, forward propagation on the TCG commences along $E18 \xrightarrow{R18} F18$ which indicates that the effort $E18^+$ will be above normal and the flow $F18^-$ is below normal. First, forward propagations will construct the effect of the increase of effort $E18^+$ along $E19 \xrightarrow{-1} E18$ implies $E19^-$ (the value of E19 decreases) then the equal relation on $E19 \xrightarrow{=} E20$ implies $E20^-$ (the value of E20 decreases). The inverse relation $E20 \xrightarrow{-1} E17$ indicates $E17^+$ (the value of E17 increases) and, in turn, this implies the flow $F17^+$ (the value of F17 increases) then the equal relation $F17 \xrightarrow{=} F11$ implies $F11^+$ (the value of F11 increases) and again, in turn, this implies $E13^+$ (the value of E13 increases).

Continuing the forward propagation, the effect of the equal relation $E20 \xrightarrow{=} E21$, indicates $E21^-$ and the inverse relation $E21 \xrightarrow{-1} E16$ implies $E16^+$, and this increase causes an increase of the flow $F16^+$ due to the relation $E16 \xrightarrow{R16} F16$, then the equality $F16 \xrightarrow{=} F12$ means the flow $F12^+$ increases which, in turn, leads to an increase of $E13^+$ from the relation $E13 = [F9 \ F8 \ F7 \ F10 \ F12 \ F11] * \frac{dl}{d\theta}$.

Third, the forward propagation that the flow $F18^-$ indicates the flow $F10^-$ is decreased which caused the electro-mechanical torque to decrease $E13^-$.

The findings from the forward propagation show that the increase of rotor resistance, caused unbalanced flow in the rotor, as well as unbalanced motor torque.

9.5.2. Stator Imbalance Fault Detection Algorithm

To simulate the stator winding imbalance, an extra resistance was added to one phase of the stator, and the algorithm for prediction of an imbalance fault started from this. Thus the qualitative fault detection of stator imbalance began by supposing that the resistance of stator phase A (R2 in the TCG, Figure 9-3) increased due to a defect in the stator winding. Then, as in Section 9.5.1, a forward propagation was carried out to predict system behaviour under the fault, using the TCG and its causality relations.

When the stator resistance in phase A (R2 in the BG Figure 9-1, and its TCG Figure 9-3) increased above its nominal value, forward propagation starts at $E2 \xrightarrow{R2} F2$ which caused the effort $E2$ to increase (voltage drop on the resistance of phase A) and decreased the flow $F2$ (the current through Rsa, stator resistance).

First, forward propagations will construct the effect of the increase of $E2^+$. From the relation $E2 \xrightarrow{1} E9$ the effort E9 will increase. Thus from the relation that connect the current flow with the efforts at IC-field the current flow through inductance stator B (F8) and the current flow through inductance stator C (F7) will increase as $E9^+$ increase. This implies that the motor induced torque (Te) $E13$ will increase as expressed in the following relation:

$$E13 = [f9 \ f8 \ f7 \ f10 \ f12 \ f \ 11] * \frac{dl}{d\theta}.$$

Forward propagation considering the effects of the flow $f2^-$ indicates that flow $f9^-$ (current flow through inductance stator A) decreased which causes the electro-magnetic torque $E13^-$ to decrease .

The findings from the forward propagation show that the increase of stator resistance, caused unbalanced current flow through the stator winding, as well as unbalanced motor torque.

9.6. Results and Discussion

9.6.1. Broken Rotor Bar Prediction Using TCG

In the ACIM, the effect of a BRB is a rise of the rotor resistance. Figure 9-4 illustrates the forward propagation of the effect of the increase of the rotor resistance, as explained in Section 9.5.1. The effects of a broken rotor bar is an unbalanced increase in the rotor resistance, causing an unbalanced current flow in the rotor bars and an unbalanced electromagnetic torque. The unbalanced electromagnetic torque is taken as an indicator of the broken rotor bar fault.

$$R18^+ \rightarrow \begin{cases} E18^+ \rightarrow E19^- \rightarrow E20^- \rightarrow \begin{cases} E17^+ \rightarrow f17^+ \rightarrow f11^+ \rightarrow \\ E21^- \rightarrow E16^+ \rightarrow f16^+ \rightarrow f12^+ \rightarrow \end{cases} \begin{cases} E13^{(\cdot)} \end{cases} \\ f18^- \rightarrow f10^- \rightarrow \end{cases}$$

Figure 9-4 Forward propagation of $R18+$

This result agrees with the simulation result of the BG model as illustrated in Figure 9-6 to Figure 9-10, which represent flows F10, F11 and F12 through the rotor phases, and the E13 electromagnetic torque for a healthy motor, and motor with broken rotor bar respectively. This is in agreement with previous work [120, 176], which confirms that a BRB results in the flow of unbalanced current and increased torque pulsations.

9.6.2. Stator Winding Imbalance

The qualitative approach aims to investigate the effect of the deviation (increase) of the resistance of one phase of the stator. Figure 9-5 represents the forward propagation of phase (A) resistance R2+. As explained in Section 9.5.2.

$$R2^+ \rightarrow \begin{cases} F2^- \rightarrow F9^- \rightarrow \\ E2^+ \rightarrow E9^+ \rightarrow \begin{cases} F8^+ \rightarrow \\ F7^+ \end{cases} \begin{cases} E13^{(\cdot)} \end{cases} \end{cases}$$

Figure 9-5 Forward propagations of the increase of stator resistance, R2+

These findings from forward propagation indicate that the increase of resistance in one phase caused unbalanced motor current and fluctuated electromagnetic torque. These results are in good agreement with the simulation result in the next section, also in good agreement with the result in the literature [159] .

9.7. Simulation Results Validation

To investigate the behaviour of the ACIM BG model it has been implemented in 20-sim under different conditions. The parameters of the motor are as shown in Table 8-1.

9.7.1. Effects of Rotor Broken Bars

Figure 9-6 and Figure 9-7 represent the electromagnetic torque (E13) in the TCG for the healthy motor and motor with BRB respectively. It can be seen from Figure 9-7 that the electromagnetic torque of the motor with a broken bar fluctuates in amplitude compared with the torque of the healthy motor.
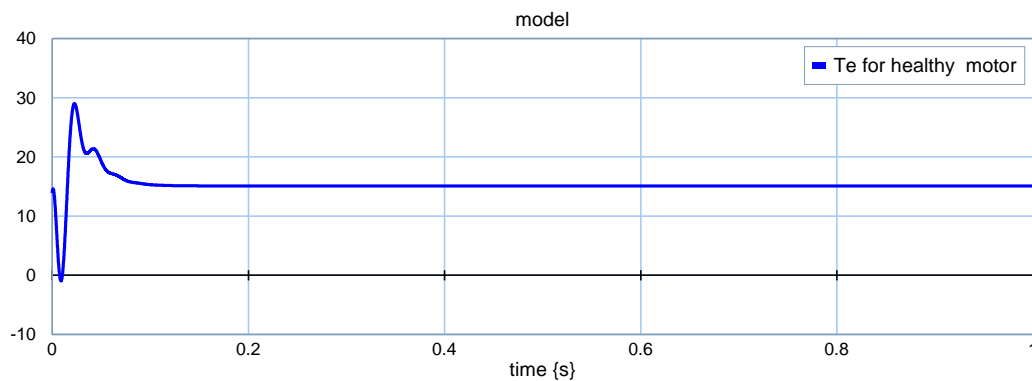
Figure 9-6 Representation of the motor electromagnetic torque T_e for a healthy motor (Effort E13 on the ACIM BG model and its TCG)
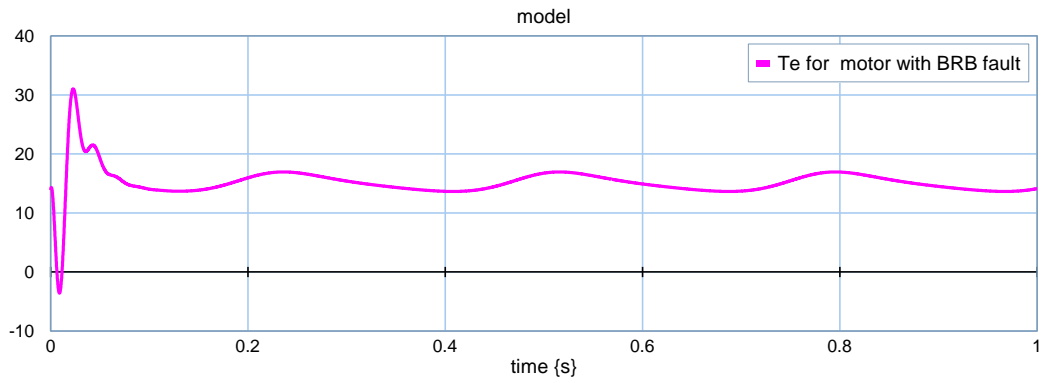
Figure 9-7 Representation of the motor electromagnetic torque T_e with broken rotor bar (Effort E13 on the ACIM BG model and its TCG)

RMS values of the current were utilized to examine the motor's condition. Figure 9-8 presents the RMS values of the current flow in bond No. 10 on the BG model and TCG that simulated the current flow in the rotor phase (A) under different load conditions for baseline motor and motor with BRB. The flow current is decreased under the effects of a broken rotor bar. This agrees with the result of the QS in Section 9.6.1. It can be seen that variations in the RMS values vary significantly with the level of fault.
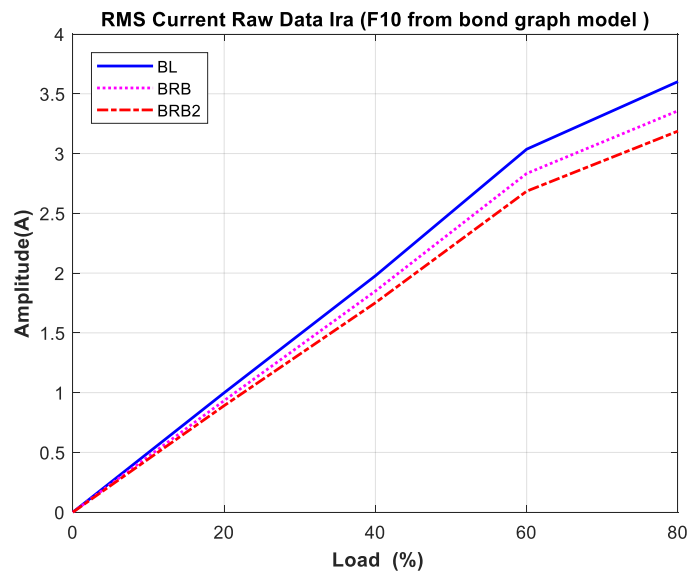
Figure 9-8 Depiction of the RMS current flow F10 under different levels of BRB fault
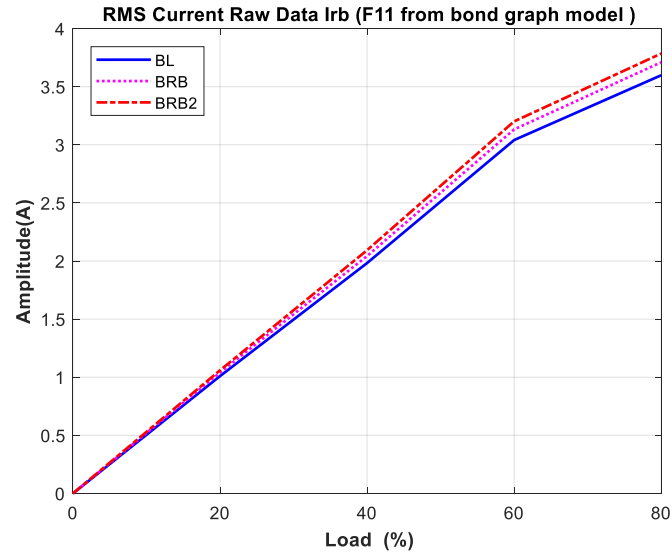
Figure 9-9 Depiction of the RMS current flow of |F11 under different levels of BRB fault
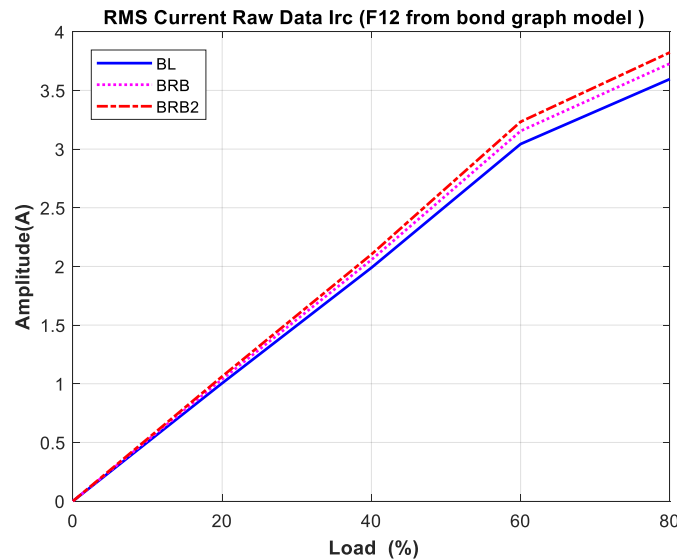
Figure 9-10 Depiction of the RMS current flow of f12 under different levels of BRB fault

Figure 9-9 and Figure 9-10 represent the current flow in the rotor conductors in phase B and phase C of the rotor. The flow of the current is seen in these two figures to increase in the presence of a broken rotor bar. These finding show the increase of rotor resistance caused by the broken rotor bar fault lead to an unbalanced current flow in the rotor, which produced unbalanced torque.

9.7.2. Effect of Stator Winding Imbalance

The current signals of stator phase A under different levels of the imbalanced stator winding are shown in Figure 9-11. It is obvious that the flow of the current is decreased significantly in the presence of the seeded defect (adding a resistance to phase A). In contrast, the current flow

of the other two phases, B and C, are increased in the presence of the fault, see Figure 9-12 and Figure 9-13.
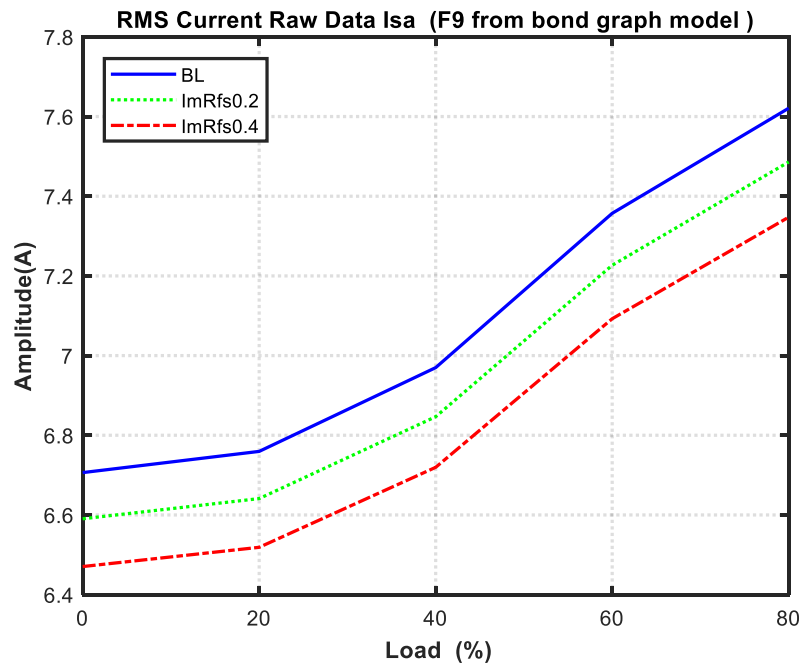
Figure 9-11 RMS current flow in stator phase A (f9 on the ACIM BG model and its TCG)
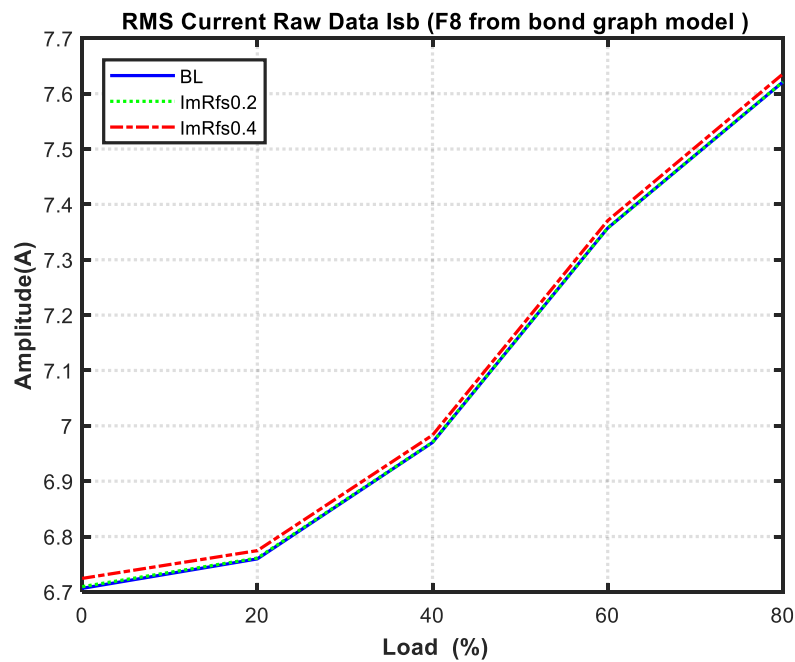
Figure 9-12 RMS current flow in stator phase B (f8 on the ACIM BG model and its TCG)
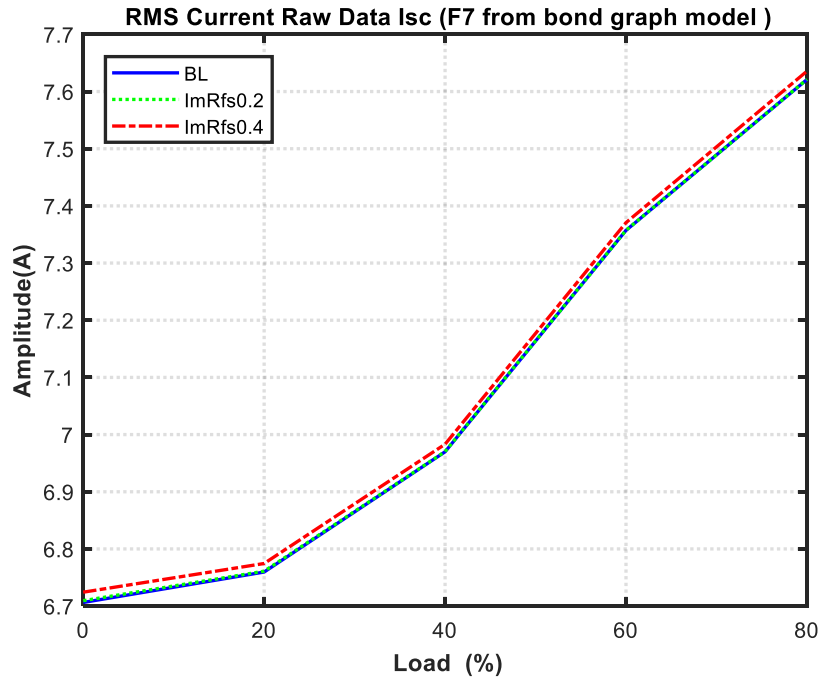
Figure 9-13 RMS current flow in stator phase C (f7 on the ACIM BG model and its TCG)

Depiction of the motor electromagnetic torque with stator imbalance is shown in Figure 9-14. It is clear from the figure that the imbalance in stator winding produced torque pulsations compared with healthy motor torque, see Figure 9-16, and much more rapid pulsations than were produced by broken rotor bar, Figure 9-7.
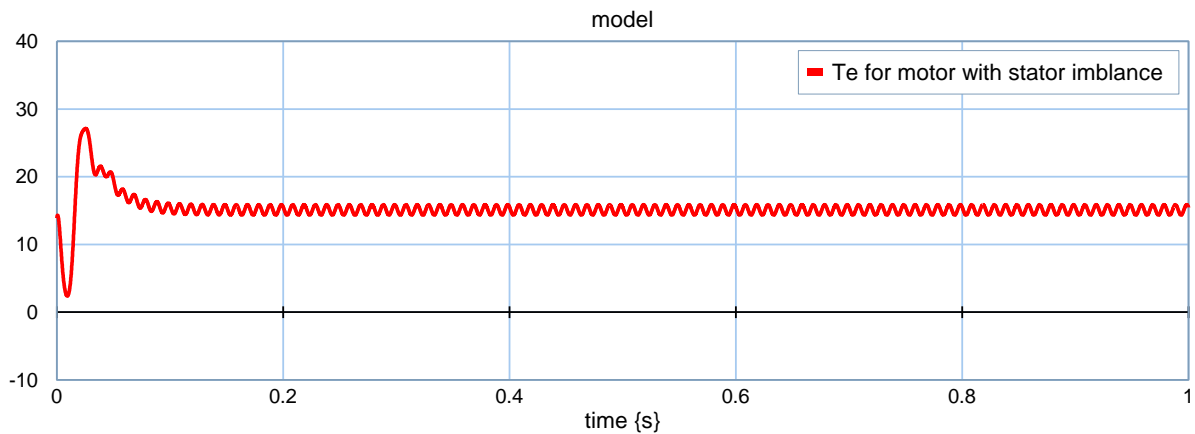
Figure 9-14 Representation of the motor electromagnetic torque Te with stator winding imbalance (Effort E13 on the ACIM BG model and its TCG)

9.8. Fault Diagnosis based on the Qualitative Influence of the Fault on the Motor Current Signals

In this section a qualitative fault diagnostic approach is developed to detect the faults discussed in Section 9.5. It is well known that any asymmetry of the motor leads to the appearance of

peaks in the current spectrum. The relationship between the amplitude of these peaks and fault occurrence is investigated.

Broken rotor bars and stator imbalance are diagnosed based on their qualitative influence on the motor current spectrum. The increase of spectral amplitude at $(f_s + 2sf_s)$ and $3f_s$, caused by a broken rotor bar and stator imbalance respectively, will be considered for fault diagnosis based on the reference values obtained for each fault case. Figure 9-15 shows the qualitative fault diagnosis procedure for a broken rotor bar fault. The fault diagnosis procedure for stator imbalance is illustrated in Figure 9-16.
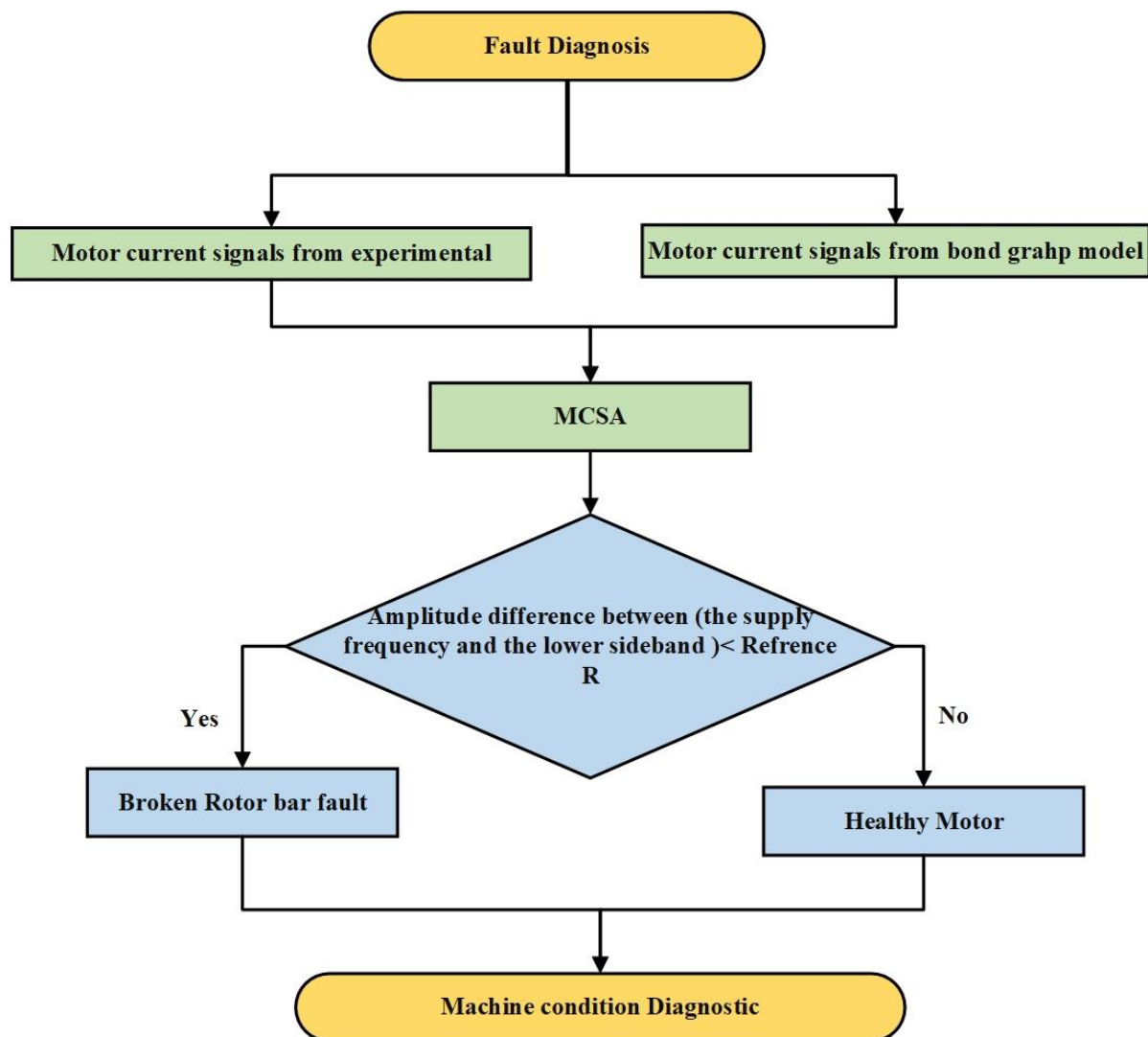
Figure 9-15 Qualitative fault diagnosis procedure for broken rotor bar fault
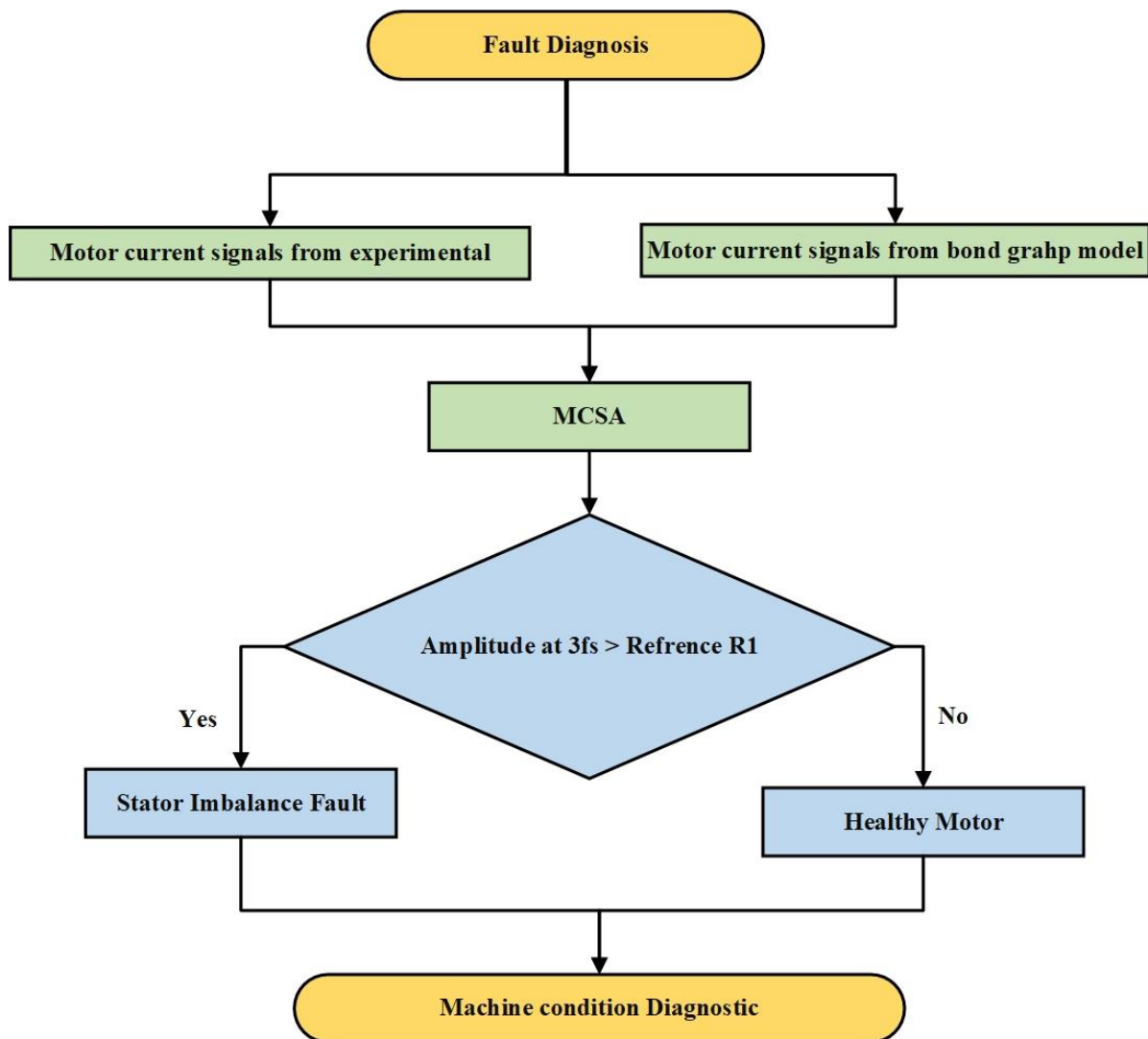
Figure 9-16 Qualitative fault diagnosis procedure stator winding imbalance fault

9.8.1. Broken Rotor Bar Fault Diagnosis Algorithm

In the case of broken rotor bar fault, the investigation was based on the amplitude difference between the supply frequency and the lower sideband around the supply frequency, so if the difference is less than a prescribed value, R say, it means there is increase in the amplitude of the lower sideband peak and a broken rotor bar is diagnosed. However, if the difference is greater than R it implies that there is no increase in the amplitude of the sideband and the motor can be considered healthy. This provides a qualitative measure that allows the amplitude of the sideband to be used as an effective indicator.

Previous studies [48, 157, 177] have stated that the amplitude difference of the lower sideband and the fundamental supply can be used as indicator of the presence of broken rotor bar fault. Detailed analysis of the model data presented in Figure 9-17 to Figure 9-21 allows tabulation of the value of R for each case, see Table 9-3.

Figure 9-17 to Figure 9-19 represent the current spectrums of the BG signals to show the amplitude differences between the baseline condition and with a broken rotor bar fault where the amplitude of the lower side band will be used as an indicator of the presence of one or more broken rotor bars.
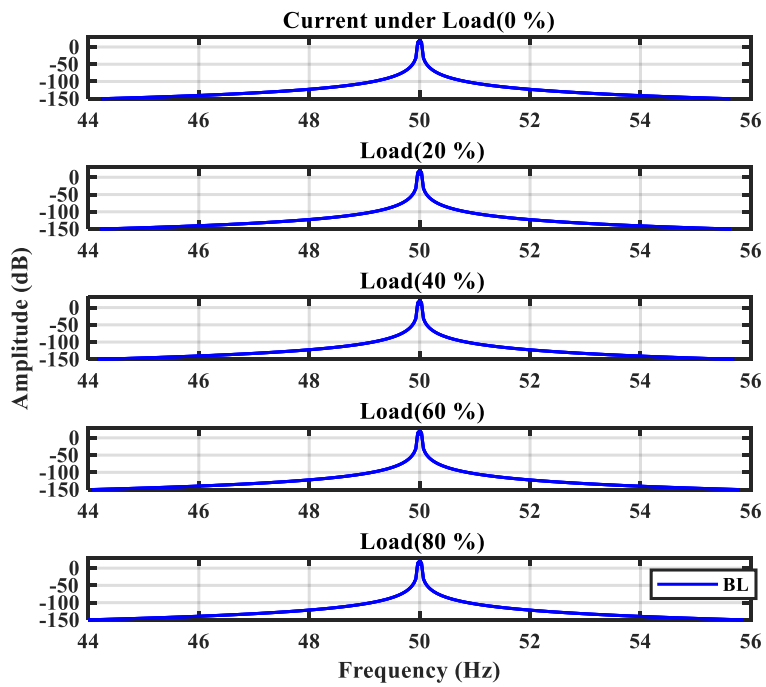
Figure 9-17 Current spectrum around the supply frequency of BG signals for baseline motor under five load conditions
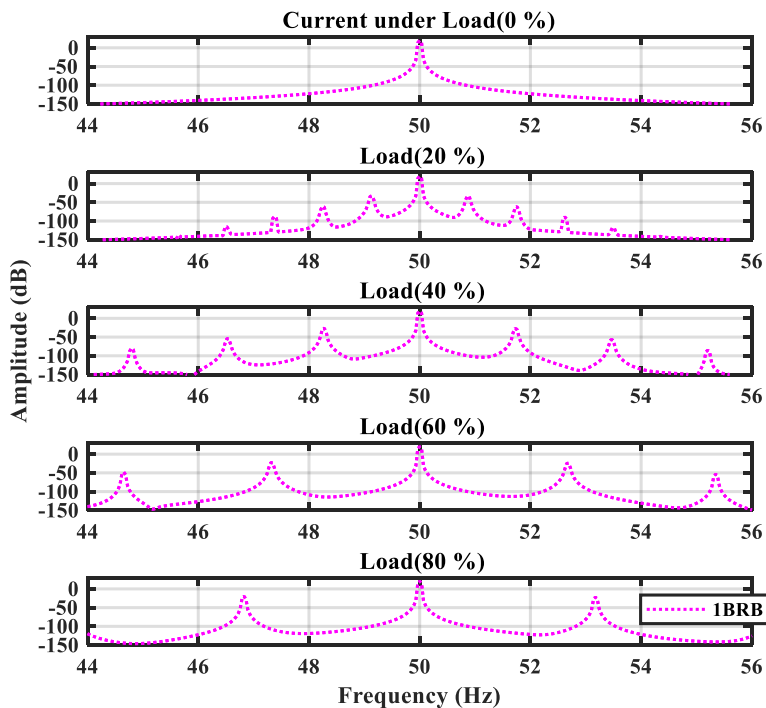
Figure 9-18 Current spectrum around the supply frequency of BG signals with one broken bar under five load conditions
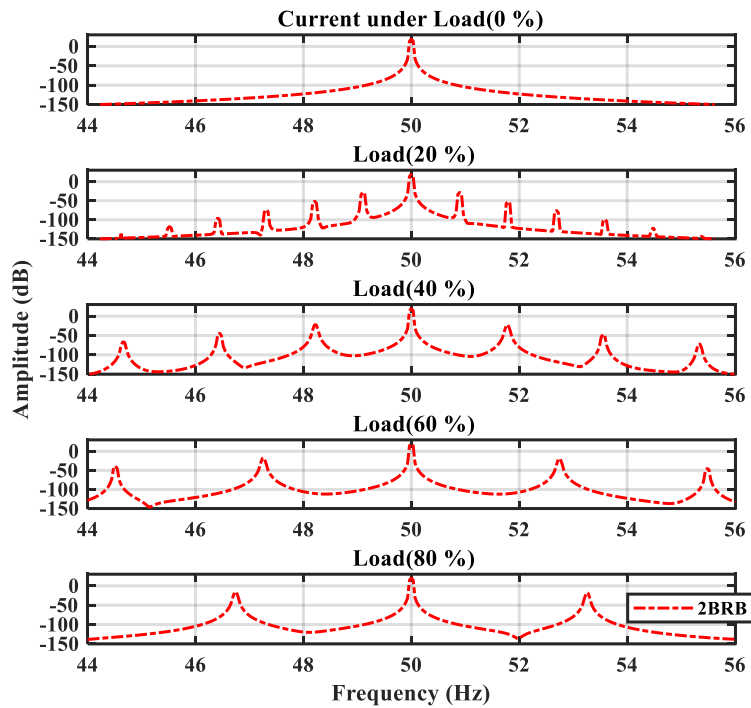
Figure 9-19 Current spectrum around the supply frequency of BG signals with two broken bars under five load conditions

Figure 9-20 to Figure 9-22 represent the measured (test rig data) current spectrum for baseline motor, and motor with one and two broken bars respectively under different load conditions. From these figures and the tabulated results the amplitude difference is seen to decrease with the increase of fault level and load.
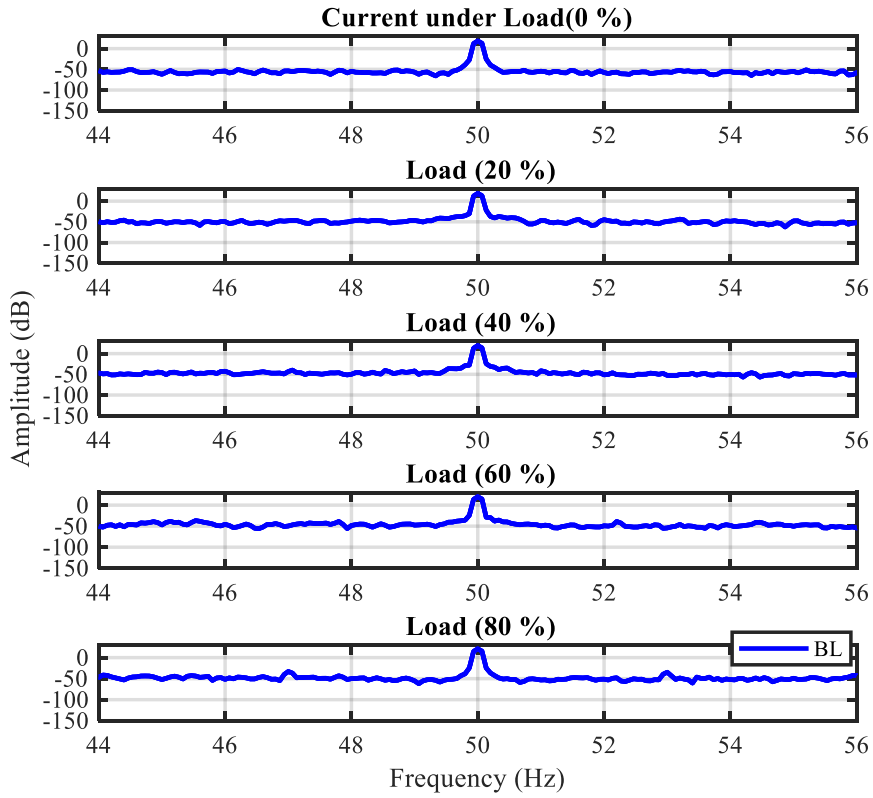
Figure 9-20 Measured current spectrum of test rig signals for baseline motor under five different loads
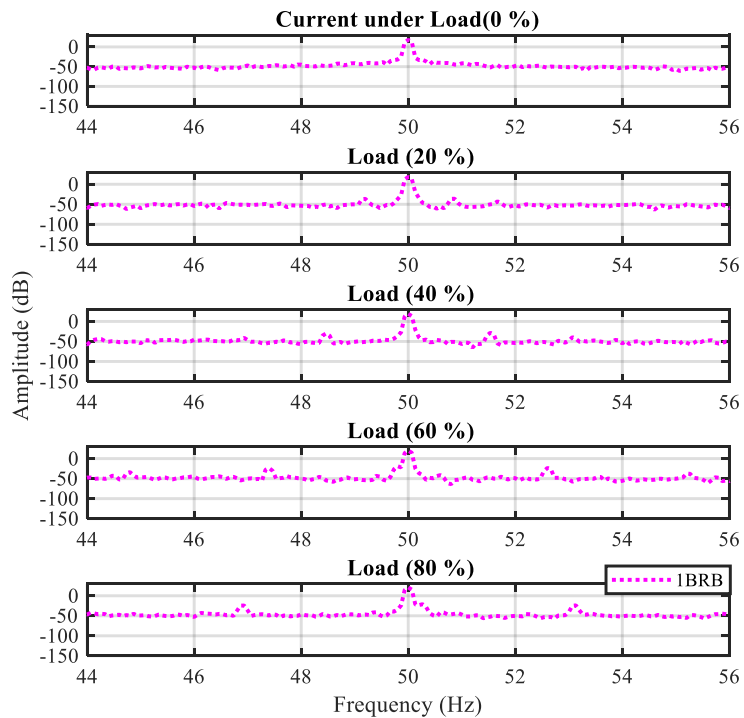
Figure 9-21 Measured current spectrum of test rig signals for motor with one broken bar under five load conditions
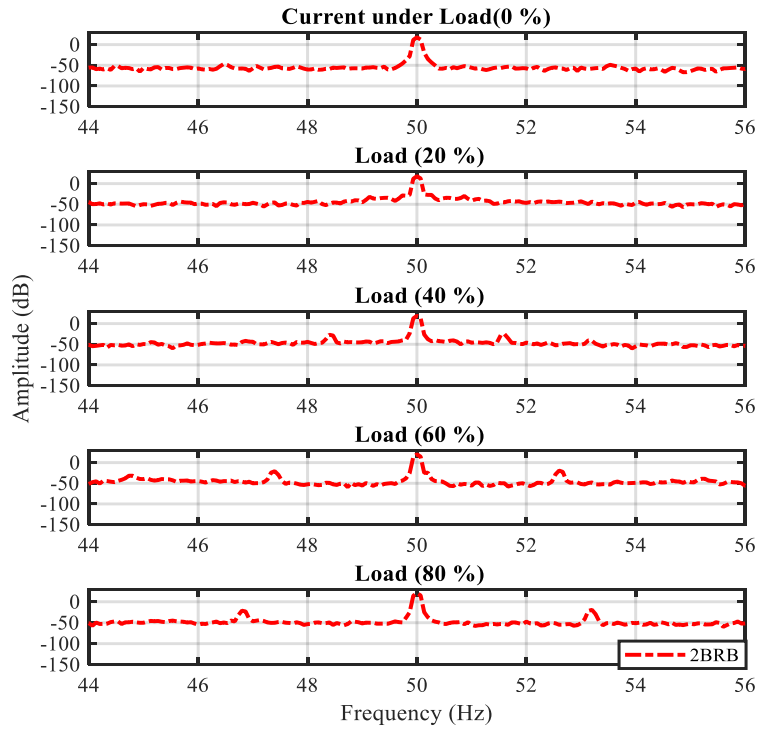
Figure 9-22 Measured current spectrum of test rig signals for motor with two broken bars under five load conditions

Table 9-3 shows the amplitude difference between the fundamental and lower side band for broken rotor bar under different loads for BG model data and experimentally measured data.

Table 9-3 Amplitude difference between fundamental and lower sideband

The amplitude difference between fundamental and lower sideband of f_{brb} (dB) BG model					
Motor condition	Load 0%	Load 20%	Load 40%	Load 60%	Load 80%
1 BRB	107.0 dB	52.3 dB	46.2 dB	43.1 dB	40.4 dB
2 BRBs	107.0 dB	47.0 dB	42.1 dB	38.2 dB	36.8 dB

The amplitude difference between fundamental and lower sideband of f_{brb} (dB) Measured data					
Motor condition	Load 0%	Load 20%	Load 40%	Load 60%	Load 80%
1 BRB	58.2 dB	54.9 dB	48.9 dB	43.6 dB	45.2 dB
2 BRB	64.9 dB	50.1 dB	46.0 dB	40.9 dB	42.0dB

9.8.1.1. Results and Discussion

From the figures above and the tabulated results, the presence of a broken rotor bar can be diagnosed based on amplitude difference. The result shows that when the difference is less than a reference value R, the amplitude at $f_s - 2sf_s$ has increased and a broken rotor bar is presented. However, under light load the amplitude with one or two broken bars is relatively small and may not exceed the reference. For loads greater than 40% full load the broken rotor bar fault can be diagnosed using amplitude difference as the criterion.

Previous studies [157, 177] have argued that if the amplitude difference is greater than 50 dB there are no broken bars.

9.8.2. Stator Imbalance Fault Detection Algorithm

In the case of stator imbalance the investigation is based on the increase of the amplitude at the 3rd harmonic in the current spectrum. From reports in the literature [112, 159, 166] and the results of the BG graph in Chapter Eight and the experimental results in Chapter Six, it is clear that stator imbalance produces an increase of the peak amplitude of the 3rd harmonic of the supply frequency. Thus this study proposes a simple test for diagnosis of imbalance faults that the amplitude of the spectral peak at 150 Hz measured under baseline conditions is taken as reference R1. If the amplitude at the 3rd harmonic is greater than R1 then stator imbalance is present.

9.8.2.1. Results and Discussion

Figure 9-22 and Figure 9-23 display the 3rd harmonic peak amplitude change (increase) under the effects of stator winding imbalance.
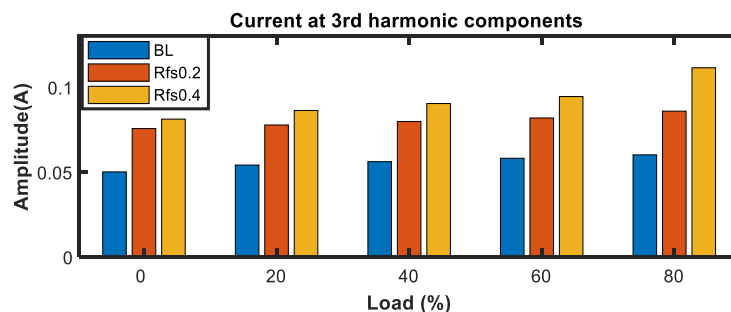
Figure 9-23 Simulated third harmonic spectral component at different loads and levels of imbalance.
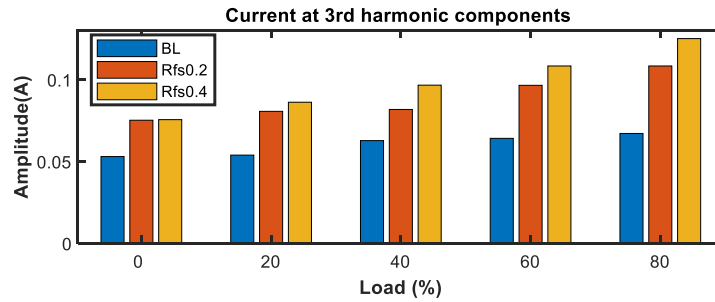
Figure 9-24 Measured amplitude of 3rd harmonic spectral peaks of current for different levels of stator imbalance (BL, and Rfs = 0.2 Ω and 0.4 Ω) for full speed at 0%, 20%, 40%, 60% and 80% full load

It is concluded from the result in Figure 9-23 and Figure 9-24, that the relative magnitudes of spectral peaks at 150 Hz for BL motor can be used for the diagnosis of stator imbalance. These findings are in good agreement with the reported literature [159] that stated the increase of the amplitude at 150Hz is the indicator of the stator imbalance.

9.9. Comparison of this Research (Graphical Causality-based Fault Detection) with Other Work in the Literature.

Series of comparison investigations have been done to evaluate the performance of the proposed graphical fault detection approach. The first comparison is based on the run time, and memory consumption of some AC induction motor fault detection approaches from the literature. All the compared systems are run using a Lenovo laptop (core i5). Table 9-4 compares the current work with some available studies reported in the literature.

Table 9-4 Comparison of the current work with the comparable work reported in the literature

Authors/Year	Types of faults	Domain used	Method used	Signals	Time (s)	Allocated Memory (Kb)
[178] Haiyang Li, et.al	Broken Rotor bar	Frequency domain	Mathematical Morphology	Instantaneous Induction Motor Electrical Signals Analysis	25.057	7771440.0
[179] Funso, et.al.	Broken Rotor bar	Frequency domain	Harmonic Order Tracking Analysis based on Motor Current Signature Analysis	Current signals	38.103	15175380.0
[180]H Li, et.al	Broken rotor bar	Frequency domain	Normalized frequency domain energy operator (FDEO)	Current signals	5.422446	3066216.0
Aisha present work Graphical causality approach	Broken rotor bar & stator winding imbalance	Time domain / Frequency domain	Structured illustration model (physical structure, causality and mathematics)	Current signals	2.175	17228.0

It is obvious from Table 9-4 that the electrical faults of AC induction motor have been detected using different methods; however, the recent work -graphical diagnostic approach has a short run time and less memory locations than other works.

A further comparison is presented in Table 9-5. It compares this research with qualitative approaches from the literature.

Table 9-5 Compares this research (graphical causality approach) with some available qualitative approaches from the literature.

Authors/Year	Type of used System	Method	Spurious predictions that do not correspond to real behaviour
[80] Kuipers, B	The U-tube	QSIM	Yes
[83] Maestri, M., et al.	Diagnosing faults in industrial processes	Automatic qualitative trend simulation	Yes
Aisha, recent Graphical fault detection approach	Diagnosing broken rotor bar / stator winding imbalance of ACIM	BG and TCG	No

It is clear from Table 9-5 that the graphical diagnostic approach has no spurious solutions, which overcomes the limitation of previous researches. This is achieved by using BG modelling and causality assignment procedure.

Table 9-6 shows another comparison between the recent graphical causality based approach with a previous BG of ACIM in the literature.

Table 9-6 Compares this research with the available bond graph model of AC induction motor.

Authors/Year	Model Type	Is it simulate a general AC induction motor	Model Framework	Fault Detection
[181] Kim, J. and M.D. Bryant	BG model considers three stator winding and only five rotor bars	No. It simulate the ACIM with individual rotor bars	It simulates the ACIM in α-β orthogonal reference frame.	No in-depth fault detection
Aisha present Graphical fault detection approach	BG model is general for Ac induction motor	Yes. It simulate the ACIM whatever the number of rotor bars.	It simulate the ACIM in the natural reference frame (three sinusoidal waveforms)using IC field to model the energy exchange and air gap flux that takes place between components of the system.	In-depth fault detection of electrical faults and used the qualitative influence for fault severity.

It can be seen from Table 9-6 that the graphical fault detection approach overcome the shortage of the previous BG fault detection. It simulates the behaviour of a general ACIM using IC field. It investigates the effect of a BRB and imbalanced stator winding faults on the system behaviour and addresses the qualitative influence of these faults on the motor current for fault severity. Farther, it validated using experimental data.

In conclusion, the graphical causality-based approach represents an efficient and meaningful technique for simulating the dynamic system behavior. The diagnostic approach based on TCG is very effective for the detection of ACIM electrical faults.

9.10. Summary

This chapter introduced the QS approach to fault detection, and it was shown that the results obtained from the TCG and forward propagation could be used for fault detection. A major advantage of this method that is it uses fewer parameters than the quantitative models. The application of QS predicted parameter changes in terms of (+) increased, (0) the same, or (-) decreased activity of the behaviour of the entire system. The results suggested that the using a QS approach based on TCG and qualitative reasoning can enable the extraction of diagnostic information that provides the basis for an accurate diagnosis.

The results obtained show that this approach could be used for the effective detection of broken rotor bars and stator winding imbalance faults in an ACIM. Then the QS approach was evaluated using a 20-SIM simulation of the ACIM BG model, which confirmed the potential of QS to detect broken rotor bars and stator imbalances.

Importantly, a series of comparisons between the simulation results and experimentally obtained data confirmed that the qualitative influence of the faults on the motor current signatures could show an accurate diagnostic tool. Where the work can be compared to previous papers (e.g., Sharma et al.,[157] and Shreve [177]), the results appear to be in good agreement.

The investigation continues to evaluate the graphical causality-based approach; it has been compared with other work in the literature. The graphical causality-based approach represents an efficient and meaningful technique for simulating the dynamic system behavior. The diagnostic approach based on TCG is very effective for the detection of ACIM electrical faults.

Chapter 10 Conclusions and Future Work

This chapter summarises and presents the key outcomes arising from this research study and extracts conclusions according to the attained outcomes. First, the chapter presents the aim and objectives mentioned in Chapter One, along with the way these objectives were accomplished. Then it presents an explanation of the contributions to knowledge provided by this research. Last, suggestions are made for further research with some recommendations for the useful development of the Bond Graph model and the qualitative simulation approach for system condition monitoring, in particular, detection of diverse sorts of malfunction from those used here, including electrical and mechanical.

10.1. Objectives and Achievements

The main aim of this research was to develop a qualitative simulation approach for the CM of AC induction motors. This primary target was successfully achieved by the development of a Bond Graph model, and the construction of a temporal causal graph for qualitative fault detection.

A summary of the objectives and their corresponding achievements are now given:

Objective 1: To review and understand conventional techniques used in CM systems, including quantitative and qualitative methods, and to complete a comprehensive review of the diagnostics of faults in electrical induction machines.

Achievement 1: A comprehensive review of common methods used for machine CM is provided in Chapter Two, Sections 2.1 and 2.2. In Section 2.3 a critical review of fault detection techniques for ACIMs was presented. MCSA was found to be an appropriate method for electrical machines fault detection, see Section 2.1.4. From this review, it was found that most of the simulations in current use tend to be based on abstract mathematical models instead of a structured representation of the system. Adopting this latter approach, this study selected BG modelling, which is based on system structure and causality relations for the detection of broken rotor bar and stator imbalance faults.

Objective 2: To investigate the effects of electrical faults, stator windings imbalance, and broken rotor bar, on the performance of an induction motor. This was accomplished by analyzing the cause and effects of these faults.

Achievement 2: Chapter Four, Section 4.4 discussed common faults of ACIMs and the effects of these faults on the motor operation, and Section 4.5 discussed the relation between motor specifications and their failure. The cause and effects of electrical faults, including broken rotor bar and stator winding imbalance, were reviewed and shown to impact the ACIM's performance in terms of an unbalanced rotating magnetic field, torque pulsations, and speed oscillation. These problems led to a decline in the system efficiency/productivity and shorten the life of the ACIM.

Objective 3: To understand models of ACIMs and develop a BG model of a healthy motor, the motor with a broken rotor bar, and motor with stator winding imbalance.

Achievement 3: Chapter Two, Section 2.3 model-based fault detection techniques have been reviewed. The review found that many of the models that have addressed electric machines' simulation are based on an abstract mathematical approach instead of a structured representation of the system. The BG method can model system behaviour dynamics based on a combination of three different aspects, conceptual, causality, and numerical. Thus the BG modelling approach was selected to build a model for fault detection in the given ACIM.

A BG model of the ACIM was developed in Chapter Seven, Section 7.5, using the neutral reference frame (A-B-C). It simulated the behaviours of the ACIM under different conditions including, a healthy motor, a motor with a broken rotor bar, and motor with stator winding imbalance. The results from this model were used as benchmarks for qualitative diagnosis.

Objective 4: To review qualitative simulation methods and develop a qualitative simulation approach for fault detection of the induction motor.

Achievement 4: A review of qualitative fault detection approaches has been reported in Chapter Three, Sections 3.1 and 3.2. This provided general information on qualitative simulation approaches and principles. A review of existing qualitative simulation methods, including BG methods, is discussed in Section 3.3. This review found that the qualitative reasoning method is a common qualitative fault detection technique and that BG modelling is a potential solution for qualitative simulation. BGs are pictorial models that construct system behaviour based on cause and effect relations.

Chapter Five gives a description of BG modelling principles, including energy variables, standard BG elements and causality, and a brief description of the sequential assignment procedure and the TCG (temporal causal graph). To evaluate the qualitative simulation performance, this study developed an ACIM qualitative BG model based on the TCG and forward propagation, see Chapter Nine. The qualitative BG model investigated the behaviour of the ACIM under the effects of two electrical faults: broken rotor bar and stator imbalance. It addressed the effects of the increase of rotor resistance that occurs because of a broken rotor bar on the system behaviour in Section 9.5.1, and investigated the effects of stator winding imbalance in Section 9.5.2.

Section 9.6 provides the results and discussion, and shows that the qualitative BG is an efficient approach for getting diagnostic information, leading to a precise diagnosis of the fault. Section 9.8 provides a diagnosis of the qualitative influence of a broken rotor bar and stator imbalance

faults on the motor current signature. The finding from the visual results of the BG model presented in Chapter Eight, the experimental results of Chapter Six, and from published literature all agree that in the presence of a broken rotor bar, the amplitude of the spectral peak in the current signature at (fs+2sfs) increased, so that the amplitude difference between the fundamental and the peak at (fs+2sfs) decreased. It is proposed that the presence of a broken rotor bar can be diagnosed by examining the amplitude difference between the fundamental supply and the amplitude of the lower sideband. If this difference is less than the reference value, say R, this would imply the presence of a broken rotor bar, see Section 9.8.1.

The diagnosis of the influence of stator imbalance was investigated based on the increase in of the third harmonic (3fs) amplitude of the fundamentals in the current spectrum. This increase is compared with the spectral peak at this frequency under baseline (healthy) conditions. If the increase is greater than a reference value, say R1, then this would imply the presence of an imbalance fault, see Section 9.8.2.

Objective 5: To build a three-phase ACIM bench rig suitable for testing different motor faults with different levels of severity and providing experimental data sets.

Achievement 5: Chapter Six provides details of the test bench used in this study to examine the effects of a broken rotor bar and stator winding imbalance on the motor current signature. Details of the test bench components and measuring equipment, sensors, and data acquisition system can be found in Section 6.2.

Objective 6: To evaluate the performance of developed techniques based on the experimental data sets.

Achievement 6: Chapter Six provides the experimental results from the tests performed on the baseline motor, the motor with a broken rotor bar, and the motor with stator imbalance. Motor current signals were collected for different load conditions under full speed. The effects of a broken rotor bar and stator imbalance investigated using the current spectrum; see Sections 6.5.1 and 6.5.2, respectively. The spectra obtained provided visual validation of the result obtained from the BG model, Section 8.2, and the results obtained from the qualitative fault diagnosis, see Section 9.8.

Objective 7: To provide suggestions and recommendations for future research in this area of study.

Achievement 7: Section 10.4 suggests useful directions for future research on the CM of AC induction motors advancing the technique developed in this research for the diagnosis of other different seeded faults.

10.2. Conclusions

This research investigated AC induction motor behaviour in the case of the electrical faults of a broken rotor bar and stator imbalance. The developed BG model can simulate the motor behaviour under different conditions, including a healthy motor, a motor with two levels of broken rotor bar faults (one and two broken bars), and a motor with two different stator winding imbalance levels.

The investigation was based on motor current analysis and the harmonic components in the current signal spectrum. In the case of a broken rotor bar, the amplitude of spectral peaks around the fundamental supply ($f_s \mp 2sf_s$) increased with fault severity and load. Stator imbalance increased the peak amplitude at the 3rd harmonic component with fault severity whatever the load. Comparing BG results with the corresponding results from the experimental study shows good agreement and good agreement with reports in the literature.

Importantly, the study has developed a qualitative simulation fault detection approach based on temporal causal graphs. The TCG and forward propagation result indicated that this approach could be used for the CM of ACIMs. An advantage of this method is that it involves fewer parameters compared with the quantitative methods.

The qualitative analysis that was applied, accurately predicted the effects of a broken rotor bar and a stator imbalance on the system's behaviour. This is taken to indicate that the QS technique proposed of combining TCG with qualitative reasoning and qualitative equations is a suitable means of extracting useful diagnostic information to provide an accurate diagnosis of broken rotor bar and stator imbalance faults.

The applied qualitative analysis predicts the effects of broken rotor bar and stator imbalance faults on the whole system behaviour, indicating that the proposed QS technique is an effective method for extracting diagnostic information, leading to an accurate fault diagnosis by combining TCG and qualitative equations with qualitative reasoning.

The QS approach was evaluated based on the implementation of the ACIM BG using 20-SIM software. The visual presentation of the simulation results, see Figure 9-6 to Figure 9-14 confirm that using the QS approach can detect BRB and IM faults accurately.

The investigation continued by investigating the qualitative effect of the seeded electrical faults on the motor current signatures based on the reference values. In the case of a broken rotor bar(s) the reference is related to the amplitude difference between the fundamental frequency in the current signal spectrum and the lower sideband frequency.

In the case of stator imbalance, the 3rd harmonic amplitude in the current signal spectrum is compared with the reference value measured under baseline (healthy) condition. A significant stator imbalance is indicated if the peak amplitude at 3rd harmonic is greater than the reference.

The results from both the BG and experimental studies show that the qualitative influence diagnosis gives accurate results.

In order to evaluate the graphical causality-based approach, it has been compared with work in the literature. The graphical causality-based approach represents an efficient and meaningful technique for simulating the dynamic system behavior. The diagnostic approach based on TCG is very effective for the detection of ACIM electrical faults. Moreover, it overcomes the limitations of some studies in the literature.

10.3. Research Contributions to Knowledge

Contribution 1: The development of a Bond Graph model of the three-phase induction motor in the natural reference frame using the IC- field that coupled the electrical and mechanical components of the electro-mechanical system has not been used before for the simulation of an ACIM. In this thesis, a BG model has been developed for fault detection in ACIMs based on motor current analysis, to the author's knowledge, MCSA has not been previously used in this way. Further, the model has been successfully used for the detection of broken rotor bar and stator imbalance faults based on MCSA, which would be a cost-effective technique for the detection of motor faults.

Contribution 2: The author believes that qualitative simulation for fault detection is a potential solution for the detection of AC induction motor faults. There has been no

research reported in the literature that used TCGs and forward propagation for the CM of ACIMs.

Contribution 3: The influence of the broken rotor bar and the stator imbalance on the system behaviour were detected based on causality and qualitative reasoning to overcome the limitations of the comparable work in the literature.

10.4. Suggestions for Further Work

The presented results show the effectiveness of using BG modelling and a qualitative approach for ACIM condition monitoring. Suggested future work could include the following:

➤ The use of the BG model for other electrical and mechanical faults in ACIMs, such as stator short circuit, stator open circuit, mechanical imbalance, and bearing faults.

➤ Fuzzy logic, already used widely for fault detection and classifications, could be fused with a qualitative BG approach to provide a more robust fault diagnosis for ACIMs.

➤ A combination of the qualitative influence diagnosis with rule-based approaches can be used to identify fault severity.

➤ The author recommends combining qualitative simulation with machine learning techniques that already play a significant role in fault detection and classification to be used for fault classification.

➤ More research is required to use the proposed qualitative detection method on the ACIM fed by a variable frequency drive (VFD) to understand the effects of the inverter on the ACIM behaviour, especially under the fault conditions.

➤ The BG model should be extended to simulate other motor-driven machineries such as pumps and engines.

References

1. Abu Saad, S., The Untilisation of Information Available in a Sensorless Control System of an AC Induction Motor for Condition Monitoring. 2015.
2. Gao, Z., et al., A frequency demodulation approach to induction motor speed detection. IEEE Transactions on Industry Applications, 2011. 47(4): p. 1632-1642.
3. Alashter, A., et al. Fault Diagnosis of Broken Rotor Bar in AC Induction Motor based on A Qualitative Simulation Approach. in 2019 25th International Conference on Automation and Computing (ICAC). 2019. IEEE.
4. Mehala, N., Condition monitoring and fault diagnosis of induction motor using motor current signature analysis. 2010, National Institute of Technology Kurukshetra, INDIA.
5. Venkatasubramanian, V., R. Rengaswamy, and S.N. Kavuri, A review of process fault detection and diagnosis: Part II: Qualitative models and search strategies. Computers & chemical engineering, 2003. 27(3): p. 313-326.
6. Mosterman, P.J. and G. Biswas, Diagnosis of continuous valued systems in transient operating regions. IEEE Transactions on Systems, Man, and Cybernetics-Part A: Systems and Humans, 1999. 29(6): p. 554-565.
7. Linkens, D. and H. Wang. Qualitative bond graph reasoning in control engineering: Fault diagnosis. in Int. Conf. Bond Graph Modeling Simulation. 1995.
8. Lu, Q., Fault Diagnosis and Fault Tolerant Control of DFIG Based Wind Turbine System. 2012.
9. Samantaray, A.K. and B.O. Bouamama, Model-based process supervision: a bond graph approach. 2008: Springer Science & Business Media.
10. Lu, Q., Fault diagnosis and fault tolerant control of DFIG based wind turbine system. 2012, University of Manchester.
11. Toliyat, H.A., et al., Electric machines: modeling, condition monitoring, and fault diagnosis. 2012: CRC press.
12. Davies, A., Handbook of condition monitoring: techniques and methodology. 2012: Springer Science & Business Media.
13. Seera, M., et al., Condition monitoring of induction motors: A review and an application of an ensemble of hybrid intelligent models. Expert Systems with Applications, 2014. 41(10): p. 4891-4903.
14. Rao, B., Handbook of condition monitoring. 1996: Elsevier.
15. Jardine, A.K., D. Lin, and D. Banjevic, A review on machinery diagnostics and prognostics implementing condition-based maintenance. Mechanical systems and signal processing, 2006. 20(7): p. 1483-1510.
16. Liu, R., et al., Artificial intelligence for fault diagnosis of rotating machinery: A review. Mechanical Systems and Signal Processing, 2018. 108: p. 33-47.
17. Vogl, G.W., B.A. Weiss, and M. Helu, A review of diagnostic and prognostic capabilities and best practices for manufacturing. Journal of Intelligent Manufacturing, 2019. 30(1): p. 79-95.
18. Venkatasubramanian, V., et al., A review of process fault detection and diagnosis: Part I: Quantitative model-based methods. Computers & chemical engineering, 2003. 27(3): p. 293-311.
19. Serridge, M., Ten crucial concepts behind trustworthy fault detection in machine condition monitoring, in Vibration and Wear in High Speed Rotating Machinery. 1990, Springer. p. 729-740.
20. Lei, T., Doubly-fed induction generator wind turbine modelling, control and reliability. 2014, The University of Manchester (United Kingdom).
21. Medjaher, K., A bond graph model-based fault detection and isolation. 2011.
22. Maurya, M.R., R. Rengaswamy, and V. Venkatasubramanian, A systematic framework for the development and analysis of signed digraphs for chemical processes. 1. Algorithms and analysis. Industrial & engineering chemistry research, 2003. 42(20): p. 4789-4810.

23. Kral, C., et al. A comparison of rotor fault detection techniques with respect to the assessment of fault severity. in Diagnostics for Electric Machines, Power Electronics and Drives, 2003. SDEMPED 2003. 4th IEEE International Symposium on. 2003. IEEE.

24. Li, W. and C.K. Mechefske, Detection of induction motor faults: a comparison of stator current, vibration and acoustic methods. Journal of vibration and Control, 2006. 12(2): p. 165-188.

25. Sethiya, S., Condition Based Maintenance (CBM). Secy. to CME/WCR/JBP, 2006.

26. Gong, X., Online nonintrusive condition monitoring and fault detection for wind turbines. 2012.

27. Bloch, H.P., Practical Machinery Management for Process Plants: Volume 1: Improving Machinery Reliability. Vol. 1. 1998: Gulf Professional Publishing.

28. Li, W., et al., A study of the noise from diesel engines using the independent component analysis. Mechanical Systems and Signal Processing, 2001. 15(6): p. 1165-1184.

29. Rajul Misra , A.A., Condition Monitoring and Fault Diagnosis in Induction Motor: Case Study. MIT International Journal of Electrical and Instrumentation Engineering, 2015. 5(1): p. 6.

30. Milimonfared, J., et al., A novel approach for broken-rotor-bar detection in cage induction motors. IEEE Transactions on Industry Applications, 1999. 35(5): p. 1000-1006.

31. Thomson, W.T. and R.J. Gilmore. Motor current signature analysis to detect faults in induction motor drives–fundamentals, data interpretation, and industrial case histories. in Proceedings of 32nd Turbo machinery Symposium, A&M University, Texas, USA. 2003.

32. Boashash, B., Time-frequency signal analysis and processing: a comprehensive reference. 2015: Academic Press.

33. G. N. Surya , M.S.B., and Z. J. Khan A Survey on Progress and Development of Induction Motors' Incipient Fault Detection Techniques during Last Three Decades. Journal of Research in Engineering and Applied Sciences, 2016. 01 (02): p. 56-83.

34. Yoon, J., et al., Vibration-based wind turbine planetary gearbox fault diagnosis using spectral averaging. Wind Energy, 2016. 19(9): p. 1733-1747.

35. Chattopadhyaya, A., et al., Wavelet decomposition based skewness and kurtosis analysis for assessment of stator current harmonics in a PWM–fed induction motor drive during single phasing condition. AMSE J, 2016: p. 1-14.

36. Lebold, M., et al. Review of vibration analysis methods for gearbox diagnostics and prognostics. in Proceedings of the 54th meeting of the society for machinery failure prevention technology. 2000.

37. Subrata Karmakar, S.C., Madhuchhanda Mitra, Samarjit Sengupta, Induction Motor Fault Diagnosis: Approach through Current Signature Analysis. 2016.

38. Lee, S.-H., et al. Extraction of induction motor fault characteristics in frequency domain and fuzzy entropy. in IEEE International Conference on Electric Machines and Drives, 2005. 2005. IEEE.

39. Kral, C., A. Haumer, and C. Grabner. Modeling and simulation of broken rotor bars in squirrel cage induction machines. in Proceedings of the World congress on engineering. 2009.

40. Kaikaa, M.Y., M. Hadjami, and A. Khezzar, Effects of the simultaneous presence of static eccentricity and broken rotor bars on the stator current of induction machine. IEEE Transactions on Industrial Electronics, 2013. 61(5): p. 2452-2463.

41. Shi, P., et al., A new diagnosis of broken rotor bar fault extent in three phase squirrel cage induction motor. Mechanical Systems and Signal Processing, 2014. 42(1-2): p. 388-403.

42. Heckbert, P., Fourier transforms and the fast Fourier transform (FFT) Algorithm. Computer Graphics, 1995. 2: p. 15-463.

43. Abdusslam, S.A., Detection and diagnosis of rolling element bearing faults using time encoded signal processing and recognition. 2012, University of Huddersfield.

44. Suh, I.-S., Application of time-frequency representation techniques to the impact-induced noise and vibration from engines. SAE Transactions, 2002: p. 952-960.

45. Liu, Y. and A.M. Bazzi, A review and comparison of fault detection and diagnosis methods for squirrel-cage induction motors: State of the art. ISA transactions, 2017. 70: p. 400-409.

46. Gandhi, A., T. Corrigan, and L. Parsa, Recent advances in modeling and online detection of stator interturn faults in electrical motors. IEEE Transactions on Industrial Electronics, 2010. 58(5): p. 1564-1575.

47.   Gaeid, K.S., et al., Fault diagnosis of induction motor using MCSA and FFT. Electrical and Electronic Engineering, 2011. 1(2): p. 85-92.

48.   Miljković, D., Brief review of motor current signature analysis. HDKBR Info magazin, 2015. 5(1): p. 14-26.

49.   Gu, F., et al., Electrical motor current signal analysis using a modified bispectrum for fault diagnosis of downstream mechanical equipment. Mechanical Systems and Signal Processing, 2011. 25(1): p. 360-372.

50.   Gu, F., et al., A new method of accurate broken rotor bar diagnosis based on modulation signal bispectrum analysis of motor current signals. Mechanical Systems and Signal Processing, 2015. 50: p. 400-413.

51.   Zolfaghari, S., et al., Broken rotor bar fault detection and classification using wavelet packet signature analysis based on fourier transform and multi-layer perceptron neural network. Applied Sciences, 2017. 8(1): p. 25.

52.   Douglas, H., P. Pillay, and P. Barendse. The detection of interturn stator faults in doubly-fed induction generators. in Fourtieth IAS Annual Meeting. Conference Record of the 2005 Industry Applications Conference, 2005. 2005. IEEE.

53.   Sonje, D.M., P. Kundu, and A. Chowdhury, A Novel Approach for Sensitive Inter-turn Fault Detection in Induction Motor Under Various Operating Conditions. Arabian Journal for Science and Engineering, 2019. 44(8): p. 6887-6900.

54.   Göktas, T., M. Arkan, and Ö.F. Özgüven. A new method to separate broken rotor failures and low frequency load oscillations in three-phase induction motor. in 2013 9th IEEE international symposium on diagnostics for electric machines, power electronics and drives (SDEMPED). 2013. IEEE.

55.   Mustafa, M.O., Faults detection and diagnosis for three phase induction machines. 2012, Luleå tekniska universitet.

56.   Chen, S., Induction machine broken rotor bar diagnostics using prony analysis. 2008.

57.   Gyftakis, K.N., et al., A novel approach for broken bar fault diagnosis in induction motors through torque monitoring. IEEE Transactions on Energy Conversion, 2013. 28(2): p. 267-277.

58.   Lu, Q., Z. Cao, and E. Ritchie. Model of stator inter-turn short circuit fault in doubly-fed induction generators for wind turbine. in Power Electronics Specialists Conference, 2004. PESC 04. 2004 IEEE 35th Annual. 2004. IEEE.

59.   Djurovic, S., et al. Condition monitoring artefacts for detecting winding faults in wind turbine DFIGs. in Proc. EWEC. 2009.

60.   Tallam, R.M., T.G. Habetler, and R.G. Harley, Transient model for induction machines with stator winding turn faults. IEEE Transactions on Industry Applications, 2002. 38(3): p. 632-637.

61.   Ritchie, E., Deng, X., and Jokinen, T., Dynamic Model of Three-Phase Squirrel Cage Induction Motors with Rotor Faults. ICEM'94, Paris, France,, (1994). 2: p. 694-698.

62.   Filho, E.R. and R.M. de Souza. Three-phase induction motor dynamic mathematical model.

63.   Alwodai, A., Motor fault diagnosis using higher order statistical analysis of motor power supply parameters. 2015, University of Huddersfield.

64.   Khater, F.M., et al., Proposed fault diagnostics of a broken rotor bar induction motor fed from PWM inverter. Journal of Electrical Systems and Information Technology, 2016. 3(3): p. 387-397.

65.   Bednarz, S.A. and M. Dybkowski, Induction motor windings faults detection using flux-error based MRAS estimators. Diagnostyka, 2019. 20(2): p. 87--96.

66.   Nemec, M., et al., Induction Motor Broken Rotor Bar Detection Based on Rotor Flux Angle Monitoring. Energies, 2019. 12(5): p. 794.

67.   Ould-Bouamama, B., et al., Bond graphs for the diagnosis of chemical processes. Computers and Chemical Engineering, 2012. 36(1): p. 301-324.

68.   Merzouki, R., et al., Intelligent mechatronic systems: modeling, control and diagnosis. 2012: Springer Science & Business Media.

69.   Forbus, K.D., Qualitative process theory. Artificial intelligence, 1984. 24(1-3): p. 85-168.

70.   Hocaoğlu, M.F., Qualitative Reasoning for Quantitative Simulation. Modelling and Simulation in Engineering, 2018. 2018.

71. Tanaka, H., et al., Fault-tree analysis by fuzzy probability. IEEE Transactions on reliability, 1983. 32(5): p. 453-457.

72. Mouzakitis, A., Classification of fault diagnosis methods for control systems. Measurement and Control, 2013. 46(10): p. 303-308.

73. Linkens, D. and H. Wang, Fault diagnosis based on a qualitative bond graph model, with emphasis on fault localisation. 1995.

74. Hang Wang, D.A.L., Intelligent Supervisory Control: A Qualitative Bond Graph Reasoning Approach. . 1996.

75. Garani, G. and G. Adam, Qualitative Modelling at the Design of Concrete Manufacturing Machinery. International Journal of Computers and Applications, 2008. 30(4): p. 325-330.

76. Kuipers, B. The Limits of Qualitative Simulation. in IJCAI. 1985. Citeseer.

77. Zhang, P., et al., A survey of condition monitoring and protection methods for medium-voltage induction motors. IEEE Transactions on Industry Applications, 2011. 47(1): p. 34-46.

78. Feenstra, P.J., et al., Bond graph modeling procedures for fault detection and isolation of complex flow processes. 2001.

79. Kuipers, B., Qualitative simulation. Artificial intelligence, 1986. 29(3): p. 289-338.

80. Kuipers, B., Qualitative simulation. Encyclopedia of physical science and technology, 2001. 3: p. 287-300.

81. Say, A.C. and S. Kuru, Qualitative system identification: deriving structure from behavior. Artificial Intelligence, 1996. 83(1): p. 75-141.

82. WU, C.-g., T. Xia, and B.-k. ZHANG, The Qualitative Simulation Based on Deep Knowledge Model of Signed Directed Graph [J]. Acta Simulata Systematica Sinica, 2003. 10.

83. Maestri, M., et al., Automatic qualitative trend simulation method for diagnosing faults in industrial processes. Computers & Chemical Engineering, 2014. 64: p. 55-62.

84. Vedam, H. and V. Venkatasubramanian, Signed digraph based multiple fault diagnosis. Computers & chemical engineering, 1997. 21: p. S655-S660.

85. Yong-kuo, L., et al., A cascade intelligent fault diagnostic technique for nuclear power plants. Journal of Nuclear Science and Technology, 2018. 55(3): p. 254-266.

86. Tarifa, E.E. and N.J. Scenna, Fault diagnosis for MSF dynamic states using a SDG and fuzzy logic. Desalination, 2004. 166: p. 93-101.

87. Tarifa, E.E. and N.J. Scenna, Fault diagnosis, direct graphs, and fuzzy logic. Computers & Chemical Engineering, 1997. 21: p. S649-S654.

88. Gao, D., et al., Signed Directed Graph and Qualitative Trend Analysis Based Fault Diagnosis in Chemical Industry. Chinese Journal of Chemical Engineering, 2010. 18(2): p. 265-276.

89. Bregon, A., M. Daigle, and I. Roychoudhury, Qualitative fault isolation of hybrid systems: A structural model decomposition-based approach. 2016.

90. Daigle, M.J., et al., A qualitative event-based approach to multiple fault diagnosis in continuous systems using structural model decomposition. Engineering Applications of Artificial Intelligence, 2016. 53: p. 190-206.

91. Thoma, J.U., Introduction to bond graphs and their applications. 2016: Elsevier.

92. Daigle, M.J., A qualitative event-based approach to fault diagnosis of hybrid systems. 2008.

93. Yu, L. and X. Qi. Bond-graph modeling in system engineering. in Systems and Informatics (ICSAI), 2012 International Conference on. 2012. IEEE.

94. Lo, C., Y.-K. Wong, and A.B. Rad, Intelligent system for process supervision and fault diagnosis in dynamic physical systems. IEEE Transactions on Industrial Electronics, 2006. 53(2): p. 581-592.

95. Biswas, G., X. Yu, and K. Debelak, A Formal Modeling Scheme for Continuous-valued Systems: Focus on Diagnosis. 1992.

96. Xia, S., D. Linkens, and S. Bennett, Automatic modelling and analysis of dynamic physical systems using qualitative reasoning and bond graphs. Intelligent Systems Engineering, 1993. 2(3): p. 201-212.

97. Manders, E.-J., et al., A combined qualitative/quantitative approach for fault isolation in continuous dynamic systems. IFAC Proceedings Volumes, 2000. 33(11): p. 505-510.

98. Lo, C., Y.-K. Wong, and A.B. Rad, Bond graph based Bayesian network for fault diagnosis. Applied soft computing, 2011. 11(1): p. 1208-1212.

99. Mekki, T., S. Triki, and A. Kamoun, Diagnosis of switching systems using hybrid bond graph. arXiv preprint arXiv:1312.2047, 2013.

100. Zhang, P., et al., A survey of condition monitoring and protection methods for medium-voltage induction motors. IEEE Transactions on Industry Applications, 2010. 47(1): p. 34-46.

101. Fitzgerald, A.E., et al., Electric machinery. Vol. 5. 2003: McGraw-Hill New York.

102. Electrical Academia. Three Phase Induction Motor Construction. [cited 2020 21 August].

103. Karmakar, S., et al., Induction motor fault diagnosis. Vol. 25. 2016: Springer.

104. Vas, P., Parameter estimation, condition monitoring, and diagnosis of electrical machines. Vol. 27. 1993: Oxford University Press.

105. Parekh, R., AC Induction Motor Fundamentals. Microchip Technology Inc, 2003(DS00887A): p. 1-24.

106. Payne, B.S., Condition monitoring of electric motors for improved asset management. 2003: University of Manchester.

107. Gajare, A.M. and N.R. Bhasme, A review on speed control techniques of single phase induction motor. International Journal of Computer Technology and Electronics Engineering, 2012. 2(5): p. 33-39.

108. Automation, R., Application basics of operation of three-phase induction motors. Sprecher+ Schuh AG Rockwell Automation, Aarau. 1996.

109. Pandey, K., P. Zope, and S. Suralkar, Review on fault diagnosis in three-phase induction motor. MEDHA–2012, Proceedings published by International Journal of Computer Applications (IJCA), 2012.

110. Thomson, W.T. and M. Fenger, Current signature analysis to detect induction motor faults. IEEE Industry Applications Magazine, 2001. 7(4): p. 26-34.

111. Lebaroud, A. and G. Clerc. Diagnosis of induction motor faults using instantaneous frequency signature analysis. in 2008 18th International Conference on Electrical Machines. 2008. IEEE.

112. Sridhar, S. and K.U. Rao. Detection of simultaneous unbalanced under-voltage and broken rotor fault in induction motor. in 2013 IEEE 1st International Conference on Condition Assessment Techniques in Electrical Systems (CATCON). 2013. IEEE.

113. Deleroi, W., BROKEN BAR IN A SQUIRREL-CAGE ROTOR OF AN INDUCTION-MOTOR. 1. DESCRIPTION BY SUPERIMPOSED FAULT-CURRENTS. Archiv fur Elektrotechnik, 1984. 67(2): p. 91-99.

114. Mustafa, M.O., et al., A fault detection scheme based on minimum identified uncertainty bounds violation for broken rotor bars in induction motors. Control Engineering Practice, 2016. 48: p. 63-77.

115. Said, M.N., M.E.H. Benbouzid, and A. Benchaib, Detection of broken bars in induction motors using an extended Kalman filter for rotor resistance sensorless estimation. IEEE Transactions on energy conversion, 2000. 15(1): p. 66-70.

116. Bellini, A., et al. Assessment of induction machines rotor fault severity by different approaches. in 31st Annual Conference of IEEE Industrial Electronics Society. IECON 2005.: IEEE.

117. Joksimovic, G.M. and J.J.I.T.o.I.e. Penman, The detection of inter-turn short circuits in the stator windings of operating motors. 2000. 47(5): p. 1078-1084.

118. Shaeboub, A., The Monitoring of Induction Machines Using Electrical Signals from the Variable Speed Drive. 2018, University of Huddersfield.

119. Cira, F., et al. Analysis of stator inter-turn short-circuit fault signatures for inverter-fed permanent magnet synchronous motors. in IECON 2016-42nd Annual Conference of the IEEE Industrial Electronics Society. 2016. IEEE.

120. Chen, S. and R. Živanović, Modelling and simulation of stator and rotor fault conditions in induction machines for testing fault diagnostic techniques. European Transactions on Electrical Power, 2010. 20(5): p. 611-629.

121. Cruz, S.M. and A.M. Cardoso, Diagnosis of stator inter-turn short circuits in DTC induction motor drives. IEEE Transactions on Industry Applications, 2004. 40(5): p. 1349-1360.

122. Bouzid, M. and G. Champenois. Experimental compensation of the negative sequence current for accurate stator fault detection in induction motors. in IECON 2013-39th Annual Conference of the IEEE Industrial Electronics Society. 2013. IEEE.

123. Messaoudi, M. and L. Sbita, Multiple Faults Diagnosis in Induction Motor Using the MCSA Method. International Journal of Signal & Image Processing, 2010. 1(3).

124. Nandi, S., H.A. Toliyat, and X. Li, Condition monitoring and fault diagnosis of electrical motors—A review. IEEE transactions on energy conversion, 2005. 20(4): p. 719-729.

125. Mustafa, M.O., On Fault Detection, Diagnosis and Monitoring for Induction Motors. 2015, Luleå tekniska universitet.

126. Cira, F., M. Arkan, and B. Gumus, Detection of stator winding inter-turn short circuit faults in permanent magnet synchronous motors and automatic classification of fault severity via a pattern recognition system. J. Electr. Eng. Technol, 2016. 11(2): p. 416-424.

127. Tanvir, M.R. https://grabcad.com/library/tag/bearing. [cited 2020 25 August].

128. Bonaldi, E.L., et al., Predictive maintenance by electrical signature analysis to induction motors, in Induction Motors-Modelling and Control. 2012, IntechOpen.

129. Rokseth, B., A bond graph approach for modelling systems of rigid bodies in spatial motion. 2014, Institutt for marin teknikk.

130. Paynter, H., Analysis and Design of Engineering Systems; Class Notes for MIT Course 2,751. 1961.

131. Karnopp, D. and R.C. Rosenberg, Analysis and simulation of multiport systems: The bond graph approach to physical system dynamics. 1968.

132. Broenink, J.F., 20-sim software for hierarchical bond-graph/block-diagram models. Simulation Practice and Theory, 1999. 7(5-6): p. 481-492.

133. Granda, J.J. and J. Reus. New developments in bond graph modeling software tools: the computer aided modeling program CAMP-G and MATLAB. in 1997 IEEE International Conference on Systems, Man, and Cybernetics. Computational Cybernetics and Simulation. 1997. IEEE.

134. Mukherjee, A. and A. Samantaray, System modelling through bond graph objects on SYMBOLS 2000. Simulation Series, 2001. 33(1): p. 164-170.

135. Mezghani, D., et al., A New Optimum Frequency Controller of Hybrid Pumping System: Bond Graph Modeling-Simulation and Practice with ARDUINO Board. International Journal of Advanced Computer Science and Applications, 2017. 8(1): p. 78-87.

136. Mosterman, P.J., R. Kapadia, and G. Biswas. Using bond graphs for diagnosis of dynamic physical systems. in Proceedings of the 5th International Workshop on Principles of Diagnosis. 1995.

137. Mashadi, B. and D. Crolla, An Introduction to Bond Graph Modelling. Vehicle Powertrain Systems: p. 511-528.

138. Karnopp, D., D.L. Margolis, and R.C. Rosenberg, System dynamics: modeling and simulation of mechatronic systems. 3rd ed. 2000, Chichester;New York, N.Y;: Wiley.

139. Zrafi, R., S. Ghedira, and K. Besbes, A Bond Graph Approach for the Modeling and Simulation of a Buck Converter. Journal of Low Power Electronics and Applications, 2018. 8(1): p. 2.

140. Karnopp, D.C., D.L. Margolis, and R.C. Rosenberg, System dynamics: modeling, simulation, and control of mechatronic systems. 2012: John Wiley & Sons.

141. Hang Wang, D.A.L., Intelligent Supervisory Control: A Qualitative Bond Graph Reasoning Approach. 1996.

142. Borutzky, W., Bond graph modelling of engineering systems. Vol. 103. 2011: Springer.

143. Borutzky, W., Bond graph modelling and simulation of multidisciplinary systems–an introduction. Simulation Modelling Practice and Theory, 2009. 17(1): p. 3-21.

144. Borutzky, W., Bond Graph Modelling of Engineering Systems. Theory, Applications and Software Support .2010

145. Lattmann, Z., A multi-domain functional dependency modeling tool based on extended hybrid bond graphs. 2010, Vanderbilt University.

146. Jallut, B.M.C., Introduction to bond graph theory. Second part: multiport field and junction structures, and thermodynamics.

147. Mosterman, P.J., E.J. Manders, and G. Biswas, Qualitative Diagnosis of Systems With Models That Include a Class of Algebraic Loops. 2000, Mar.

148. Samantaray, A.K., et al., Diagnostic bond graphs for online fault detection and isolation. Simulation Modelling Practice and Theory, 2006. 14(3): p. 237-262.

149. Bouamama, B.O., et al., Supervision of an industrial steam generator. Part I: Bond graph modelling. Control Engineering Practice, 2006. 14(1): p. 71-83.

150. Touati, Y., R. Merzouki, and B.O. Bouamama, Fault estimation and isolation using bond graph approach. IFAC Proceedings Volumes, 2012. 45(20): p. 138-143.

151. Said, M., et al., Decentralized fault detection and isolation using bond graph and PCA methods. The International Journal of Advanced Manufacturing Technology, 2018. 99(1-4): p. 517-529.

152. Bouallegue, W., S. Bouslama, and M. Tagina, Robust fault detection and isolation in bond graph modelled processes with Bayesian networks. International Journal of Computer Applications in Technology, 2017. 55(1): p. 46-54.

153. Kleijn, C., 20-sim 4.1 Reference Manual. 2009: Getting Started with 20-sim.

154. Mini, V. and S. Ushakumari, Rotor fault detection and diagnosis of induction motor using fuzzy logic. AMSE JOURNALS 2014-Series: Modelling A, 2014. 87(2): p. 19-40.

155. Nadir, B., R.M. Faouzi, and B. Ahmed, The investigation of induction motors under abnormal condition. TOJSAT, 2013. 3(4): p. 150-158.

156. Mirabbasi, D., G. Seifossadat, and M. Heidari. Effect of unbalanced voltage on operation of induction motors and its detection. in 2009 International Conference on Electrical and Electronics Engineering-ELECO 2009. 2009. IEEE.

157. Sharma, A., L. Mathew, and S. Chatterji. Analysis of Broken Rotor bar Fault Diagnosis for Induction Motor. in 2017 International Conference on Innovations in Control, Communication and Information Systems (ICICCI). 2017. IEEE.

158. Babaa, F., et al. Condition monitoring of stator faults in induction motors: Part II-A more sensitive indicator of inter-turn shortcircuits fault in stator windings under unbalanced supply voltage. in 2007 International Aegean Conference on Electrical Machines and Power Electronics. 2007. IEEE.

159. Benbouzid, M.E.H. and G.B. Kliman, What stator current processing-based technique to use for induction motor rotor faults diagnosis? IEEE Transactions on Energy Conversion, 2003. 18(2): p. 238-244.

160. Touati, Y., R. Merzouki, and B.O. Bouamama, Robust diagnosis to measurement uncertainties using bond graph approach: Application to intelligent autonomous vehicle. Mechatronics, 2012. 22(8): p. 1148-1160.

161. Hussein, H.I., Mathematical driving model of three phase induction motors in stationary coordinate frame. Diyala Journal of engineering sciences, 2015. 8(4): p. 255-265.

162. P. Pillay, V.L., Mathematical models for induction machines. Conference Record, Industry Applications Society, IEEE-IAS Annual Meeting, 1995. 1: p. 606-616.

163. Simion, A., L. Livadaru, and A. Munteanu, Mathematical Model of the Three-Phase Induction Machine for the Study of Steady-State and Transient Duty Under Balanced and Unbalanced States. Induction Motors: Modelling and Control, 2012: p. 1.

164. Krause, P.C., O. Wasynczuk, and S.D. Sudhoff, Analysis of Electric Machinery.–The Institute of Electrical and Electronics Engineers. Inc., New York, 1995.

165. Santos, P., et al. A simplified induction machine model to study rotor broken bar effects and for detection. in 2006 37th IEEE Power Electronics Specialists Conference. 2006.

166. Bellini, A., et al., Quantitative evaluation of induction motor broken bars by means of electrical signature analysis. IEEE Transactions on industry applications, 2001. 37(5): p. 1248-1255.

167. Chen, S. and R. Živanović, Modelling and simulation of stator and rotor fault conditions in induction machines for testing fault diagnostic techniques. International Transactions on Electrical Energy Systems, 2010. 20(5): p. 611-629.

168. Cai, Z., A. Gao, and J. Jiang, Modelling for interior faults of induction motors and its simulation on EMTDC. Electric Power College, South China University of Technology, Guangzhou, 2003. 510640.

169. Filippetti, F., et al. Development of expert system knowledge base to on-line diagnosis of rotor electrical faults of induction motors. in Industry Applications Society Annual Meeting, 1992., Conference Record of the 1992 IEEE. 1992. IEEE.

170. Liang, H., et al., Fault Detection of Stator Inter-Turn Short-Circuit in PMSM on Stator Current and Vibration Signal. Applied Sciences, 2018. 8(9): p. 1677.

171. Benbouzid, M.E.H., M. Vieira, and C. Theys, Induction motors' faults detection and localization using stator current advanced signal processing techniques. IEEE Transactions on power electronics, 1999. 14(1): p. 14-22.

172. Barnish, T.J., M.R. Muller, and D.J. Kasten. Motor Maintenance: A Survey of Techniques and Results. in Proceedings of the 1997 ACEEE Summer Study on Energy Efficiency in Industry. American Council for an Energy-Efficient Economy, Washington, DC. 1997.

173. Calvo, J.A., C. Álvarez-Caldas, and J.L. San Román, Analysis of Dynamic Systems Using Bond Graph Method Through SIMULINK, in Engineering Education and Research Using MATLAB. 2011, InTech.

174. Feenstra, P.J., et al. Modeling and instrumentation for fault detection and isolation of a cooling system. in Proceedings of the IEEE SoutheastCon 2000.'Preparing for The New Millennium'(Cat. No. 00CH37105). 2000. IEEE.

175. Manders, E.J., P.J. Mosterman, and G. Biswas. Signal to symbol transformation techniques for robust diagnosis in TRANSCEND. in Tenth International Workshop on Principles of Diagnosis. 1999.

176. Mehrjou, M.R., et al., Rotor fault condition monitoring techniques for squirrel-cage induction machine—A review. Mechanical Systems and Signal Processing, 2011. 25(8): p. 2827-2848.

177. Shreve, D., Motor Current Signature Analysis Theory and Practice, GE Bently, Commtest, ppt, 6th Annual Meeting. 2013.

178. Li, H., et al. Broken Rotor Bar Detection Using Mathematical Morphology Based on Instantaneous Induction Motor Electrical Signals Analysis. in 2019 25th International Conference on Automation and Computing (ICAC). 2019. IEEE.

179. Funso Otuyemi , F.G., Andrew D. Ball, Broken Rotor Bar Fault Detection Working at a Low Slip Using Harmonic Order Tracking Analysis based on Motor Current Signature Analysis., in IncoME-V & CEPE Net-2020. 2020: Beijing institute of Technology, Zhuhai Chaina.

180. Li, H., et al., A Normalized Frequency Domain Energy Operator for Broken Rotor Bar Fault Diagnosis. IEEE Transactions on Instrumentation and Measurement, 2020.

181. Kim, J. and M.D. Bryant, Bond graph model of a squirrel cage induction motor with direct physical correspondence. J. Dyn. Sys., Meas., Control, 2000. 122(3): p. 461-469.